



TotalEnergies EP South Africa B.V. (TEEPSA)

Offshore Production Right and Environmental Authorisation
Applications for Block 11B/12B

Oil Spill Modelling Technical Report
Project No 42803622

September 12, 2023

Prepared for WSP Group Africa (Pty) Ltd





DHI Water & Environment, Inc • PO Box 32120 Preston • N3H 5M2 Cambridge, ON • Canada
Telephone: +1 519 650 4545 • jka@dhigroup.com • www.dhigroup.com

TotalEnergies EP South Africa B.V.

Offshore Production Right and Environmental Authorisation Applications for Block 11B/12B

Oil Spill Modelling Technical Report

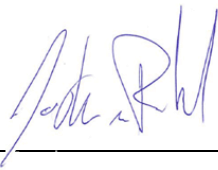
Prepared for: WSP Group Africa (Pty) Ltd

Represented by Sundar Prasad

Contact person: Sundar Prasad
Project Manager: Joshua Jon van Berkel
Quality Mads N Madsen
Supervisor:
Author: Maraya Syifa Widyastuti, Mohammad Madani, Yong Kai Saw
Project No.: 42803622
Approved by: Mads Madsen
Approval date: 9/12/2023
Revision: Final 5.0
Classification: Restricted
File name: 1. 120923_TEEPSA_Block11B12B_ESIA_OS_Modelling_230530_ComPTA__rev01.docx

Approved by Joshua Jon van Berkel

X

A handwritten signature in blue ink, appearing to read 'Joshua Jon van Berkel', written over a horizontal line.

Approved by

Contents

1	Introduction.....	8
1.1	Background.....	8
1.2	Scope of the Study	9
1.3	Modelling Scenarios Characteristics	10
2	Applied Methodologies and Data.....	11
2.1	MIKE OS.....	11
2.2	Metocean and Environmental Input.....	11
2.2.1	Mesh	12
2.2.2	SAT-Ocean Input and Model Resolution.....	13
2.2.3	Waves, Salinity and Temperature	14
2.3	General Modelling Approach	14
2.3.1	Considered Thresholds	15
3	Study Area Conditions.....	17
3.1	Available Metocean Conditions	17
3.2	Wind Rose and Current Rose	17
3.3	Water Temperature and Salinity.....	19
4	Oil Spill Modelling Set-up Parameters	21
4.1	Introduction	21
4.1.1	Distillation Curve.....	21
4.1.2	Applied Oil Properties Used in the Simulations	21
4.2	Oil Spill Scenarios Set-up Parameters	23
4.3	Model Limitations.....	25
5	Oil Spill Modelling Results	26
5.1	Results Illustration and Interpretation.....	26
5.1.1	Results Metrics	26
5.1.2	Key Points of Interest and Summarised Metrics	26
5.2	Scenario 1 – Well Blow-out - ‘Discharge 5’	27
5.2.1	Stochastic Model Results	27
5.2.2	Deterministic Model Result.....	36
5.2.3	Results Summary	45
5.3	Scenario 2 – Pipeline Rupture.....	47
5.3.1	Stochastic Model Result	47
5.3.2	Deterministic Model Result.....	54
5.3.3	Results Summary	63
6	Bibliographic References	65

Figures

Figure 1.1	Project development area and LOC locations	8
Figure 2.1	SAT-Ocean data Coverage (blue rectangle)	12
Figure 2.2	Bathymetry and the mesh of the study area	13
Figure 3.1	Wind rose at Discharge 5 location (left) and Pipeline Rupture location (right).....	18

Figure 3.2	Depth-Averaged-Current rose at Discharge 5 location (left) and Pipeline Rupture location (right)	18
Figure 3.3	Cross-section profile of water temperature and salinity at Discharge 5 Location	19
Figure 3.4	Cross-section profile of water temperature and salinity at Pipeline Rupture Location .	19
Figure 3.5	Time series representation of surface water temperature and salinity at Discharge 5 Location	20
Figure 3.6	Time series representation of surface water temperature and salinity at Pipeline Rupture Location	20
Figure 4.1	Distillation curve of oil used for the simulations	21
Figure 4.2	Model Domain and Locations of the two Oil Spill Events	24
Figure 5.1	Scenario 1 model results statistics, all simulations (all seasons): Probability of surface oil presence (top) and minimum time to oil slick exposure (bottom)	28
Figure 5.2	Scenario 1 model results statistics, all simulations that start in all seasons: Probability of shoreline oiling, zoomed-in on the impacted shoreline.....	29
Figure 5.3	Scenario 1 model results statistics, all simulations that start in Season 1 (December-February): Probability of surface oil presence (top) and minimum time to oil slick exposure (bottom)	30
Figure 5.4	Scenario 1 model results statistics, all simulations that start in Season 2 (March - May): Probability of surface oil presence (top) and minimum time to oil slick exposure (bottom)	31
Figure 5.5	Scenario 1 model results statistics, all simulations that start in Season 2 (March - May): Probability of shoreline oiling, zoomed-in on the impacted shoreline.....	32
Figure 5.6	Scenario 1 model results statistics, all simulations that start in Season 3 (June - August): Probability of surface oil presence (top) and minimum time to oil slick exposure (bottom)	33
Figure 5.7	Scenario 1 model results statistics, all simulations that start in Season 3 (June - August): Probability of shoreline oiling, zoomed-in on the impacted shoreline.....	34
Figure 5.8	Scenario 1 model results statistics, all simulations that start in Season 4 (September - November): Probability of surface oil presence (top) and minimum time to oil slick exposure (bottom)	35
Figure 5.9	Scenario 1 model results statistics, all simulations that start in Season 4 (September - November): Probability of shoreline oiling, zoomed-in on the impacted shoreline	36
Figure 5.10	Scenario 1 model results mass balance, the worst-case from all simulations (all seasons). Top - all components; bottom - zoomed-in for low value components.....	38
Figure 5.11	Scenario 1 model results mass balance, the worst-case from all simulations that start in Season 1 (December – February). Top - all components; bottom - zoomed-in for low value components.....	39
Figure 5.12	Scenario 1 model results mass balance, the worst-case from all simulations that start in Season 2 (March – May). Top - all components; bottom - zoomed-in for low value components.....	40
Figure 5.13	Scenario 1 model results mass balance, the worst-case from all simulations that start in Season 3 (June – August). Top - all components; bottom - zoomed-in for low value components.....	41
Figure 5.14	Scenario 1 model results mass balance, the worst-case from all simulations that start in Season 4 (September – November). Top - all components; bottom - zoomed-in for low value components.....	42

Figure 5.15	Scenario 1 model result drift evolution, the worst-case from all simulations that start in Season 1 (December – February)	43
Figure 5.16	Scenario 1 model result drift evolution, the worst-case from all simulations that start in Season 2 (March – May).....	43
Figure 5.17	Scenario 1 model result drift evolution, the worst-case from all simulations that start in Season 3 (June – August).....	44
Figure 5.18	Scenario 1 model result drift evolution, the worst-case from all simulations that start in Season 4 (September – November)	44
Figure 5.19	Scenario 2 model results statistics, all simulations (all seasons): Probability of surface oil presence (top) and minimum time to oil slick exposure (bottom)	48
Figure 5.20	Scenario 2 model results statistics, all simulations that start in Season 1 (December-February): Probability of surface oil presence (top) and minimum time to oil slick exposure (bottom)	49
Figure 5.21	Scenario 2 model results statistics, all simulations that start in Season 2 (March - May): Probability of surface oil presence (top) and minimum time to oil slick exposure (bottom)	50
Figure 5.22	Scenario 2 model results statistics, all simulations that start in Season 3 (June - August): Probability of surface oil presence (top) and minimum time to oil slick exposure (bottom)	51
Figure 5.23	Scenario 2 model results statistics, all simulations that start in Season 3 (June - August): Shoreline oiling probability, zoomed-in on the impacted shoreline	52
Figure 5.24	Scenario 2 model results statistics, all simulations that start in Season 4 (September - November): Probability of surface oil presence (top) and minimum time to oil slick exposure (bottom)	53
Figure 5.25	Scenario 2 model results statistics, all simulations that start in Season 4 (September - November): Shoreline oiling probability, zoomed-in on the impacted shoreline	54
Figure 5.26	Scenario 2 model results mass balance, the worst-case from all simulations (all seasons). Top - all components.....	55
Figure 5.27	Scenario 2 model results mass balance, the worst-case from all simulations that start in Season 1 (December – February). Top - all components; bottom - zoomed-in for low value components.....	56
Figure 5.28	Scenario 2 model results mass balance, the worst-case from all simulations that start in Season 2 (March – May). Top - all components; bottom - zoomed-in for low value components.....	57
Figure 5.29	Scenario 2 model results mass balance, the worst-case from all simulations that start in Season 3 (June – August). Top - all components; bottom - zoomed-in for low value components.....	58
Figure 5.30	Scenario 2 model results mass balance, the worst-case from all simulation that start in Season 4 (September – November). Top - all components; bottom - zoomed-in for low value components.....	59
Figure 5.31	Scenario 2 model result drift evolution, the worst-case from all simulations.....	60
Figure 5.32	Scenario 2 model result drift evolution, the worst-case from all simulations that start in Season 1 (December – February)	60
Figure 5.33	Scenario 2 model result drift evolution, the worst-case from all simulations that start in Season 2 (March – May).....	61
Figure 5.34	Scenario 2 model result drift evolution, the worst-case from all simulations that start in Season 3 (June – August).....	61

Figure 5.35 Scenario 2 model result drift evolution, the worst-case from all simulations that start in Season 4 (September – November) 62

Tables

Table 1.1	General Characteristics of Loss of Containment Scenarios.....	10
Table 2.1	Threshold Used in the Post-processing of Modelling Results.....	15
Table 4.1	Characterisation of Released Condensate.....	22
Table 4.2	Summary of study scenarios for both release points.....	24
Table 4.3	Repetition of the deterministic simulations per season and per year.....	25
Table 5.1	Starting Date of Deterministic Simulations.....	36
Table 5.2	Summary of Scenario 1 Results- Well Blow-out Discharge 5.....	46
Table 5.3	Starting Date of Deterministic Simulations.....	54
Table 5.4	Summary of Scenario 2 Results- Pipeline Rupture.....	64

Appendices

Appendix A: MIKE 21 & MIKE 3 Flow Model FM, Oil Spill Module - Short Description

Appendix B: Offshore Production Right and Environmental Authorisation Applications for Block 11B/12B – Analysis of Metocean Data for Oil Spill and Drilling Discharge Modelling

1 Introduction

This report presents the methodology and results of oil spill modelling for the Project Development Area in Block 11B/12B. The modelling was performed on predetermined loss of containment (LOC) scenarios associated with oil and gas well and subsea production system (SPS) operations.

1.1 Background

TotalEnergies EP South Africa B.V. (TEEPSA), together with its joint venture partners, QatarEnergy, Canadian Natural Resources International South Africa Limited, and a South African consortium, MainStreet 1549, held an Exploration Right (Exploration Right Ref. No.: 12/3/067) over Block 11B/12B that expired on 06 September 2022. TEEPSA submitted a Production Right (PR) application in terms of Section 83 of the Mineral and Petroleum Resources Development Act, 2002 (Act 28 of 2002) (MPRDA), as amended to the Competent Authority (CA) on 05 September 2022. The CA acknowledged receipt of the application on 19 September 2022.

Licence Block 11B/12B is located offshore the southern cape coast, South Africa and the application area is approximately 12 000 km² (Figure 1.1). The north-eastern point of the Block 11B/12B application area is approximately 75 km offshore of Cape St Francis and the north-western point is approximately 120 km offshore of Mossel Bay.

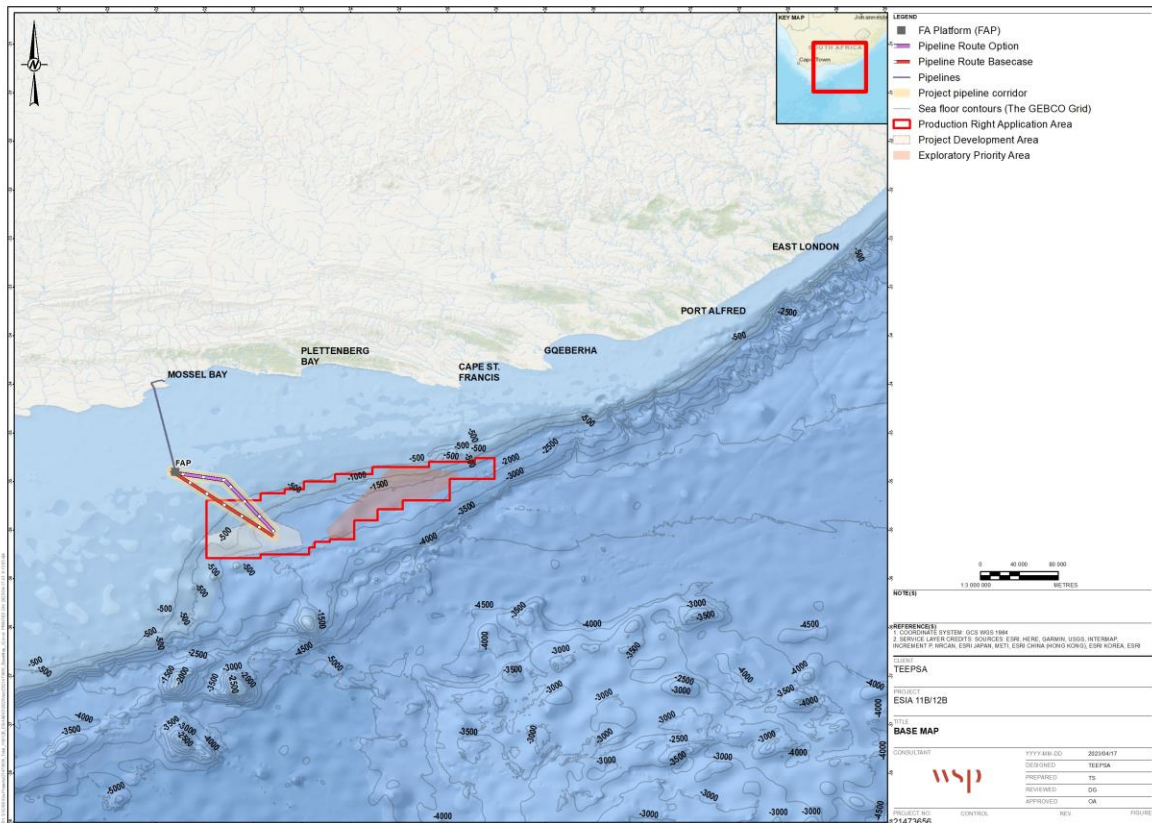


Figure 1.1 Project development area and LOC locations

Exploration activities in Block 11B/12B commenced in 2012 and ended in 2020. Drilling efforts focused on the south-west section of the Block, the Production Development Area, where the drilling of the Brulpadda – 1AX exploration well was completed in February 2019 and the drilling of the Luiperd – 1X exploration well was completed in October 2020. Extensive 3D seismic survey data was acquired between 2019 and 2020. This exploration programme led to an important gas discovery and after further completion of technical and feasibility studies, the commercial viability of the gas and associated condensates resources was confirmed. TEEPSA is planning to develop Block 11B/12B if a PR is granted and if commercial agreements for the sale of the gas onto the domestic market can be achieved.

The development of Block 11B/12B will involve the drilling of five production wells, with the option of drilling a sixth well, in the Project Development Area. In this area, the wells will be connected via subsea infrastructure to a multiphase pipeline carrying both gas and associated condensates to the existing F-A Platform located approximately 40 km northwest of Block 11B/12B. Owned and operated by PetroSA, the F-A Platform was constructed in the early 1990's and processed gas and condensate from the Block 9 gas fields to supply the PetroSA Gas-to-Liquid (GTL) plant located outside Mossel Bay. The Platform was placed in care and maintenance mode in November 2020 and it is intended that this facility will be used to process gas and condensate from Block 11B/12B. The processed products will be conveyed from the Platform to shore via existing subsea pipelines.

No exploratory drilling has been conducted to date in the east-northeast area of Block 11B/12B, the Exploratory Priority Area where crude oil is possibly the main hydrocarbon. TEEPSA intends to conduct an exploration drilling campaign of up to four exploration and appraisal wells in this area with the objective to further define the resource.

Survey works (sonar, coring, etc.) will possibly be conducted at specific locations within Block 11B/12B to support activities within the Project Development Area and the Exploratory Priority Area.

1.2 Scope of the Study

This report provides the following content as it relates to the scope of analysis:

- A description of the modelling approach as it relates to the applied numerical model and key oceanographic inputs
- A description of modelling set-up inputs (e.g., applied oil properties)
- An explanation of modelled oil spill scenarios, and
- Oil spill modelling results.

In general, the executed analysis applied SAT-OCEAN input provided by the end-Client (TotalEnergies, 2022) and the MIKE Oil Spill (OS) module from the suite of MIKE Powered by DHI models. This SAT-OCEAN hydrodynamic database can be found in WSP's Analysis of Metocean Data for Oil Spill and Drilling Discharge Modelling in Appendix B.

Two modelling scenarios were analysed, namely:

- Block 11B/12B well blow-out with condensate LOC 'Discharge 5' at the wellhead
- Block 11B/12B full pipeline rupture of condensate in the middle of the Critical Biodiversity Area (CBA).

The study derives results from two modelling approaches, namely:

- Stochastic simulations: statistical calculations / analyses based on the results from ensemble modelling of the LOC scenario under a wide range of weather and/or seasonal conditions, and

- Deterministic simulations: where the trajectory and fate of an oil slick from an individual LOC event (e.g., worst-case) was isolated amongst the ensemble model runs.

1.3 Modelling Scenarios Characteristics

The analysed scenarios were specified by TEEPSA and, generally, selected based on proximity to sensitive coastal areas and given worst-case scenario wind and wave conditions.

Discharge Location 5 was selected as a representative location for drilling occurring both to the east and the west of this location, *i.e.*, a central location within the proposed production development area. The point is in close proximity to the previously drilled explorations well Luiperd-1X upon which the oil spill characteristics for the study are based.

The location selected for the LOC spill from a pipeline rupture is deemed conservative in that it represents a shallower location (~146 m) offshore of the FA platform that is in close proximity to sensitive areas and in an area strongly influenced by both the wind-driven flows and shear edge features and strong currents associated with the Agulhas Current. This allows a wider distribution of spilled condensate, particularly shoreward, and therefore is deemed a location that will result in a sufficiently conservative assessment of the consequences of a condensate spill.

Key characteristics of the LOC release point locations are presented in Table 1.1.

Table 1.1 General Characteristics of Loss of Containment Scenarios

LOC Scenario Characteristics	Well Blow-out - 'Discharge 5'	Pipeline Rupture
LOC Event Characteristics	Condensate LOC discharge - Luiperd condensate Deepsea blow out at wellhead Release assumed to last 20 days until containment is re-established via a capping stack Spill rate of 18350 bbl/day	Condensate LOC discharge - Luiperd condensate Full rupture of the pipe in first year of production (<i>i.e.</i> , highest condensate yield) Two hours to shut-down the wells (worst-case) <i>i.e.</i> , as there is no valve between the Production Manifold in Paddavissie and FA platform riser in B9 Assumption is that entire volume inside the pipe will be released within 1 day Assumed rate of discharge: 0-2h: 19320 bbl/d, 2-24h: 10728 bbl/d
Release Point (WGS84)	Latitude - S 35° 35' 17.3071" Longitude - E 23° 08' 27.6914"	Latitude - S 35° 6' 58.41" Longitude - E 22° 23' 1.66"
Water Depth (mean sea level)	~1780 m	~ 146 m
Currents - main directions	Southwest	Southwest-Northeast
Winds - main directions	West – East	West – East

2 Applied Methodologies and Data

Numerical modelling was predominantly used to assess the physical effects of an oil spill from the proposed subsea well and pipeline breach. This entailed the use of the MIKE OS model and key metocean input data, which are described in more detail in the following subsections.

2.1 MIKE OS

The oil spill trajectory modelling was carried out using the MIKE OS model (see Appendix A) which is based on a particle tracking concept simulating the movement of discrete particles in a flow field. The spilled oil is represented by a collection of particles, each representing an oil mass with associated physical and bio-chemical properties. The mass and the properties of each particle will change over time due to weathering (see Appendix A). The probability of oil stranding and water re-entry is described as a function of the shoreline characteristics (*i.e.*, rocky, shingle, sandy or muddy beach, seawall or revetment, marshy, *etc.*). The present study assumes that once the oil strands on a coast/beach, it stays on the coast/beach and does not return to the sea.

2.2 Metocean and Environmental Input

The basis for oil spill modelling comprises meteorological and oceanographic (metocean) data and environmental data, including wind, waves, currents, salinity, and water temperature.

In the present study, oceanographic data from the following models was applied:

- SAT-OCEAN, current direction, current speed, wind speed, and wind direction (*i.e.*, coverage of this dataset is presented in Figure 2.1) – spatial resolution: 0.032° longitude x 0.032° latitude, temporal resolution: 3-hourly instantaneous values
- HYCOM GLBv0.08_expt_56.3, surface elevation - with 0.08° longitude x variable latitude spacing from 0.04 to 0.08°, temporal resolution: 3-hourly instantaneous values (Naval Research Laboratory 2014-2021)
- DHI's Global Wave Model (*i.e.*, using ERA5 wind dataset) wave data was applied
- HYCOM, salinity and temperature - resolution in space: 0.04° longitude x 0.04° latitude with 40 non-equidistant vertical layers, temporal resolution: daily instantaneous values.

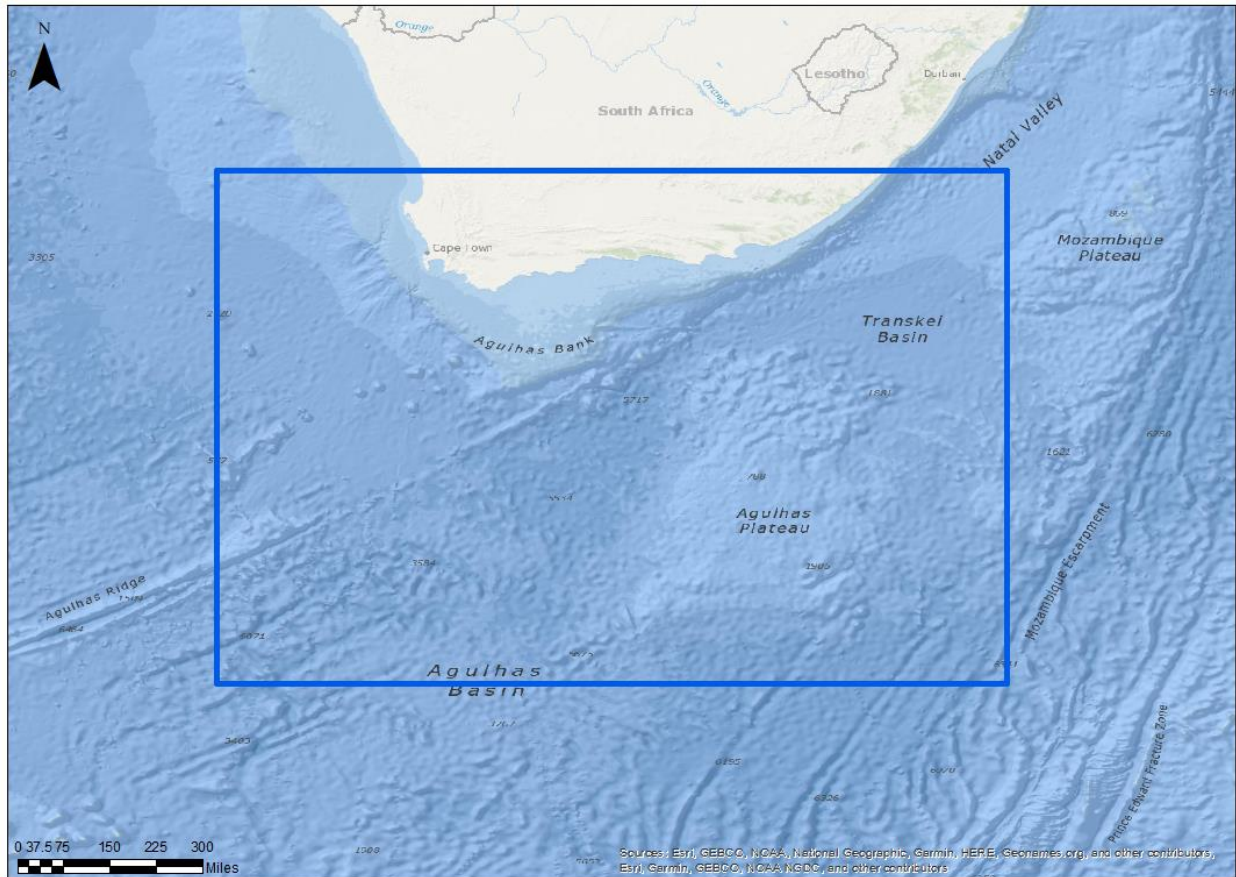


Figure 2.1 SAT-Ocean data Coverage (blue rectangle)

As evident from the bulleted overview, surface elevation data from the HYCOM dataset was used in combination with the current speed and direction from the SAT-OCEAN dataset to define the hydrodynamic conditions. Further, wave data was derived from DHI’s Global Wave Model and water temperature, and salinity was also sourced from HYCOM. The wave data are used to assess vertical dispersion of oil into the water column during wave breaking.

The coverage of the SAT-OCEAN dataset, presented in Figure 2.1 above, became the *de facto* model boundaries for the study. Further details of the metocean data used can be found in Appendix B.

2.2.1 Mesh

To model the domain in DHI’s MIKE software, the study area first needed to be discretised into a mesh network. The mesh applied for the oil spill modelling at Cape South Coast License Block in South Africa was generated using DHI’s MIKE Zero Mesh Generator and Surface-water Modelling System (SMS) developed by Aquaveo, both of which enables the generation of meshes. The mesh was established with a resolution of 300m near the shoreline and consisted of one sigma layer up to a depth of 5 meters, and 29 non-equidistant z layers. This aligned with the vertical resolution of the SAT-Ocean dataset, which ranged from around 500m near the seabed to 2.5m near the surface. Further description of SAT-OCEAN data can be found in Section 2.2.2.

The mesh has five open boundaries, with two located on the north and one at each west, east, and south direction. This highly flexible triangular mesh consisted of 82686 nodes, 159244 elements in the

horizontal plane, and 29 layers in the vertical direction, allowing for a high-resolution representation of the oil spill transport in the domain (see Figure 2.2).

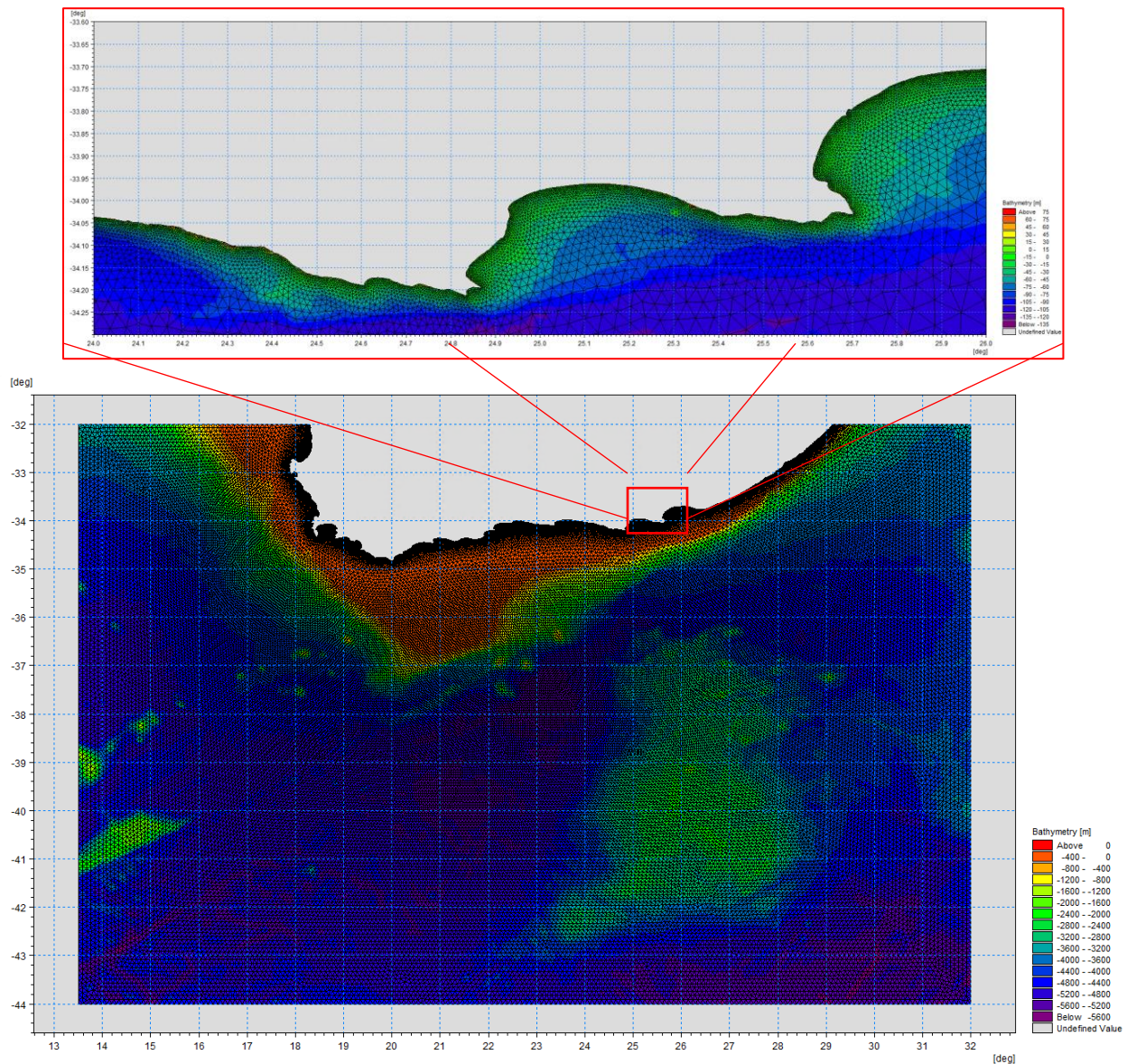


Figure 2.2 Bathymetry and the mesh of the study area

2.2.2 SAT-Ocean Input and Model Resolution

The SAT-OCEAN dataset, which was provided by TotalEnergies, includes information on current direction, current speed, wind speed, and wind direction. Initially, the data was available in netCDF format, but DHI converted it to a dfsu format (a DHI's MIKE data format) to enable compatibility with DHI's MIKE's software.

SAT-OCEAN is a source of meteorological and oceanographic (metocean) data for several industries. It provides information on current direction, current speed, wind speed, and wind direction, which are

input variables for oil spill modelling. The dataset provides high spatial resolution of 0.032° longitude x 0.032° latitude, and a temporal resolution of 3-hourly instantaneous values, which allows for the tracking of changes in wind patterns over time.

To apply the SAT-OCEAN dataset, the data had to be converted to dfsu format using a bespoke Python code. This conversion allowed the data to be compatible with the MIKE OS model and made it easier to work with. The conversion process involved several steps, including reading the data in netCDF format, converting the individual monthly data file to a dfsu format, and concatenating the data to one single dfsu file. The entire dataset i.e., from 2012-01-01 to 2016-12-31, was converted. This process ensured that the data was accurately represented in the model and that any simulation runs using the data were reliable and accurate.

2.2.3 Waves, Salinity and Temperature

Apart from the SAT-OCEAN data, several other data inputs were required to run MIKE OS. Salinity and temperature data were obtained from HYCOM and used as forcing inputs. HYCOM is an ocean data assimilation system that provides simultaneous analyses of temperature, salinity, geopotential, and vector velocity. It is a three-dimensional, multivariate, variational model that produces real-time analyses that are updated daily. The data was interpolated to a uniform grid of 0.08 degrees Lat/Long, covering a range between 80.48°S and 80.48°N. The model's high resolution makes it able to resolve eddies, which is beneficial in simulating western boundary currents and mesoscale variability. An eddy-resolving ocean model is also better at maintaining accurate and sharp ocean fronts, which is important for predicting ocean dynamics and forecasting.

HYCOM's ability to capture flow instabilities and currents allows for topographic coupling in the upper ocean. This coupling plays an important role in predicting ocean dynamics and forecasting, especially on timescales up to a month. Sea surface temperature (SST) retrievals are derived empirically using stored regressions between cloud-cleared satellite SST radiances and drifting buoy SSTs. The global regressions are calculated once and held constant, providing a reliable and consistent source of data for use in ocean modelling and forecasting.

The DHI Global Wave Model (GWM) serves as an important source of data for many oceanographic and meteorological studies, as it provides valuable information on wave and ice coverage data. This model is validated against both wave and satellite altimetry observations, proving its reliability and effectiveness when applied as boundary conditions for several models around the world. To develop the GWM, a computational mesh with a varying element size is used, resulting in a resolution of approximately 50 km in offshore areas and up to 15 km near the coastline. The model was established with the MIKE SW Release 2022, and its hindcast was run, including the following:

- the cap on wind friction
- stability-corrected wind fields
- Temporal and spatially varying ratio of air/sea density based on the ERA5.

2.3 General Modelling Approach

Two scenarios of stochastic modelling entailed the combination of one oil type (Luiperd condensate), and two locations. To consider the influence of the varying metocean conditions throughout the year and varying conditions from year to year, multiple spill simulations were required. Here, the time period of each simulated oil spill was distributed stochastically throughout the period of 2012 to 2016 for which hindcast met-ocean conditions were available.

For each of the two scenarios, a set of statistics was prepared for four representative seasons provided by the client. The four seasons adopted for the statistical analysis were S1 (December-February), S2 (March through May), S3 (June through August) S4 (September - November) in addition to all-year statistics. The number of simulations for each season and for each year is further explained in Section 4.2 and provided in Table 4.3.

The seasonal statistics comprises maps showing:

- Surface probability of exposure to an oil slick
- Probability of shoreline oiling
- The minimum time (from the start of a spill) to exposure to an oil slick.

It is emphasised that the probability maps only include contamination above pre-specified threshold levels.

To obtain a better understanding of worst-case results, eight deterministic simulations were processed, comprising of representative scenarios of the worst-case from each season and each scenario. The worst-case was defined as the simulation (among the stochastic simulations) that produced the longest impacted shoreline. The deterministic simulation provides a detailed picture of the oil trajectory during the simulation period.

2.3.1 Considered Thresholds

Thresholds values in Table 2.1 applied to this study followed those in previous related studies e.g., HES 2022. Where applicable, they were used to illustrate modelling output results.

Table 2.1 Threshold Used in the Post-processing of Modelling Results

Threshold	Threshold Value	Justification
Surface Thickness Oil	5 µm	10 µm corresponds to the thickness that would impart a lethal dose to an intersecting wildlife individual (French McCay 2009). The value of 5 µm was chosen to keep a margin and because it is also the minimum thickness at which response equipment can skim/remove oil from the surface, surface dispersants are effectively applied, or oil can be boomed/collected. Fresh oil at this thickness corresponds to a slick being a dark brown or metallic sheen
Water-Column	58 ppb	Based on extensive toxicity tests of crude oils and oil components on marine organisms, the OLF (the Norwegian Oil Industry Association) Guideline for risk assessment of effects on fish from acute oil pollution (2008) concluded that the threshold concentration for an expected No Observed Effect Concentration (NOEC) for acute exposure for THC ranges 0.05 to 0.3 ppm. Work undertaken by Neilson <i>et al.</i> (2005), as reported in OLF, 2008 proposed a value for acute exposure to dispersed oil of 58 ppb, based on the toxicity of chemically dispersed oil to various aquatic species, which showed the 5% effect level is 58 ppb.

Threshold	Threshold Value	Justification
Shoreline Oiling	10 g/m ²	Shoreline oiling calculated for deterministic scenarios assuming that a certain surface is affected by kilometre of shoreline, depending on the shoreline type. For various shoreline types, a set of maximum oil “holding capacities” is estimated along with a set of removal rates. The holding capacities are intended to reflect both shoreline slope and permeability. A 10 g/m ² threshold provides a conservative screening threshold used for potential ecological effects on shoreline fauna. Assumed as a sublethal effects threshold for birds on the shoreline (French et al. 1996; French McCay 2009; French McCay 2016).

3 Study Area Conditions

3.1 Available Metocean Conditions

A separate analysis of metocean conditions was undertaken to determine current and wind characteristics pertinent to this report and other South-west Corner - Block 11B/12B Project studies, as seen in Appendix B. This includes contextual reporting of broad-scale oceanography. Of note, the primary driver of ocean dynamics in Block 11B/12B is the strong Agulhas Current which flows southward along the east coast of Africa and is estimated to transport 70 million cubic metres of water per second. Discharge 5 and the Pipeline Rupture location are situated on the inner edge of the Agulhas Current that is strongly influenced by the predominantly strong south-westerly surface flows of the Agulhas Currents. These flows are significantly weaker at depth and more prone to current reversals. There is evidence of a more persistent current reversals in the deeper waters (> 1 500 m) on the inshore edge of the upstream regions of the Agulhas Current (Beal and Bryden, 1997; Beal, 2009; Beal *et al.*, 2015), an influence that could extend into licence Block 11B/12B but at slightly greater depths (~ 1 800m). The Pipe Leak (rupture) discharge location, in the shallower waters (~ 140 m to 150 m water depth) of the adjacent Agulhas Bank is more strongly influenced by wind driven flows, particularly in the surface waters where there is evidence of more persistent north-easterly wind-driven flows in the surface waters associated with the strong westerly winds associated with passing mid-latitude cyclones (“cold fronts”) that occur during the winter months.

3.2 Wind Rose and Current Rose

Figure 3.1 and Figure 3.2 show the general conditions of wind and current near the study area. For the most part, the wind at both scenario spill locations is in west-east directions, with the wind from the west direction stronger than the wind from the east. Meanwhile the depth-averaged current roses show the current at the Discharge 5 location is mainly in the southwest direction while the current at the Pipeline Rupture location is in northeast-southwest direction. The current condition at Discharge 5 location is stronger than at Pipeline Rupture location, where the current speed can reach up to more than 0.8m/s.

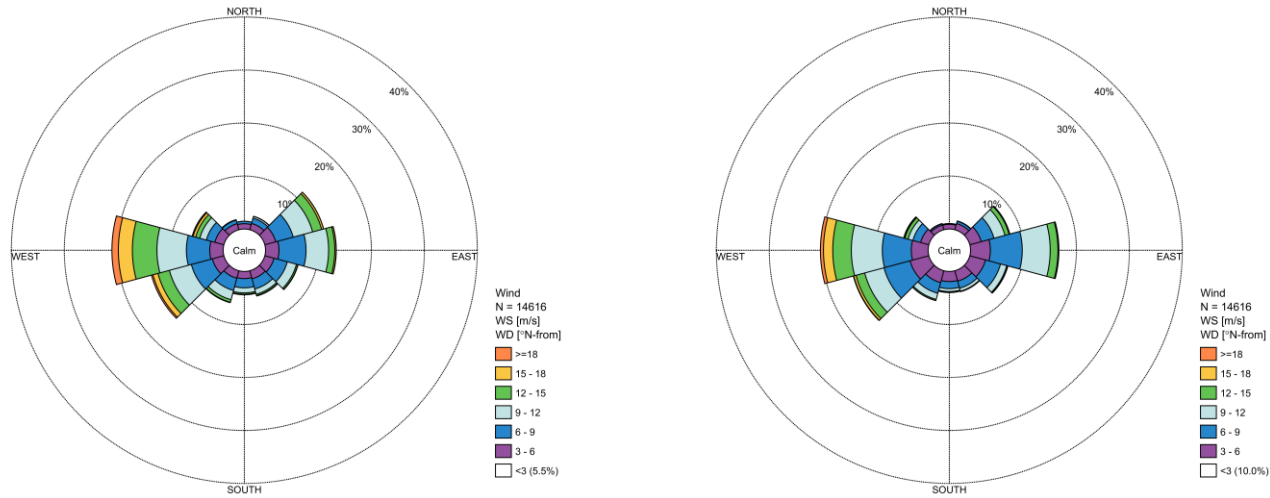


Figure 3.1 Wind rose at Discharge 5 location (left) and Pipeline Rupture location (right)

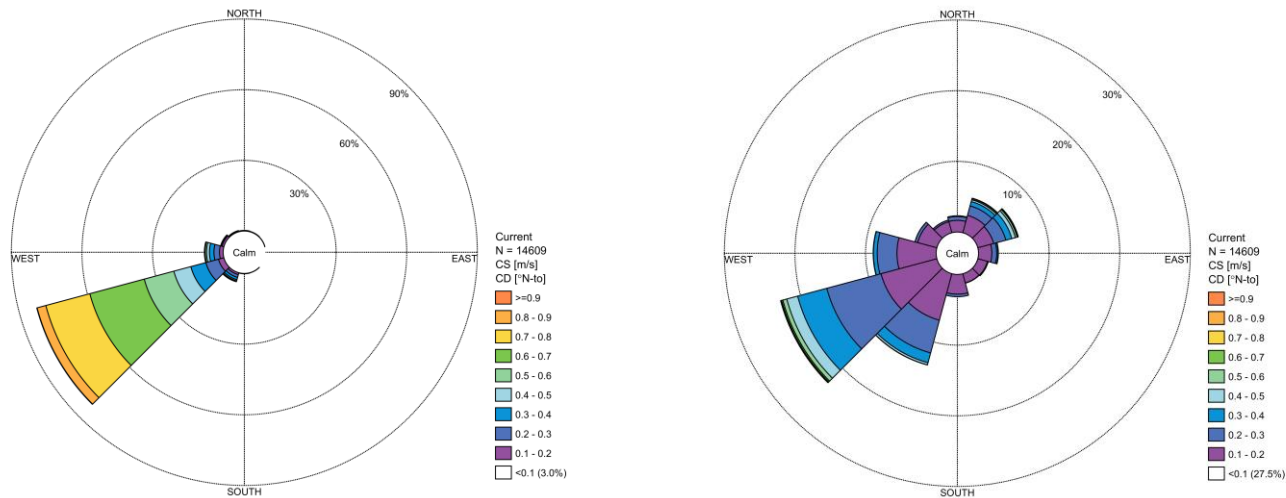


Figure 3.2 Depth-Averaged-Current rose at Discharge 5 location (left) and Pipeline Rupture location (right)

3.3 Water Temperature and Salinity

While certain oil spill models utilize static water temperature and salinity constants in their set-up, MIKE OS allows for the inclusion of spatial-temporal data to better characterise the influence of these influential parameters. To demonstrate an example of the applied HYCOM data which, as previously mentioned was sourced for this input, a selection of cross-section and time series plots at each LOC location are provided in Figure 3.3 to Figure 3.6.

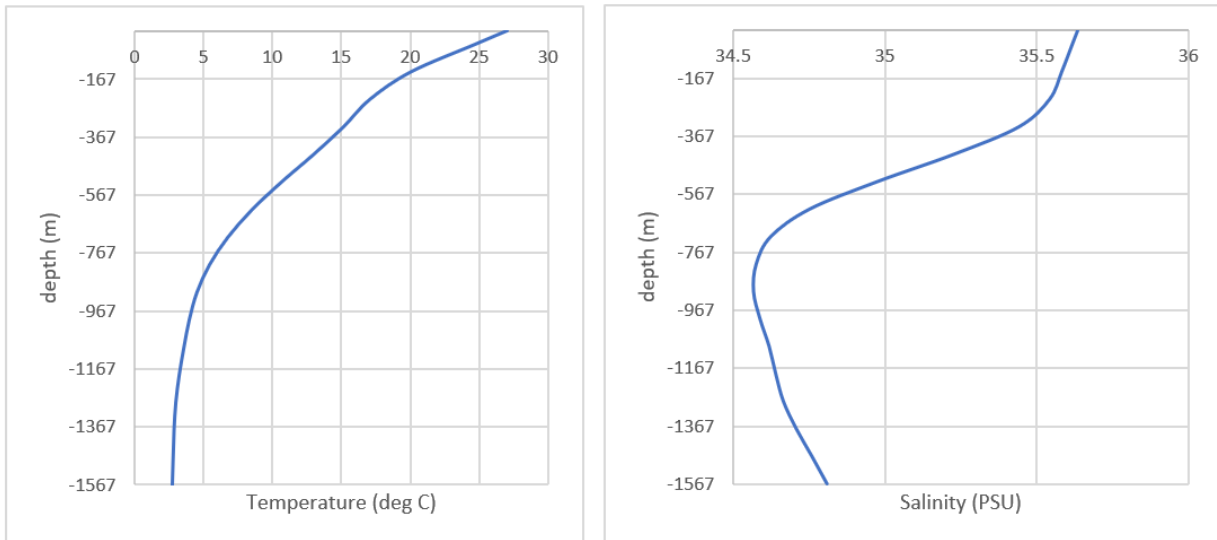


Figure 3.3 Cross-section profile of water temperature and salinity at Discharge 5 Location

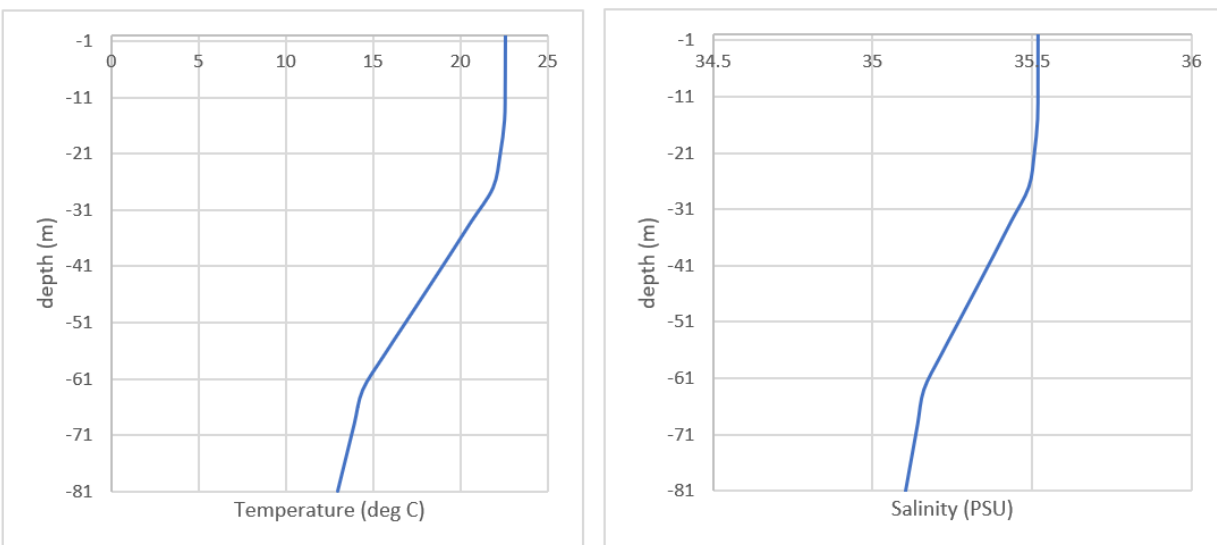


Figure 3.4 Cross-section profile of water temperature and salinity at Pipeline Rupture Location

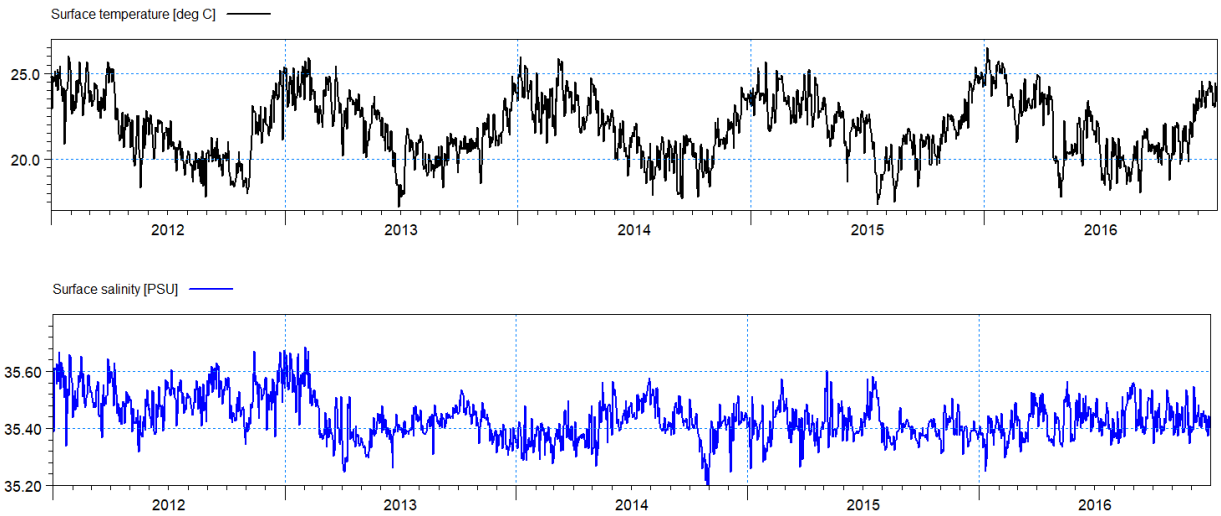


Figure 3.5 Time series representation of surface water temperature and salinity at Discharge 5 Location

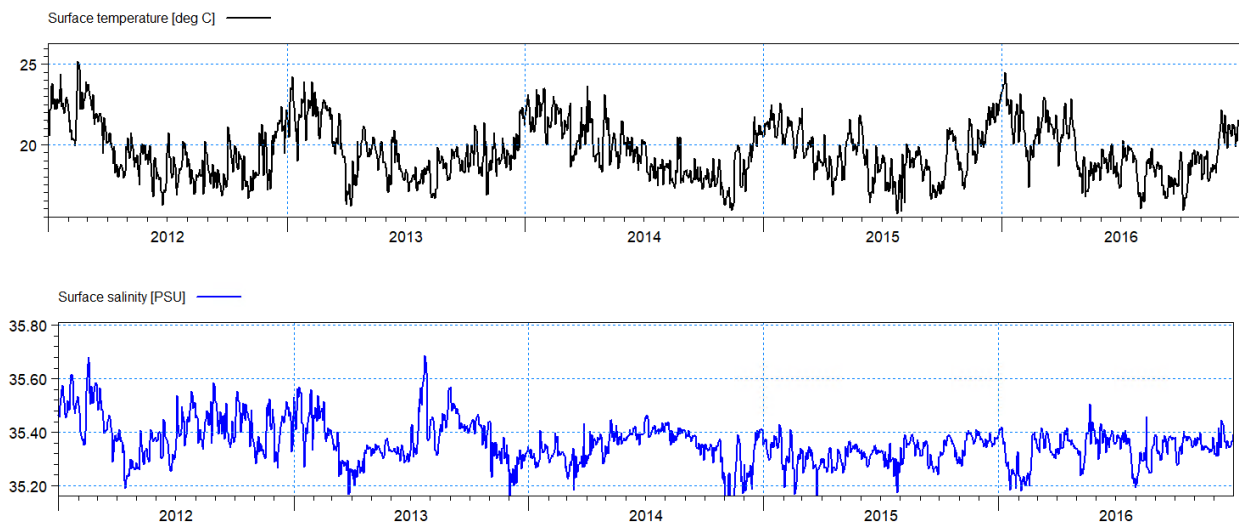


Figure 3.6 Time series representation of surface water temperature and salinity at Pipeline Rupture Location

4 Oil Spill Modelling Set-up Parameters

4.1 Introduction

TotalEnergies provided data on the TBP (True Boiling Point), density, viscosity at 10, 20 and 40°, content of asphaltenes and wax associated with the Luiperd condensate. The oil was characterised according to this information and was used in the simulations.

Oil properties are described through the percentage of each of three oil fractions: light, medium and heavy. Each of these fractions was assigned a boiling point and vapour pressure range which changed during the simulation due to the evaporation. In addition, the content of wax and asphaltenes was included in the simulations. These two fractions were assumed to be involatile.

The received information on the oil was considered sufficient for a proper and conservative characterization of the oil type.

4.1.1 Distillation Curve

The oil was characterized according to the aforementioned sources and was used to define the distillation curves, as seen in Table 4.1.

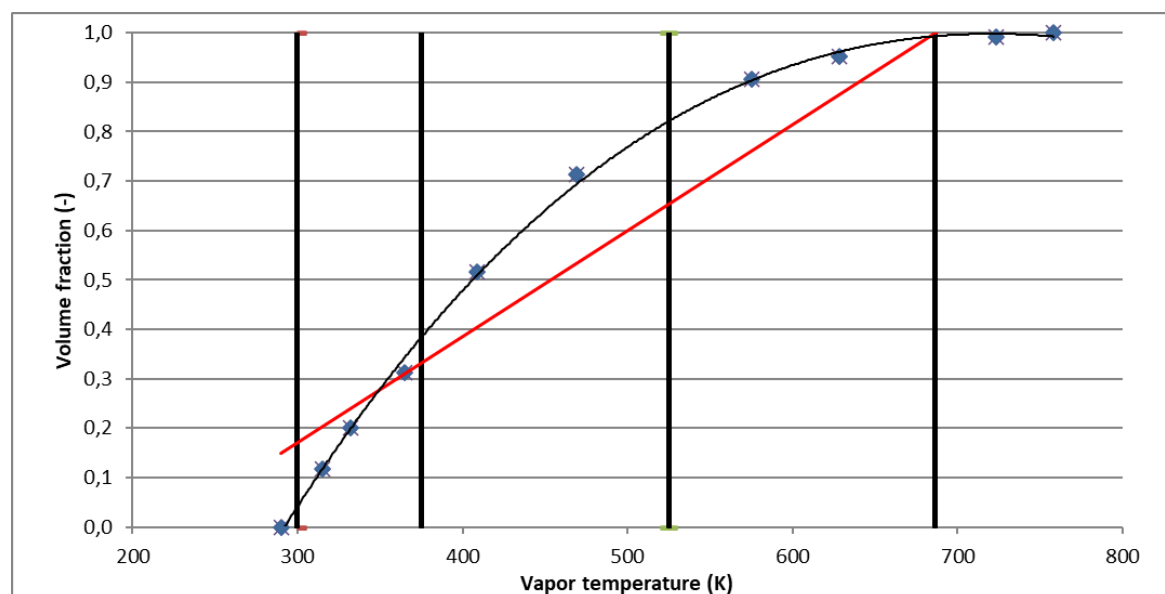


Figure 4.1 Distillation curve¹ of oil used for the simulations

4.1.2 Applied Oil Properties Used in the Simulations

A summary of the characterisation of the condensate applied in the simulations is given in Table 4.1, below.

¹ The red line is a linear trendline for the three model classes established from the distillation curve.

Table 4.1 Characterisation of Released Condensate

Parameter	Oil Fraction			Comments
	Light	Medium	Heavy	
Concentration (wt%)	32.3	32.4	34.3	See Figure 4.1
Boiling point (K)	375	525	687	See Figure 4.1
Vapor pressure (atm)				Calculated from boiling point range
Molar mass (g/mole)	107	211	286	Calculated from the average boiling point
Pour point (°C)	-20	0	36	Set values
Biodegradation (1/d)	0.005	0.001	0	Defaults
Density (kg/m³)	716	782	798	Derived from the fluid composition data
Oil Data				
Density (@288K)	(Kg/m3)	766		Information provided by TotalEnergies
Viscosity (@293K)	(cP)	0.8		Information provided by TotalEnergies
Max water content from emulsification	(%)	0		Assumed value. Due to the low content of wax and asphaltenes, it is assumed that the oil has low tendency to form water-in-oil emulsions
Asphaltene content	(%)	0.1		Information provided by TotalEnergies
Wax content	(%)	0.85		Information provided by TotalEnergies
Surface tension without surfactant	(m nM)	0.015		Default
Surface tension with surfactant	(m nM)	0.001		Default

For the oil described in Table 4.1, an assessment of the importance of photooxidation, biodegradation and sedimentation were made:

Photooxidation is usually considered to play only a relatively minor role in the overall weathering of the spilled oil. Not all oil components are susceptible to photooxidation, and the process is also dependent on the availability of light, e.g., cloudiness, night-time, time-of-year. The photooxidation

does not remove the oil components completely but transforms the oil components into more water-soluble components compared to the mother oil components and can stabilise the emulsification process and enhance the dissolution process. Photooxidation may be of interest when looking at the toxicity of the oil, as more toxic compounds than the mother oil component may be formed by photooxidation, but not concerning the mass balance of the oil. Photooxidation is considered to contribute less than 1% of the total removal and therefore were not included in modelling setup.

Biodegradation is a significant process for the total removal of oil from the environment. However, the process is very slow and very complex as it depends on the composition of the oil, availability of microorganisms, oxygen, and on temperature. Where the oil is thick, the microbial community mainly only meets the surface; as a result, very little reduction in oil volume is due to biodegradation. For very thin oil sheens and when oil droplets are dispersed in the water for a long period, then the biodegradation becomes a more dominating process. Mainly heavy weight oil components are left after evaporation (and dissolution), and many of these components are not susceptible to biodegradation until after periods of months or years have passed.

In a study of biodegradation of heavy fuel oil at good conditions for biodegradation (15°C, inoculation with creek water, nutrients), 11% degradation after 28 days was observed (Walker J.D. et al, 1976). This corresponds to a half-life of 166 days. The conditions for biodegradation for an oil spill at sea will not be as good as for the mentioned experiment – both concerning temperature and presence of microorganisms/nutrients, so a much higher biodegradation half-life than 166 days for the residual oil components (after evaporation/dissolution) is expected. At maximum, removal due to biodegradation of 10-20% of the remaining oil (after evaporation, dissolution) within a 120-day window is expected.

If the density of the oil exceeds the density of the ambient water, the settling of the oil is included. However, sedimentation due to the uptake of heavier particles is only considered relevant for oil close to the coastlines, where adsorption to sediment followed by sedimentation may be of relevance. The absorption of sediments is not included in the model. Therefore, sinking is not relevant for the oil simulated in this project.

Overall, biodegradation, sedimentation and photooxidation within a considered 120-day-window are assessed to contribute less than 10% of the total mass balance of the oil spill and for maximum 10-20% of the remaining oil (after evaporation and dissolution).

The change in oil pour point, density and viscosity is calculated in dependence of all above mentioned fate processes – the evaporation being by far the most important process.

4.2 Oil Spill Scenarios Set-up Parameters.

As mentioned, two spill scenarios (refer to Figure 4.2 below) were considered Luiperd condensate, which was already explained in previous section, was used in the simulations.

The two selected locations comprise a deep-sea blow out at well head (Discharge 5 location) and full rupture of a pipeline in first year (Pipeline Rupture location). The spill at Discharge 5 location was released over 20 days with spill rate of 18350 bbl/day, while the spill at Pipeline Rupture location was released over one day with a varying spill rate (19320 bbl/day for the first two hours, and 10728 bbl/day for the remain hours).

For each location, around 400 simulations were stochastically selected and distributed evenly over the modelling period of 2012-2016. The number of simulations for each season is provided in Table 4.3. All the simulations at the Discharge 5 location were simulated throughout 30 days while at Pipeline Rupture location, the simulations were simulated throughout 20 days. This model duration is considered to be sufficient considering the spill comprised condensate.

A map of the location of the two different spill locations is provided in Figure 4.2 and a summary overview of all oil spill scenarios can be found in Table 4.2.

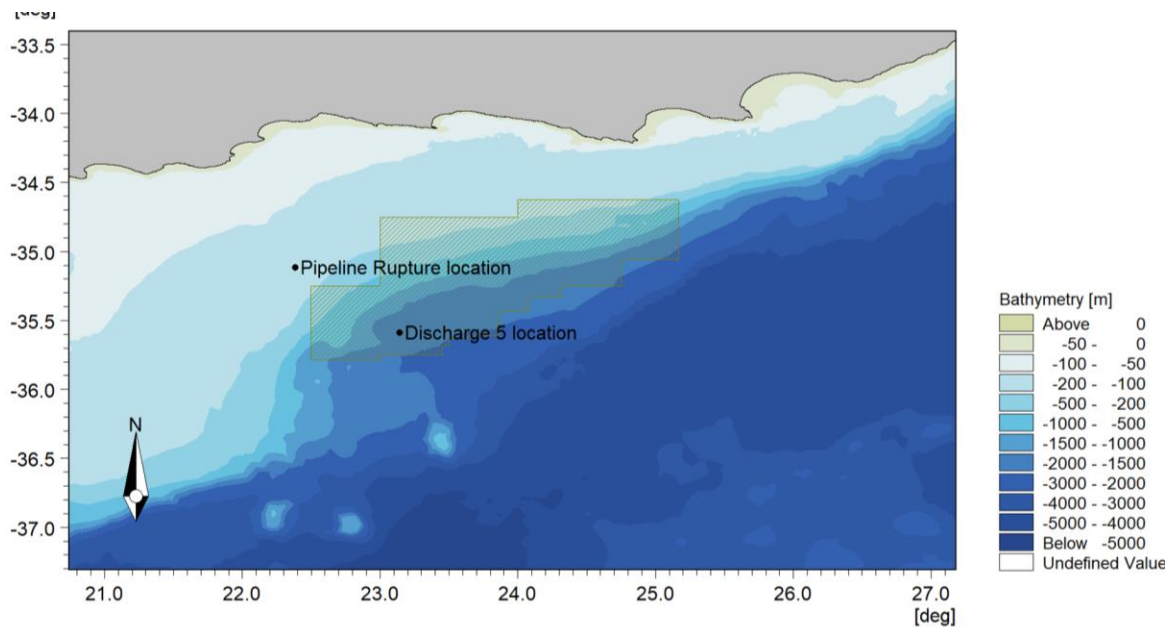


Figure 4.2 Model Domain and Locations of the two Oil Spill Events

Key scenario set-up parameters for both LOC events are summarized in Table 4.2.

Table 4.2 Summary of study scenarios for both release points

LOC Spill Location	Duration	Rate	Cause of Discharge	Coordinates (lon°, lat°)	Depth (m)	Simulation Period
Scenario 1: Well Blow-out						
Discharge 5	20 days	18350 bbl/day	Blow out at Capping Stack	E 23° 08' 27.6914" S 35° 35' 17.3071"	~1780m	30 days
Scenario 2: Pipeline Rupture						
Nearshore (Subsea Pipeline Rupture)	1 day	1-2 hour: 19320 bbl/day 2-24 hour: 10728 bbl/day	Full pipeline rupture	E 22° 23' 1.66" S 35° 6' 58.41"	~146m	20 days

As the stochastic analysis is a result from many sets of similar deterministic simulations, the following Table 4.3 presents the repetition of the number of deterministic simulations for each season in each

modelled year. As simulations were grouped to each season based on the first day of the simulation time, seasons 1 and 4 in 2016 contained fewer simulation as 2016 was the last year of modelling.

Table 4.3 Repetition of the deterministic simulations per season and per year

Number of simulations Per Season / Per Year	S1	S2	S3	S4
2012	21	21	21	21
2013	20	21	21	21
2014	21	21	21	21
2015	20	21	21	21
2016	14	21	21	11
Total	96	105	105	95

4.3 Model Limitations

As with all modelling analyses, the generated results are demonstrative interpretations of the specified scenarios and limited with respect to the various data used in establishing the applied model and the model itself. In this regard, the MIKE OS model is described in more detailed in the document, 'MIKE 21 & MIKE 3 Flow Model FM, Oil Spill Module - Short Description', in Appendix A.

5 Oil Spill Modelling Results

5.1 Results Illustration and Interpretation

The threshold levels of total hydrocarbons in the water column, associated with risk assessment of effects on fish from acute water pollution is estimated as 58 ppb (Neilson et al, 2005, as reported in OLF, 2008). Similar levels are mentioned by the OLF (Norwegian Oil Industry Association Guideline, 2008). However, the simulated mass of oil in the water column (see

Figure 5.10 and Figure 5.26) does not lead to concentrations exceeding this threshold level in the upper or lower part of the water column anywhere in the model domain. Thus, no risk maps were prepared for oil in the water column.

5.1.1 Results Metrics

The results of the statistical analysis for each of the oil spill scenario are presented as statistical maps such as:

- Surface probability of exposure to an oil slick > 5 μm [%]
- Probability of shoreline oiling larger than 10g/m² [%]
- The minimum time (from the start of a spill) to exposure to an oil slick [days]. This represents the minimum time needed for the oil to reach a specified location. The minimum time has been presented as a 95th percentile value, to avoid outliers.

It should be noted that maps of shoreline probability of exposure to an oil amount > 10g/m² are only provided for seasons where the probability is 1% or higher. The plots are not provided (i.e., as these plots are blank) for all the results that show a probability of less than 1%.

The results for the seasons S1 (December-February), S2 (March through May), S3 (June through August) S4 (September - November) together with the results for the whole year are shown in Section 5.2 and 5.2.3.

5.1.2 Key Points of Interest and Summarised Metrics

The following summarized metrics, along with maximum oil amount for key points of interest, are provided for each oil spill scenario in sections 5.2.3 and 5.3.3:

- Flow rate/amount
- Main direction of spill drift
- MAX. distance of the 90%-oil-surface-probability contour
- MAX. distance of the 1%-oil-surface-probability contour
- Offshore surface waters possibly reached by a spill
- Shoreline length that could receive oil (considering all the simulations)
- Shoreline possibly impacted
- Deterministic worst-case shoreline length impacted
- MAX. % shoreline impact probability
- MAX. oil amount onshore (tons) probability of shoreline oiling at Bird Island, De Hoop MPA, Knysna Lagoon, Klein Brak Estuary, Stilbaai Estuary, Tsitsikamma MPA, Walker Bay.

5.2 Scenario 1 – Well Blow-out - ‘Discharge 5’

The following sections present the results for stochastic and deterministic simulations for Scenario 1. The statistical maps from stochastic model result are shown in Section 5.2.1, while the deterministic results are shown in Section 5.2.2. Section 5.2.3 provides a summary with respect to the key points of interest defined in 5.1.2.

5.2.1 Stochastic Model Results

As explained in the Section 5.1.1, the results of stochastic simulations were processed into statistical maps, i.e., maps of surface oil presence probability, minimum time to oil slick exposure, and probability of shoreline oil presence (Figure 5.1 - Figure 5.9). It should be noted that, the map of shoreline oil presence probability (exposure to an oil amount $> 10\text{g/m}^2$) are not provided for Season 1, since the results from this season indicate a less than 1% probability occurrence of oiling of the shoreline. In Season 1, some oil was observed reaching the shore but the quantities were less than 10g/m^2 .

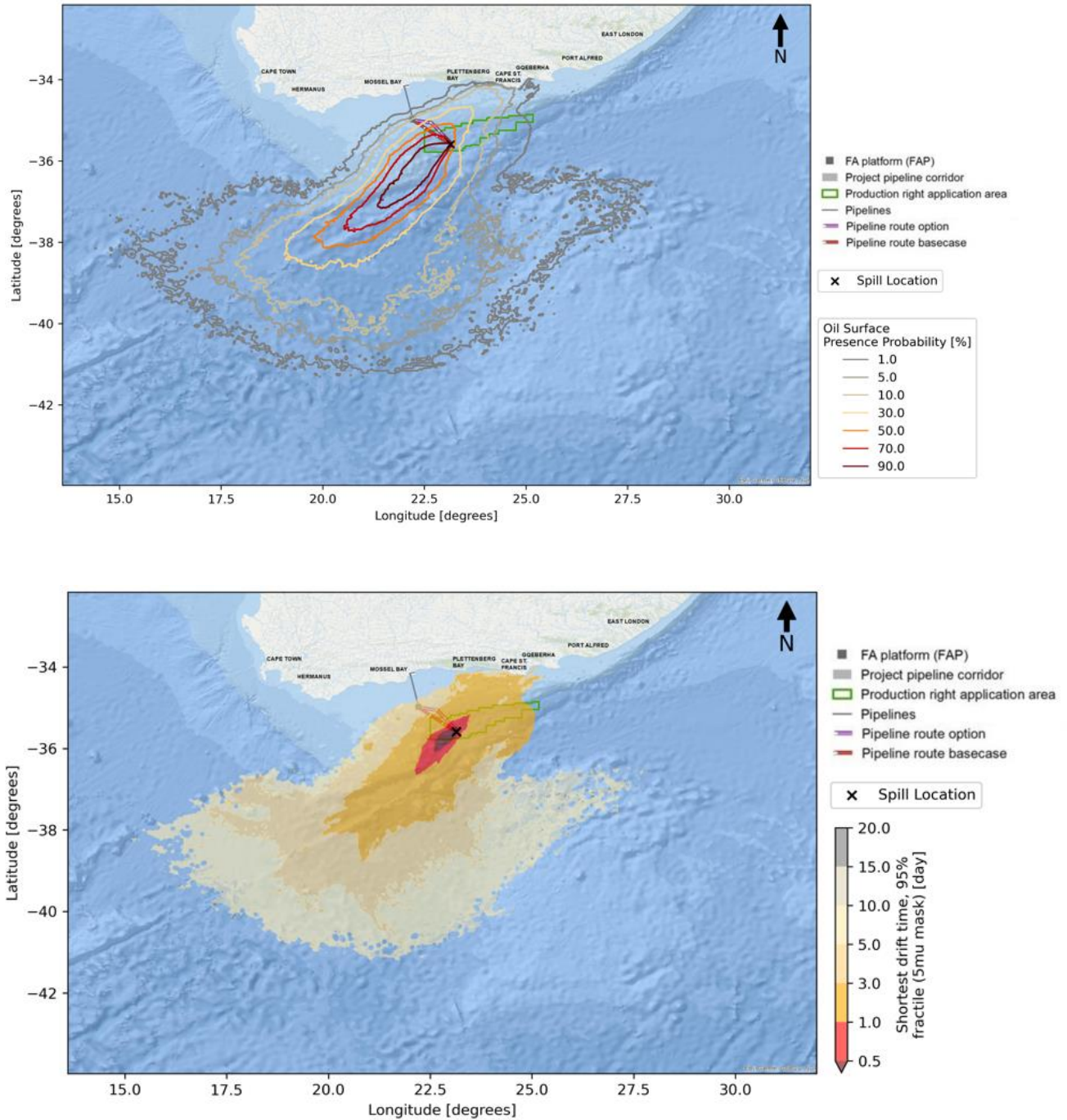


Figure 5.1 Scenario 1 model results statistics, all simulations (all seasons): Probability of surface oil presence (top) and minimum time to oil slick exposure (bottom)

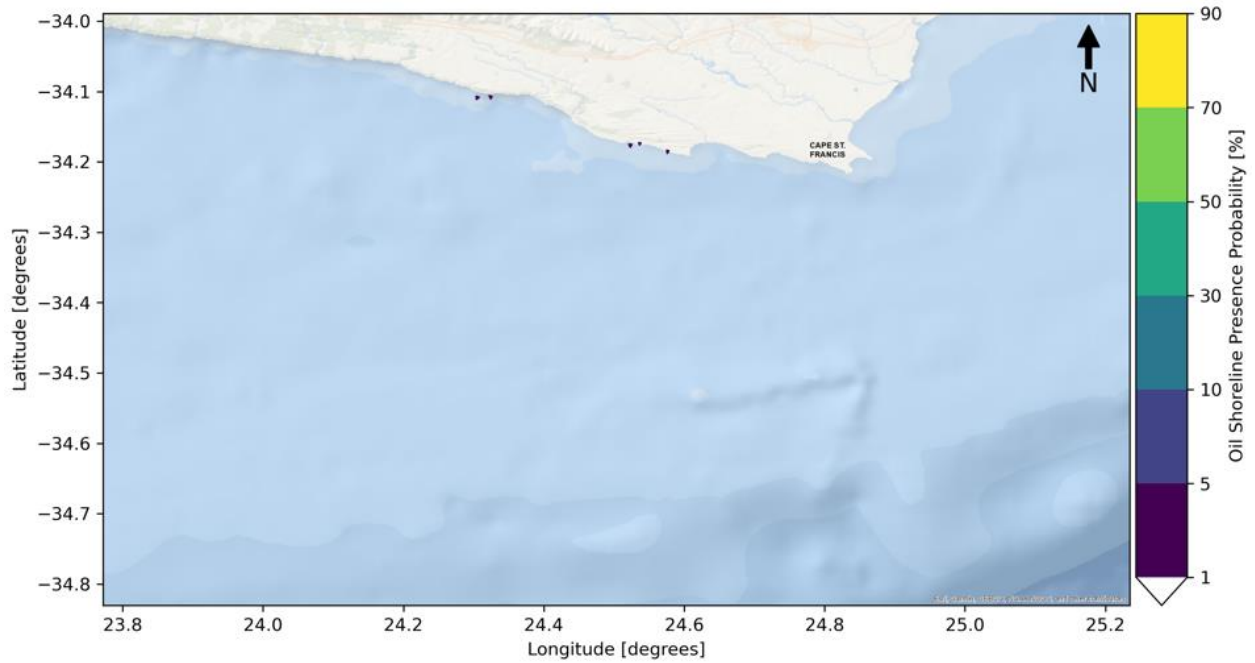


Figure 5.2 Scenario 1 model results statistics, all simulations that start in all seasons: Probability of shoreline oiling, zoomed-in on the impacted shoreline

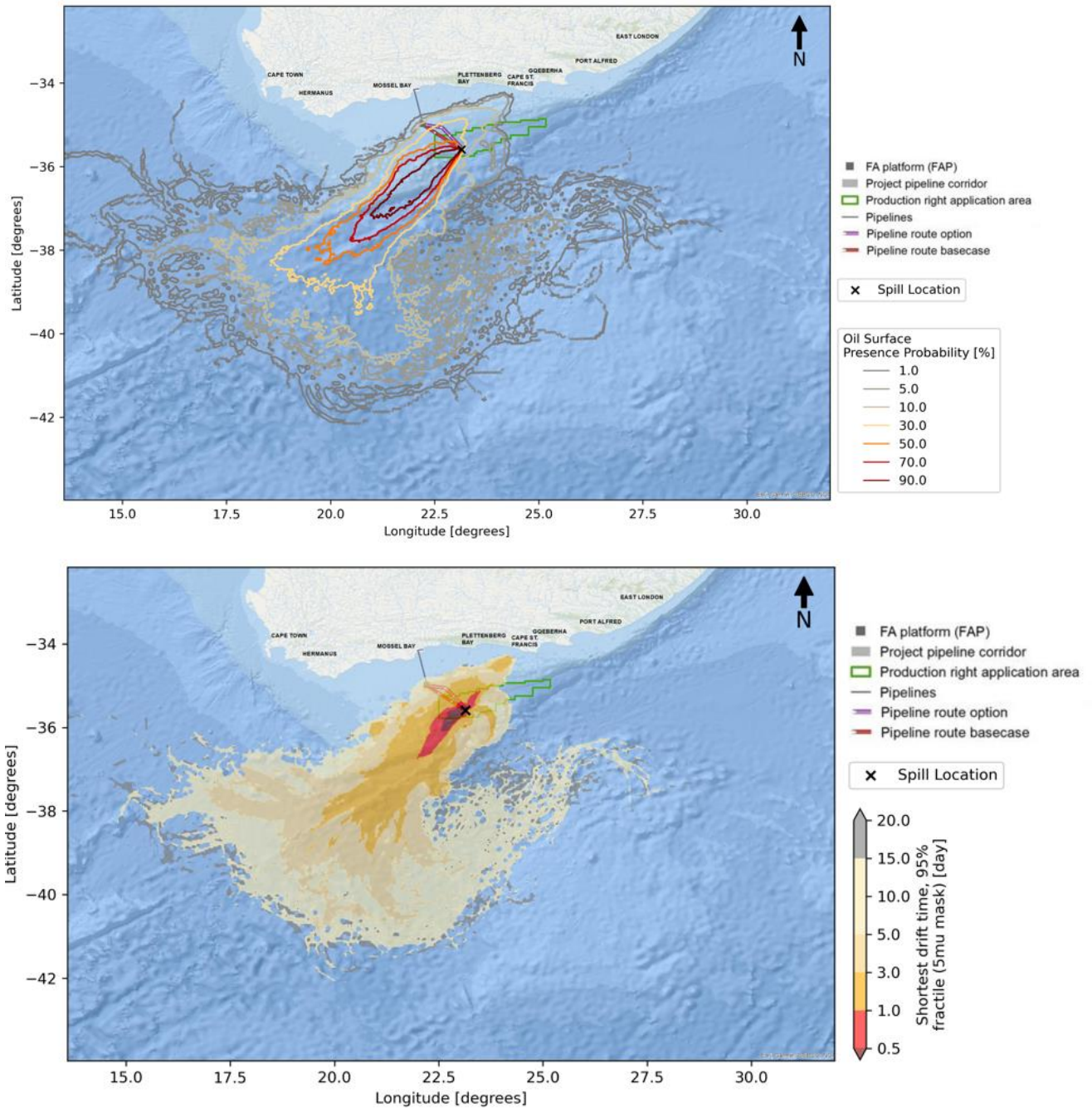


Figure 5.3 Scenario 1 model results statistics, all simulations that start in Season 1 (December-February): Probability of surface oil presence (top) and minimum time to oil slick exposure (bottom)

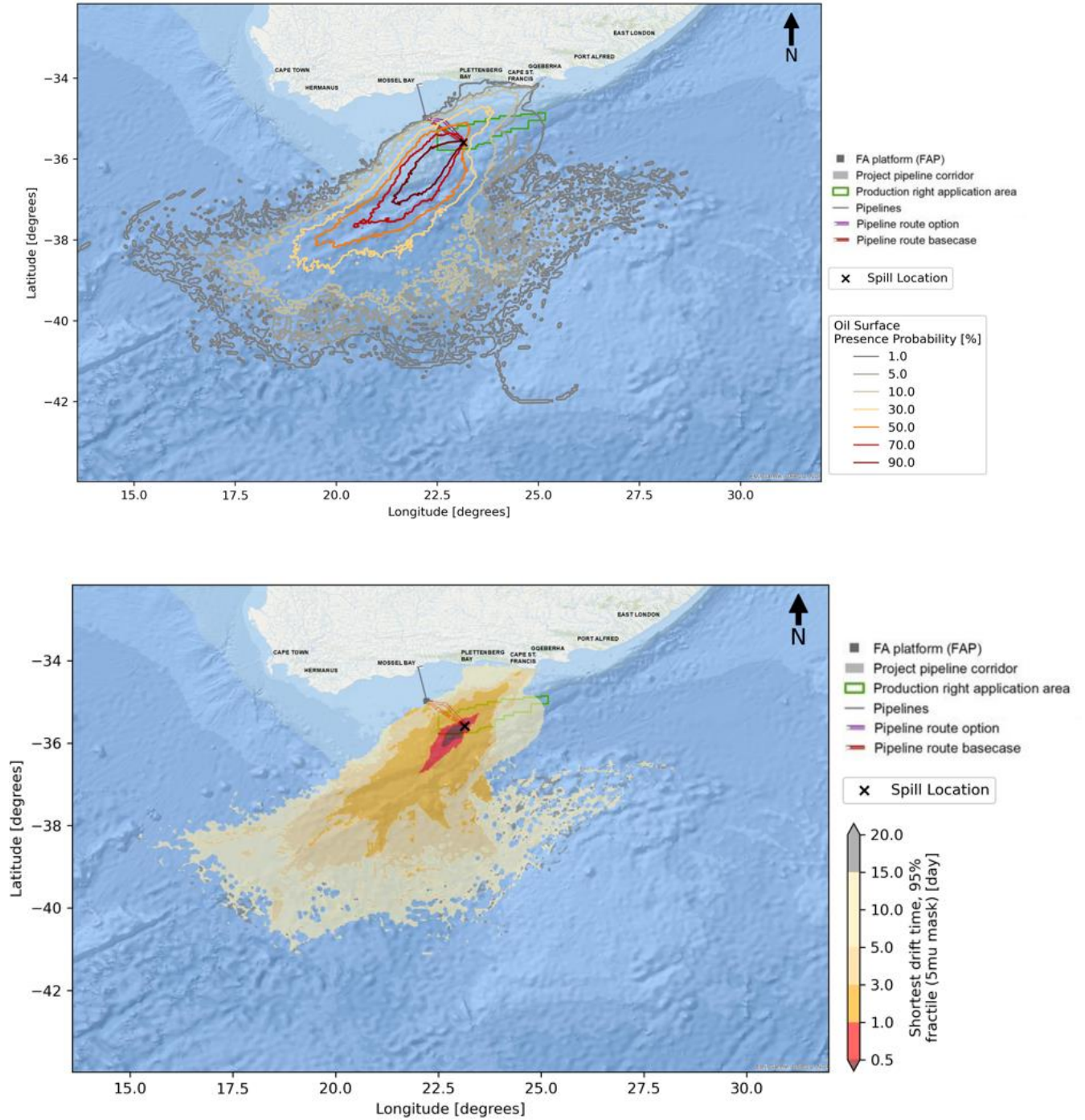


Figure 5.4 Scenario 1 model results statistics, all simulations that start in Season 2 (March - May): Probability of surface oil presence (top) and minimum time to oil slick exposure (bottom)

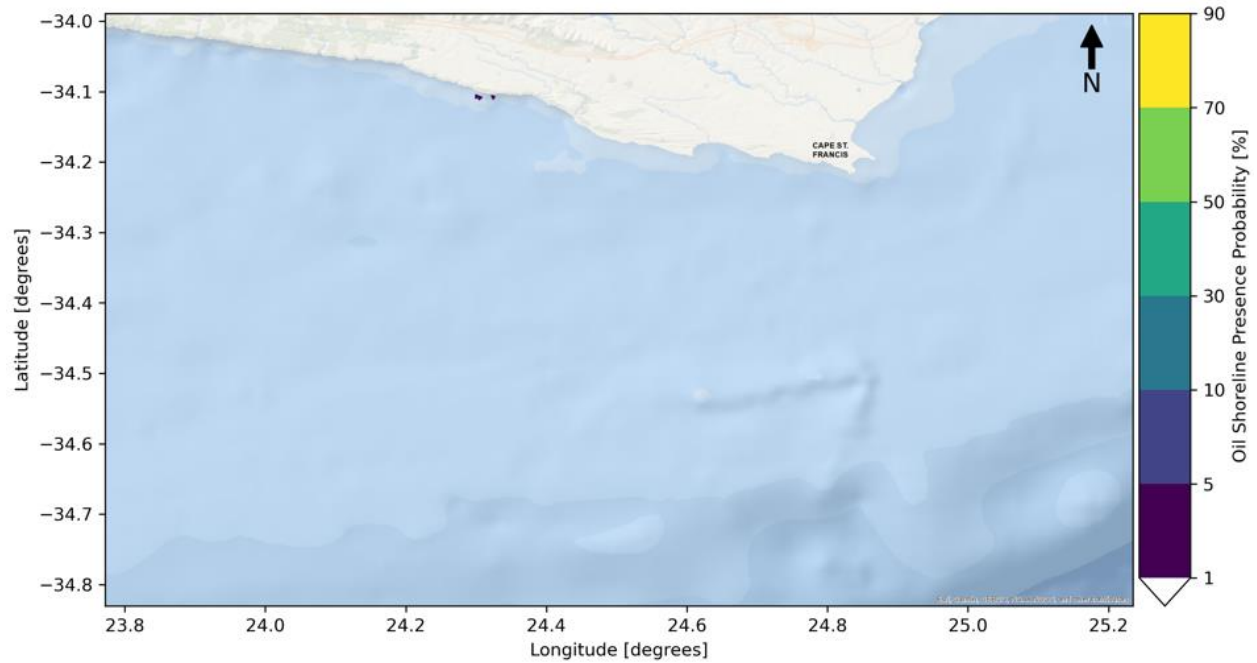


Figure 5.5 Scenario 1 model results statistics, all simulations that start in Season 2 (March - May): Probability of shoreline oiling, zoomed-in on the impacted shoreline

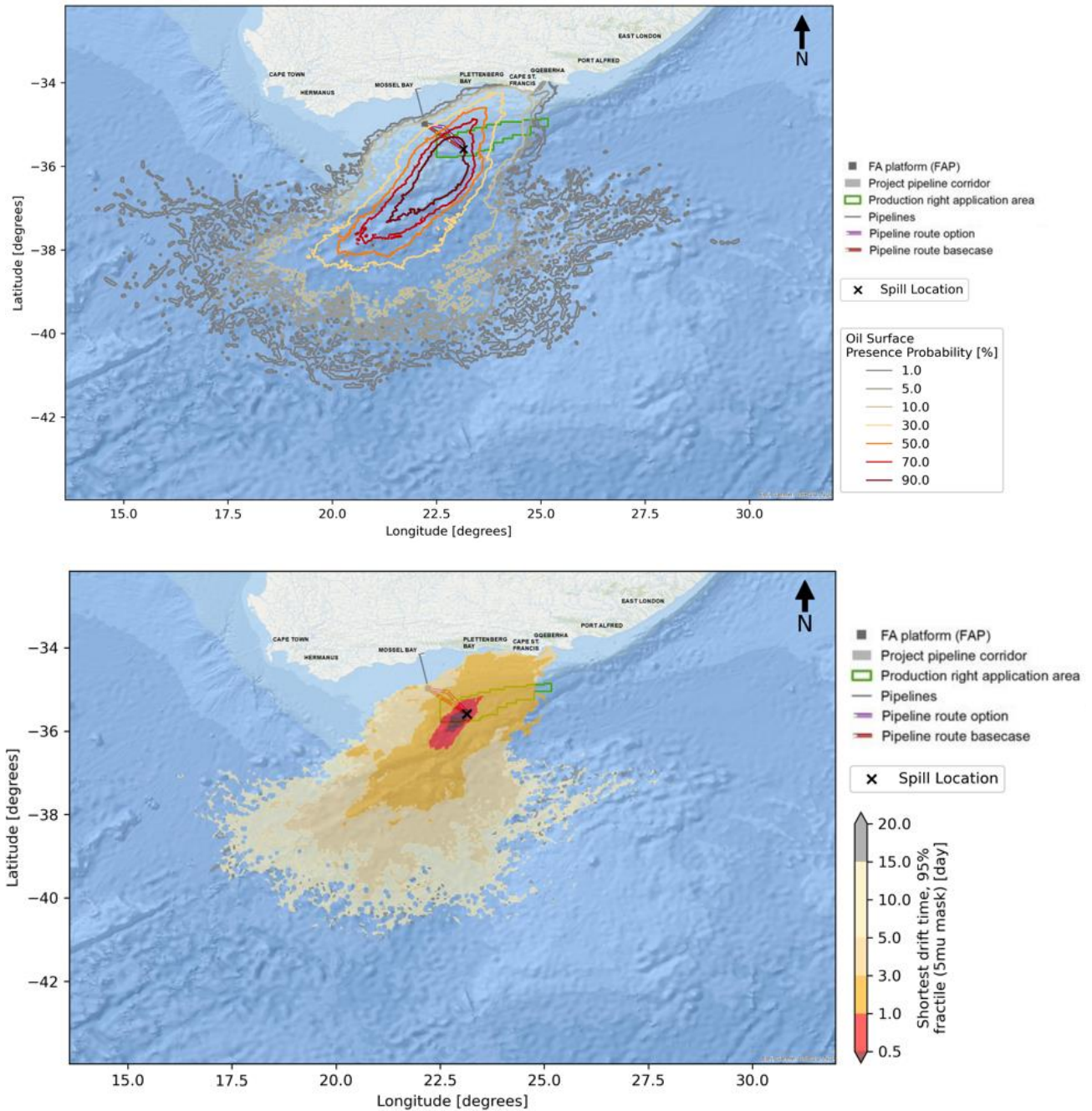


Figure 5.6 Scenario 1 model results statistics, all simulations that start in Season 3 (June - August): Probability of surface oil presence (top) and minimum time to oil slick exposure (bottom)

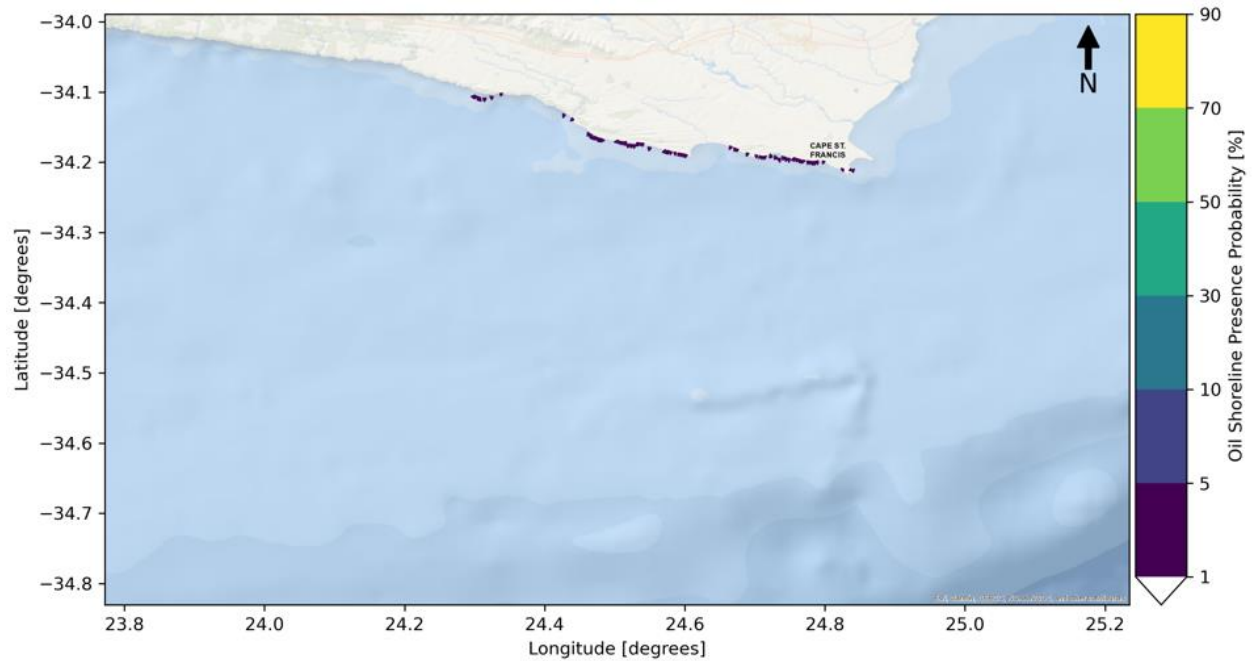


Figure 5.7 Scenario 1 model results statistics, all simulations that start in Season 3 (June - August): Probability of shoreline oiling, zoomed-in on the impacted shoreline

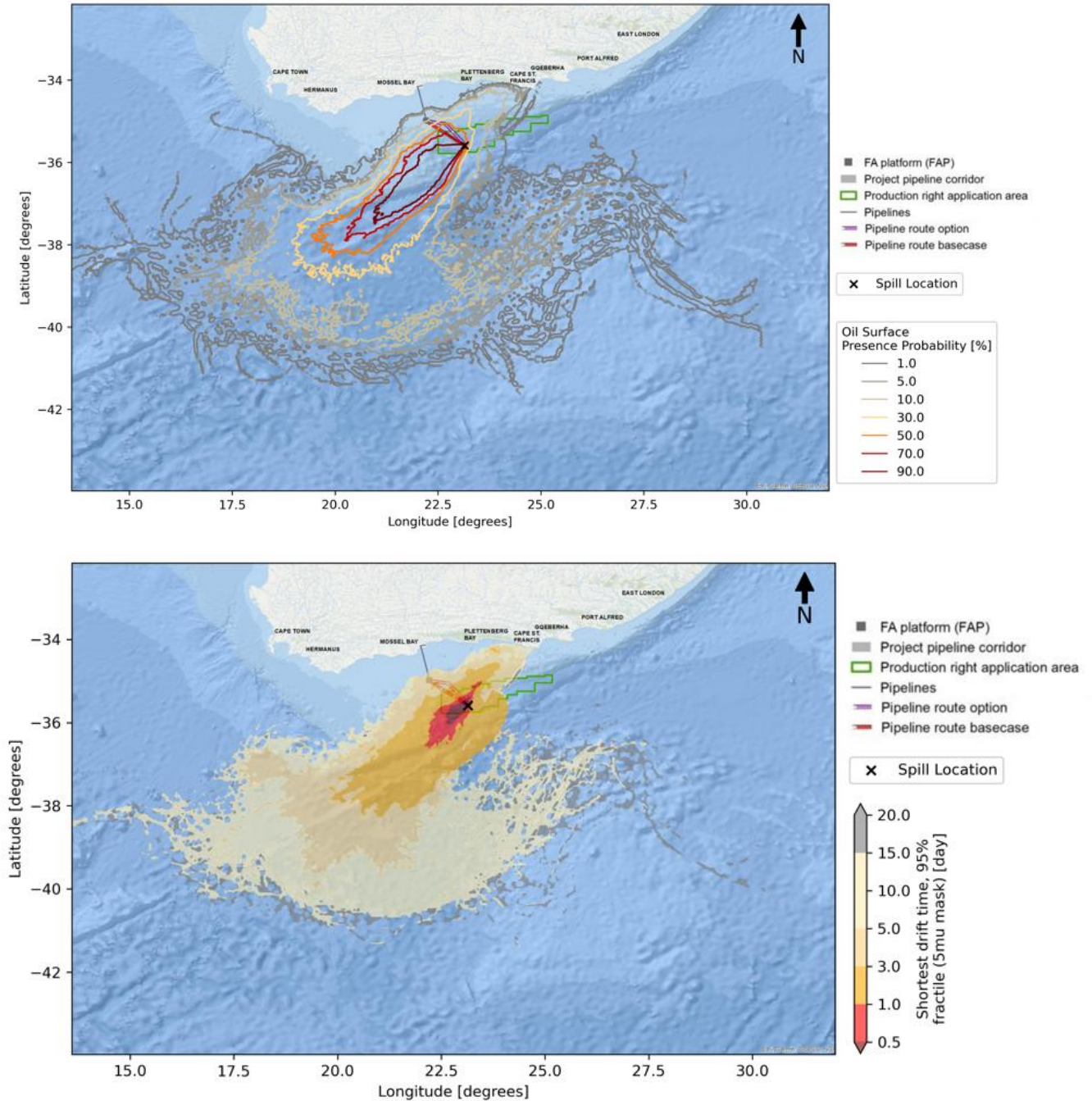


Figure 5.8 Scenario 1 model results statistics, all simulations that start in Season 4 (September - November): Probability of surface oil presence (top) and minimum time to oil slick exposure (bottom)

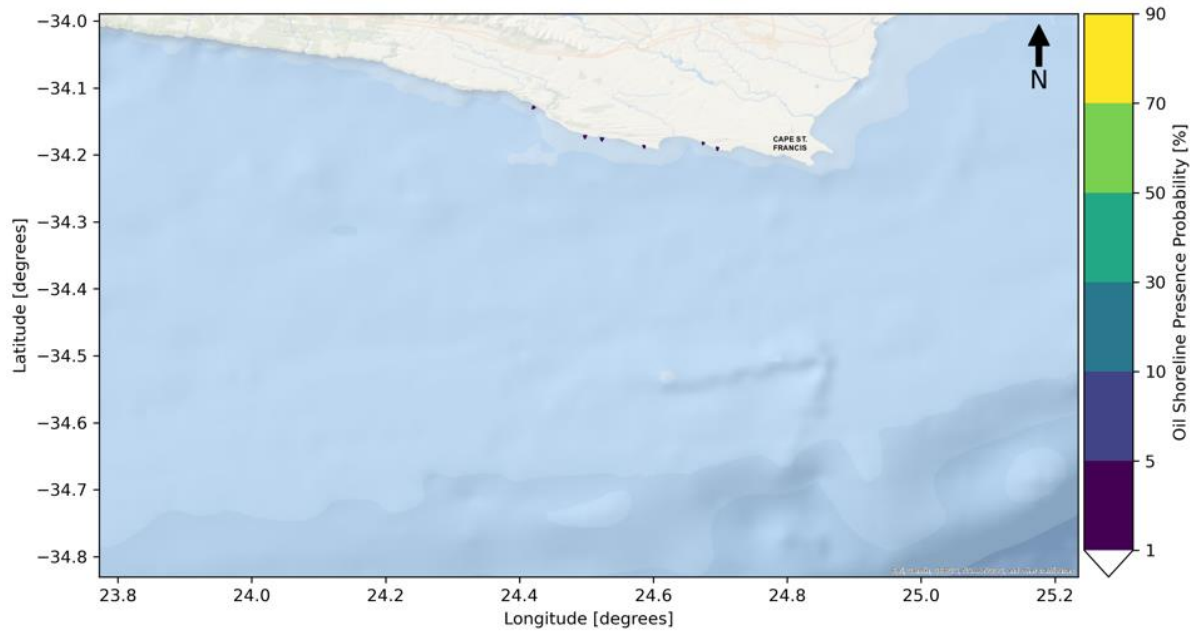


Figure 5.9 Scenario 1 model results statistics, all simulations that start in Season 4 (September - November): Probability of shoreline oiling, zoomed-in on the impacted shoreline

5.2.2 Deterministic Model Result

The worst-case simulation from stochastic simulations was re-simulated and further analysed to illustrate mass balance as well as evolution of drift. The worst-case simulations were selected from all stochastic simulation per season that produced the longest impacted shoreline. The starting date of the worst-case simulations can be seen in Table 5.1, below. From all the deterministic simulations, S3 has the longest impacted shoreline.

Table 5.1 Starting Date of Deterministic Simulations

Season	Starting Date
S1	06-02-2012
S2	26-05-2014
S3	02-08-2015
S4	28-09-2015

Figure 5.10 - Figure 5.14 illustrate the mass balance from the worst-case model results for 'all seasons' and from each season. A mass balance plot, illustrating oil from the surface slick, dispersed oil, and sedimented oil, is provided in a zoomed-out plot (i.e., consisting of all components), as well as in a zoomed-in plot (i.e., consisting of only low value components). From the 'all seasons' plots, it is apparent that evaporation is the most important weathering process for condensate, as evaporation starts immediately after LOC.

Figure 5.15- Figure 5.18 show the particle track maps by applying thin lines to illustrate drift evolution.

The condensate spill trajectories comprise the worst-case trajectories for the simulations undertaken in the various seasons. The condensate drift trajectories are shown for 1, 3, 5 and 10 days after the commencement of the spill. It should be noted that the particle track maps only show oil at the surface with slick thickness $> 5\mu\text{m}$.

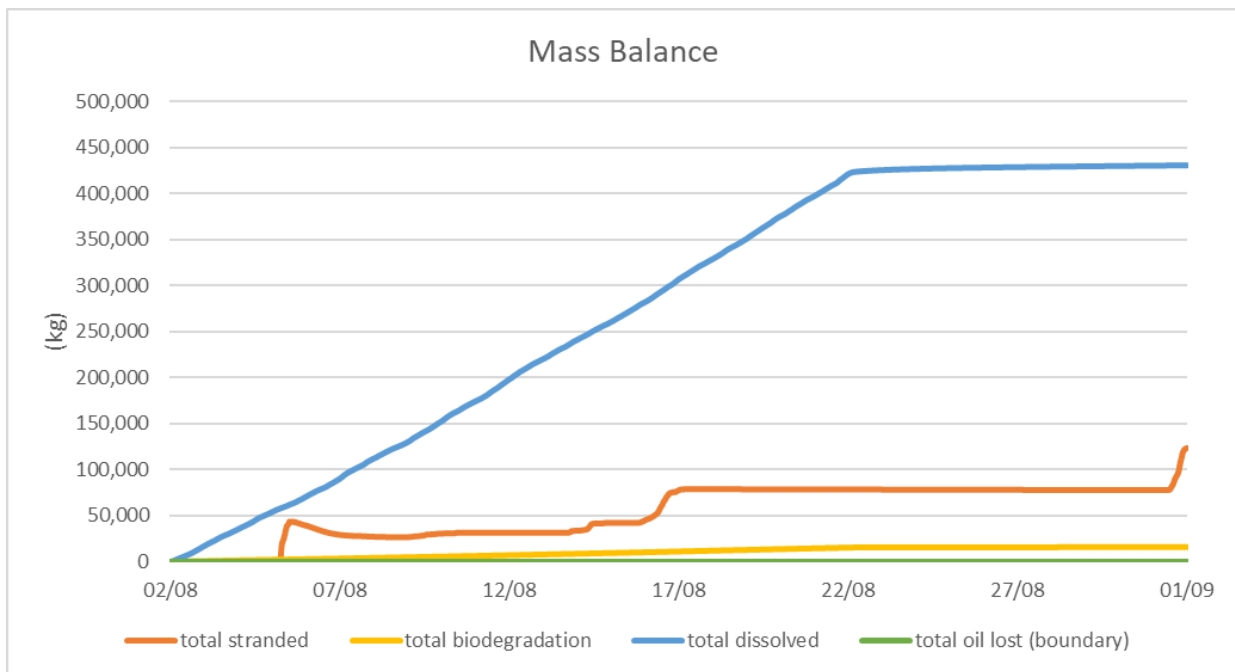
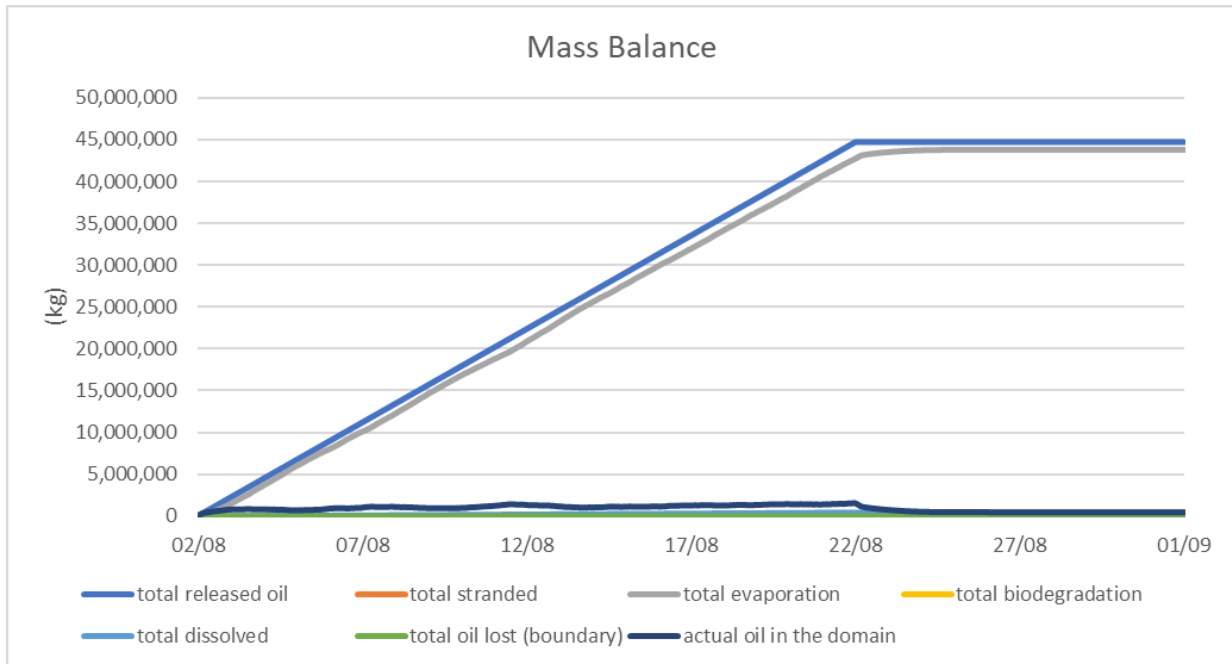


Figure 5.10 Scenario 1 model results mass balance, the worst-case from all simulations (all seasons). Top - all components; bottom - zoomed-in for low value components

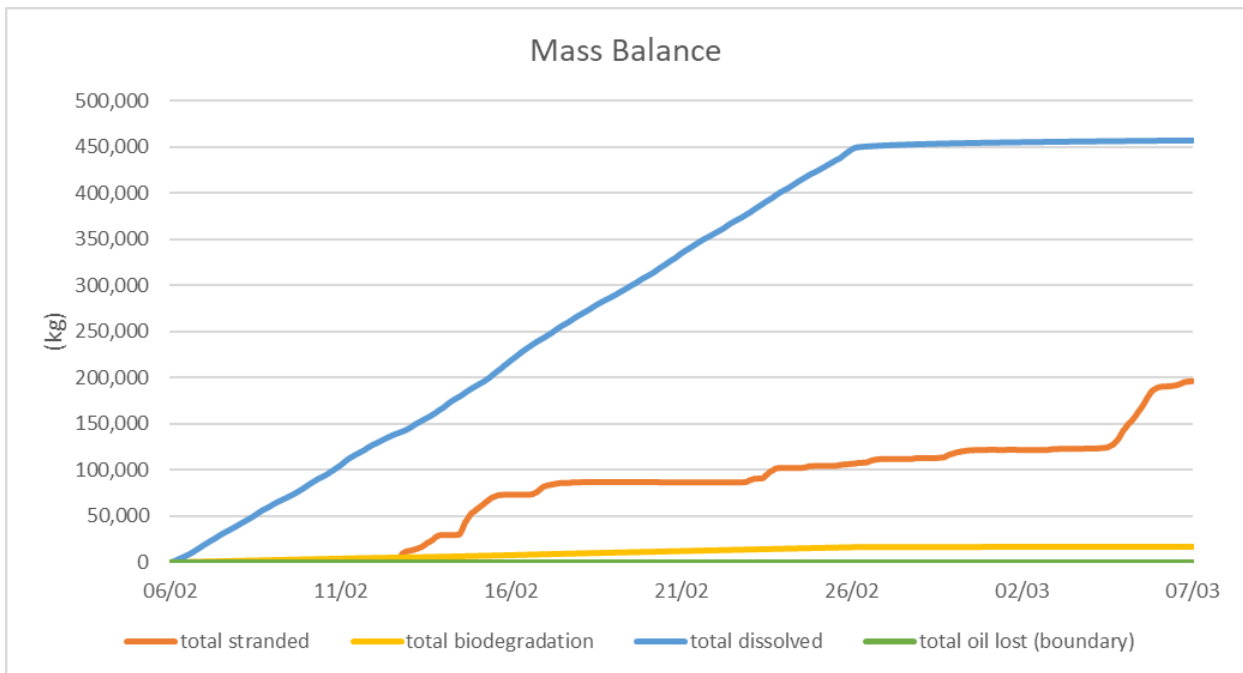
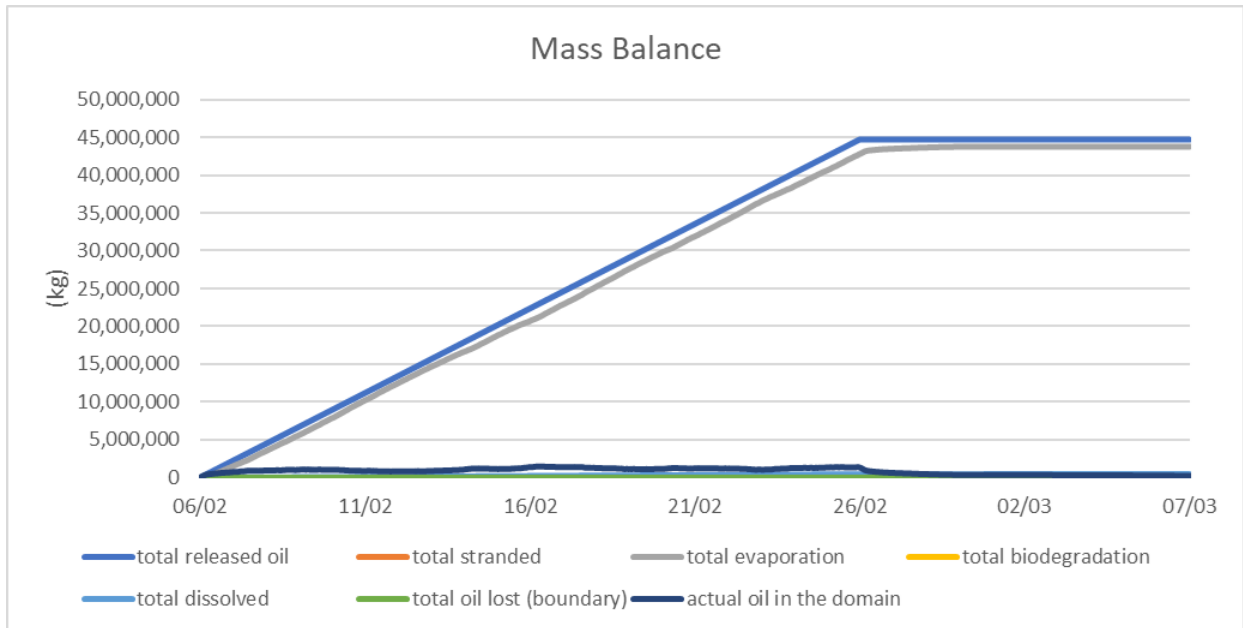


Figure 5.11 Scenario 1 model results mass balance, the worst-case from all simulations that start in Season 1 (December – February). Top - all components; bottom - zoomed-in for low value components

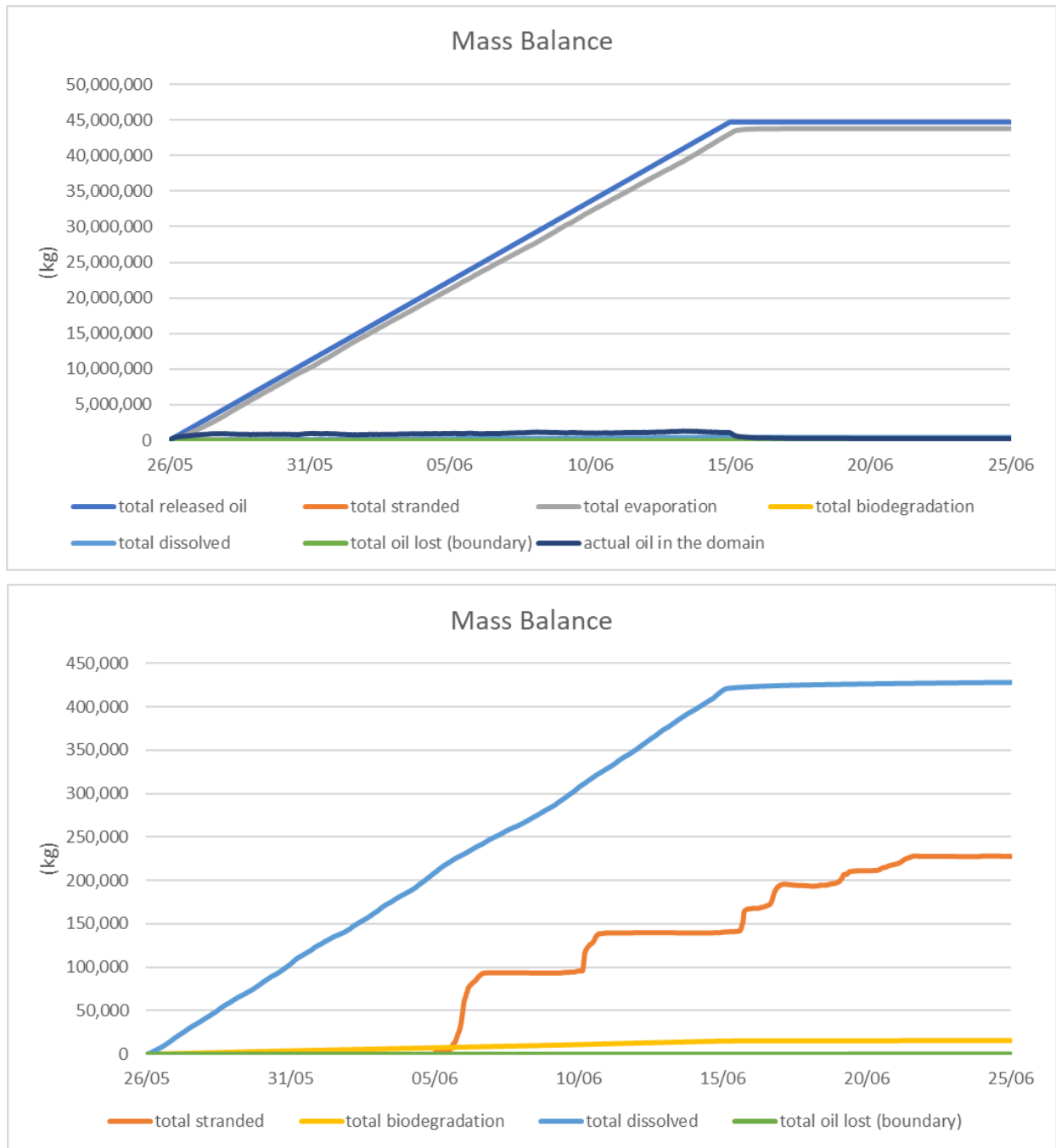


Figure 5.12 Scenario 1 model results mass balance, the worst-case from all simulations that start in Season 2 (March – May). Top - all components; bottom - zoomed-in for low value components

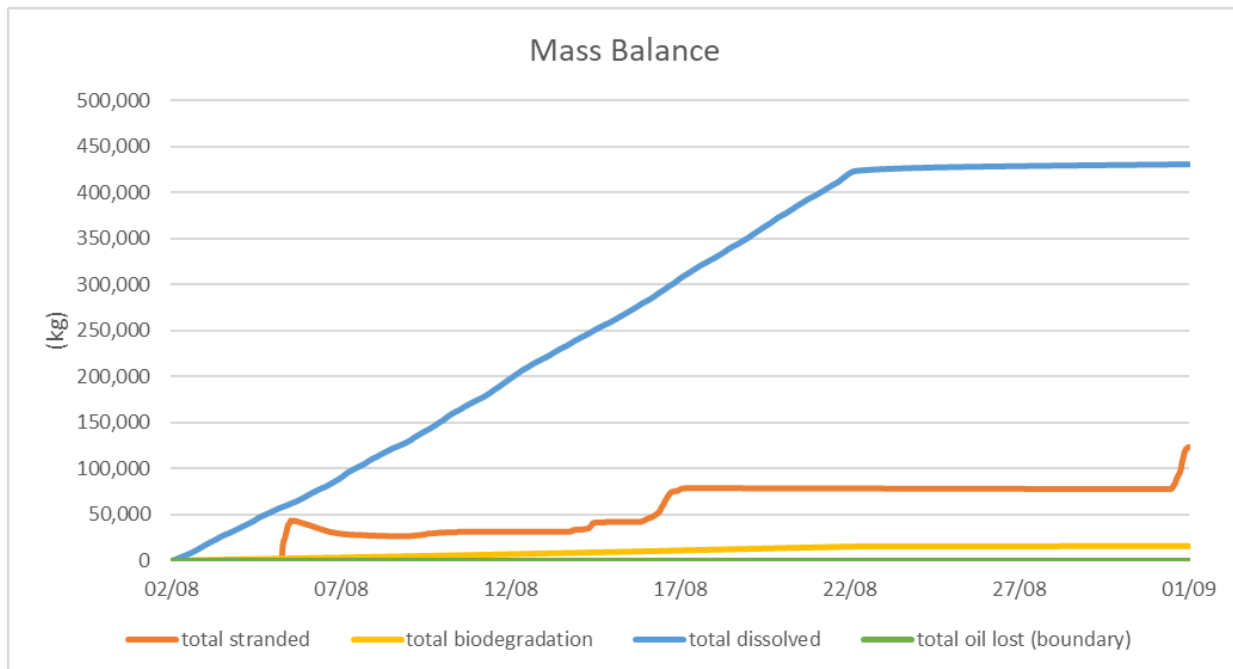
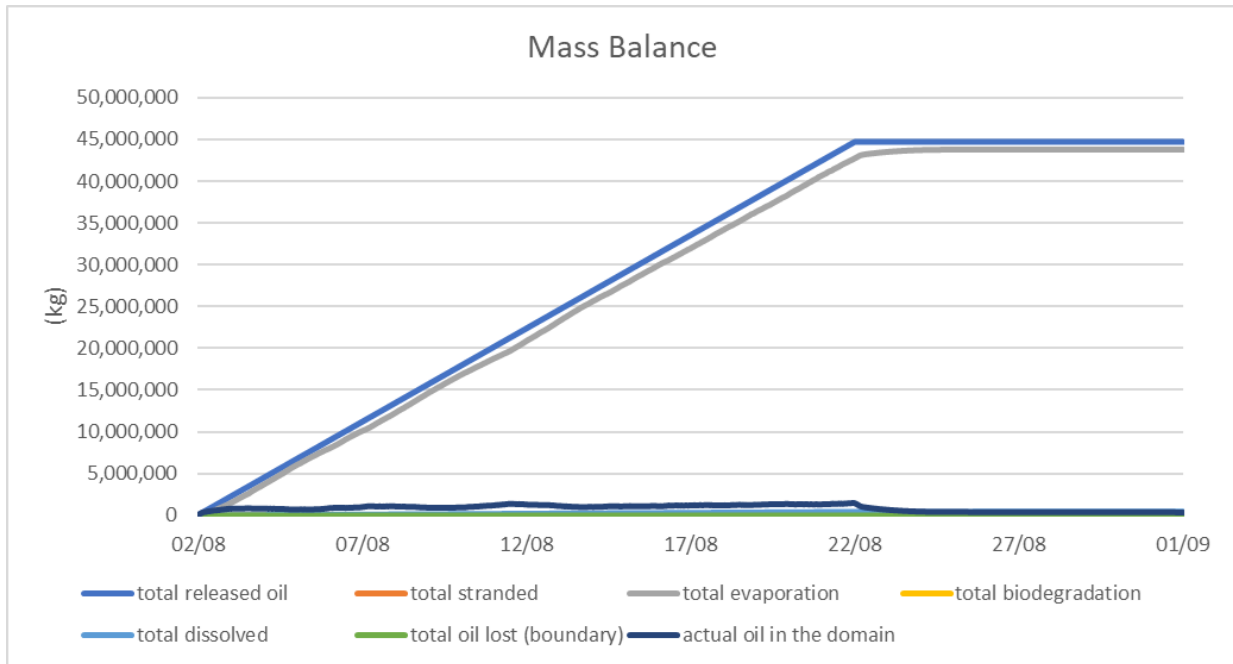


Figure 5.13 Scenario 1 model results mass balance, the worst-case from all simulations that start in Season 3 (June – August). Top - all components; bottom - zoomed-in for low value components

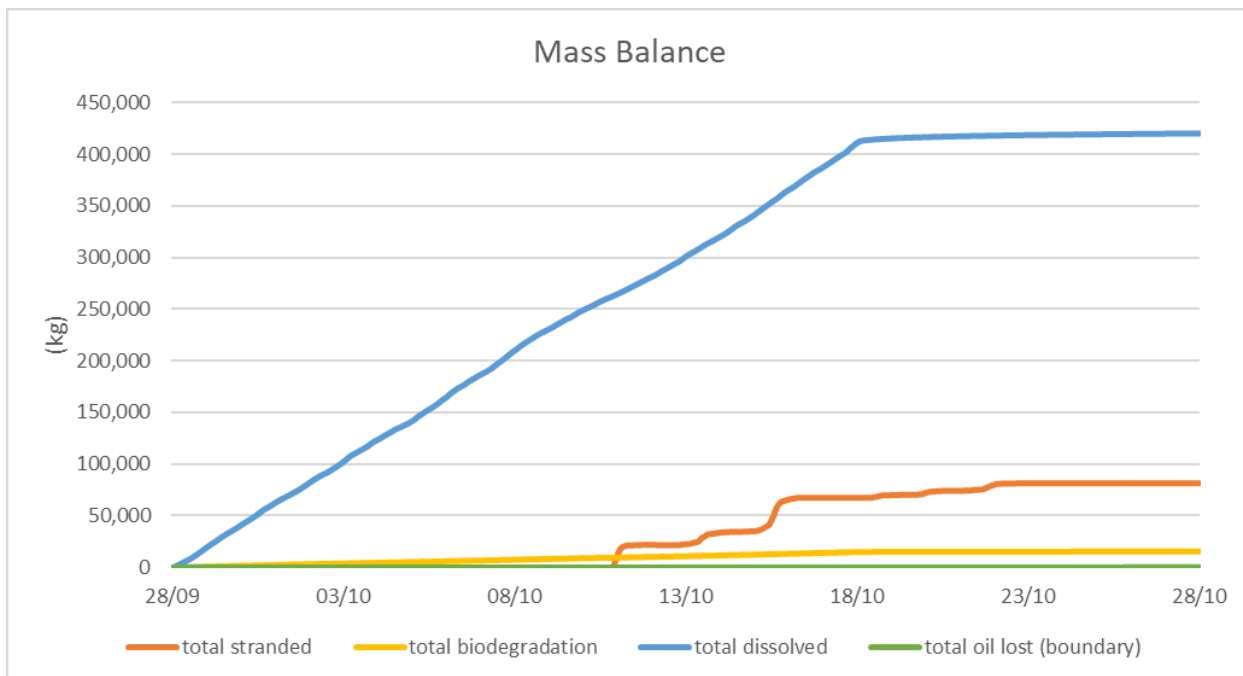
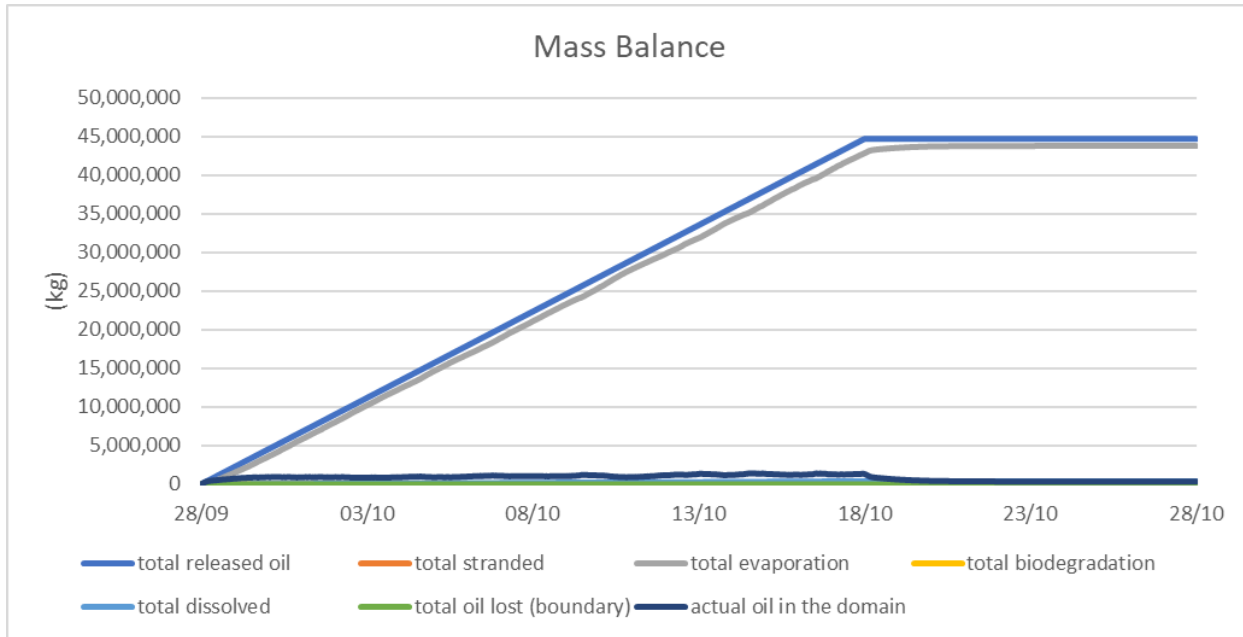


Figure 5.14 Scenario 1 model results mass balance, the worst-case from all simulations that start in Season 4 (September – November). Top - all components; bottom - zoomed-in for low value components

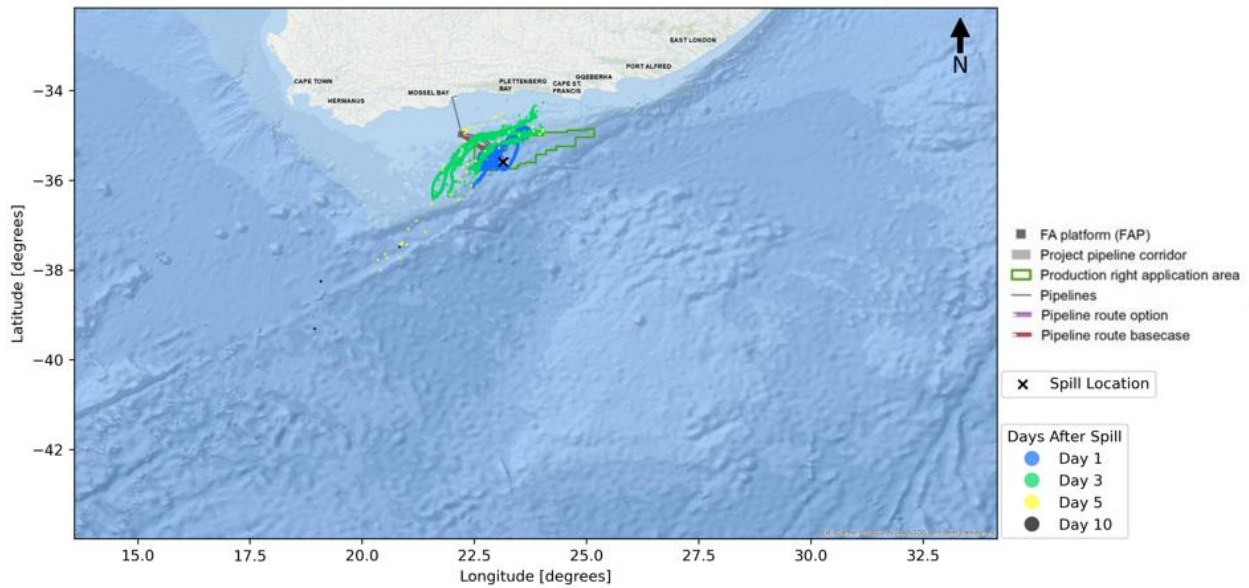


Figure 5.15 Scenario 1 model result drift evolution, the worst-case from all simulations that start in Season 1 (December – February)

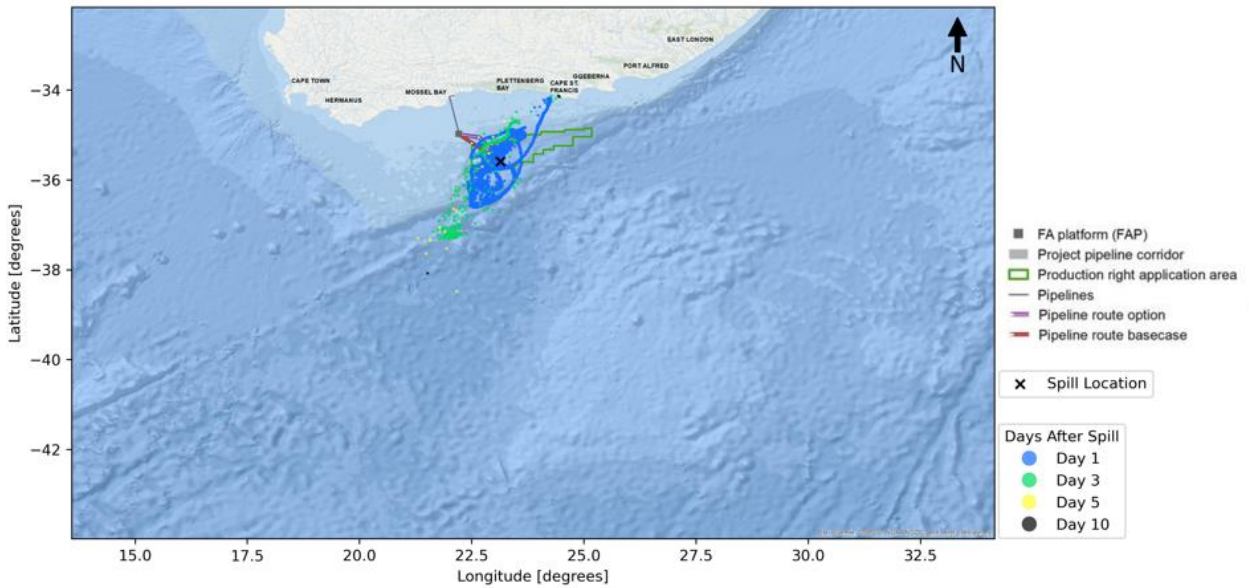


Figure 5.16 Scenario 1 model result drift evolution, the worst-case from all simulations that start in Season 2 (March – May)

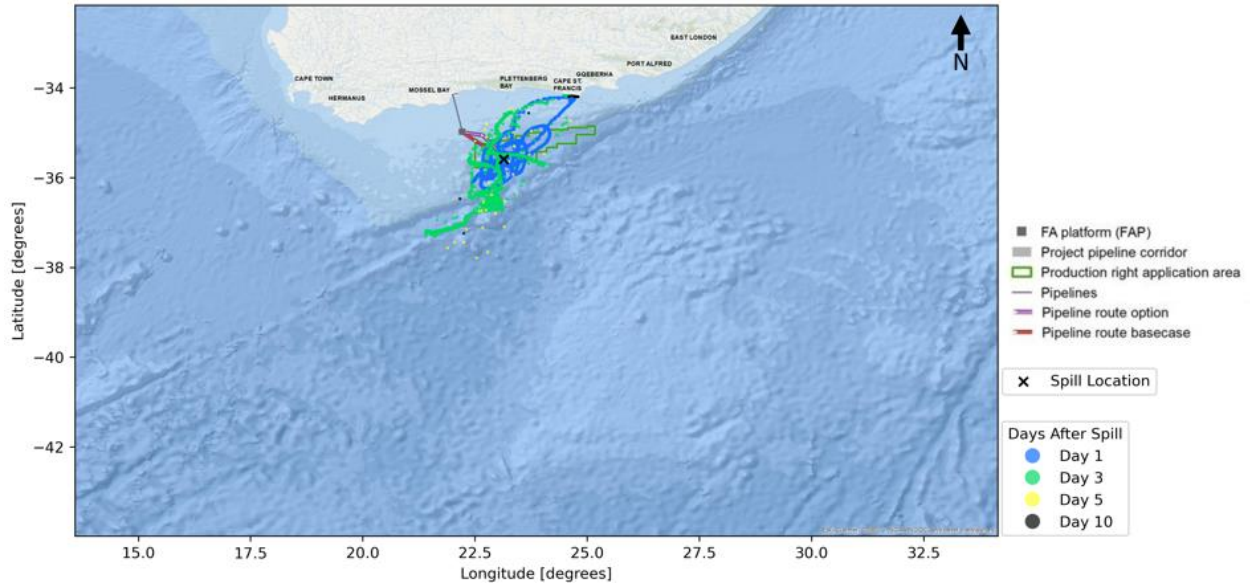


Figure 5.17 Scenario 1 model result drift evolution, the worst-case from all simulations that start in Season 3 (June – August)

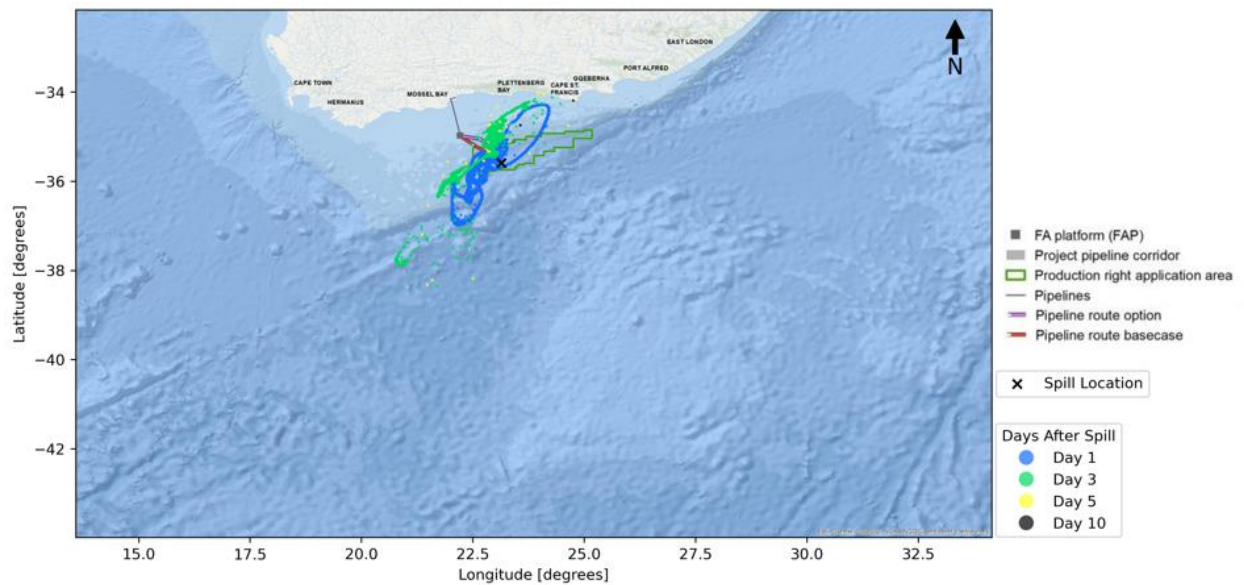


Figure 5.18 Scenario 1 model result drift evolution, the worst-case from all simulations that start in Season 4 (September – November)

5.2.3 Results Summary

The key points of interest identified for the study were Bird Island, De Hoop MPA, Knysna Lagoon, Klein Brak Estuary, Stilbaai Estuary, Tsitsikamma MPA, and Walker Bay. Results were derived for provided coordinates associated with each locale and a 500m buffer around them. Table 5.2 summarizes the model results for the affected point of interest for each of the four seasons. In all seasons, the main direction of the spill drift is southwest with the maximum distance to the 90%-oil-surface-probability contour reaching up to 230-290 km from the LOC release point.

Season 1 and Season 4 model results provide the lowest probability to oil-shoreline impact (in Season 1, shore impacted with quantities lower than 10g/m^2), whereas the highest probability occurs in Season 3. The shoreline length with oil amount $> 10\text{g/m}^2$ can reach 68 km, with impacted shoreline comprising Cape St Francis, Oyster Bay, Huisclip Nature Reserve, Thyspunt, Rebelsrus Private Nature Reserve, Wasserna's Beach. The maximum oil amount found on shore based on the worst-case scenario (deterministic simulation) is 0.9-2.8 tons (in one cell with cell area around 0.1 km^2), with the worst-case (from deterministic) shoreline length impacted is at around 0.8 – 20km. The minimum arrival time of spilled oil on shore from all stochastic simulation result is expected to be around 2-4 days.

However, in all seasons, no oil shoreline impact (based on oil $> 10\text{ g/m}^2$) is observed in focus areas such as Bird Island, De Hoop MPA, Knysna Lagoon, Klein Brak Estuary, Stilbaai Estuary, Tsitsikamma MPA, and Walker Bay.

Table 5.2 Summary of Scenario 1 Results- Well Blow-out Discharge 5

Discharge 5 (Capping stack)	All Simulations	Season 1 (Dec-Feb)	Season 2 (March-May)	Season 3 (June-Aug)	Season 4 (Sep-Nov)
Spill	Blow out – Capping Stack				
Flow Rate / Amount	Qoil: 18350 bbl/d, Qgas: 6170000 Sm ³ /d				
Main direction of the Spill Drift	Toward SW	Toward SW	Toward SW	Toward SW	Toward SW
MAX. Distance of the 90%-oil-surface-probability contour	250 km SW from release point (RP)	275 km SW from RP	230 km SW from RP	240 km SW from RP	290 km SW from RP
MAX. distance of the 1%-oil-surface-probability contour	490 km W & 850 km SW from RP	490 km W and 970 km SW from RP	490 km W and 870 km SW from RP	490 km W and 750 km SW from RP	490 km W and 970 km SW from RP
Offshore surface waters possibly reached by a spill	South African, International Waters	South African, International Waters	South African, International Waters	South African, International Waters	South African, International Waters
Shoreline length that could receive oil >10 g/m² (considering all the simulations)	68 km	0 km	4 km	64.3 km	2.5 km
Shoreline Possibly Impacted (by oil >10 g/m²)	Cape St Francis, Oyster Bay, Huisklip Nature Reserve, Thyspunt, Rebelsrus Private Nature Reserve, Wasserna's Beach	-	Huisklip Nature Reserve, Wasserna's Beach	Huisklip Nature Reserve, Thyspunt, Rebelsrus Private Nature Reserve, Wasserna's Beach	Huisklip Nature Reserve, Wasserna's Beach
Deterministic Worst-case Shoreline Length Impacted (>10g/m²)	20 km	0 km	4 km	20 km	0.8 km
MAX. % Shoreline Impact Probability (>10g/m²)	1.3%	0%	1.9%	4.8%	1.1%
MAX. oil amount onshore (tons)*	2.5	0.9	2.8	2.5	1.5
Probability of Shoreline Oiling (>10 g/m²):					
Bird Island	0%	0%	0%	0%	0%
De Hoop MPA	0%	0%	0%	0%	0%
Knysna Lagoon	0%	0%	0%	0%	0%
Klein Brak Estuary	0%	0%	0%	0%	0%
Stilbaai Estuary	0%	0%	0%	0%	0%
Tsitsikamma MPA	0%	0%	0%	0%	0%
Walker Bay	0%	0%	0%	0%	0%
Minimum Shoreline Arrival Time	2-3 days	-	3-4 days	2-3 days	4 days

* The maximum oil amount onshore corresponds to the deterministic simulation part of the stochastic scenario. The maximum oil amount onshore does not have a threshold.

NOTE: Table 5.2's content is based on stochastic model, except the Worst-case Shoreline Length Impacted and MAX. oil amount onshore which were based on deterministic model.

5.3 Scenario 2 – Pipeline Rupture

The following sections present the results for stochastic and deterministic simulations for Scenario 2. The statistical maps from stochastic model result are shown in Section 5.3.1 while the deterministic results are shown in Section 5.3.2. Section 5.3.3 provide a summary with respect to key points of interest as defined in 5.1.2

5.3.1 Stochastic Model Result

As explained in the Section 5.1.1, the results of stochastic simulations was processed into statistical maps, i.e., maps of surface oil presence probability and minimum time to exposure to an oil slick (Figure 5.19 - Figure 5.25). It should be noted that, the map of shoreline oil presence probability (exposure to an oil amount $> 10\text{g/m}^2$) is only provided for Season 3 and 4, since the results from other season indicate a less than 1% probability occurrence of oiling of the shoreline.

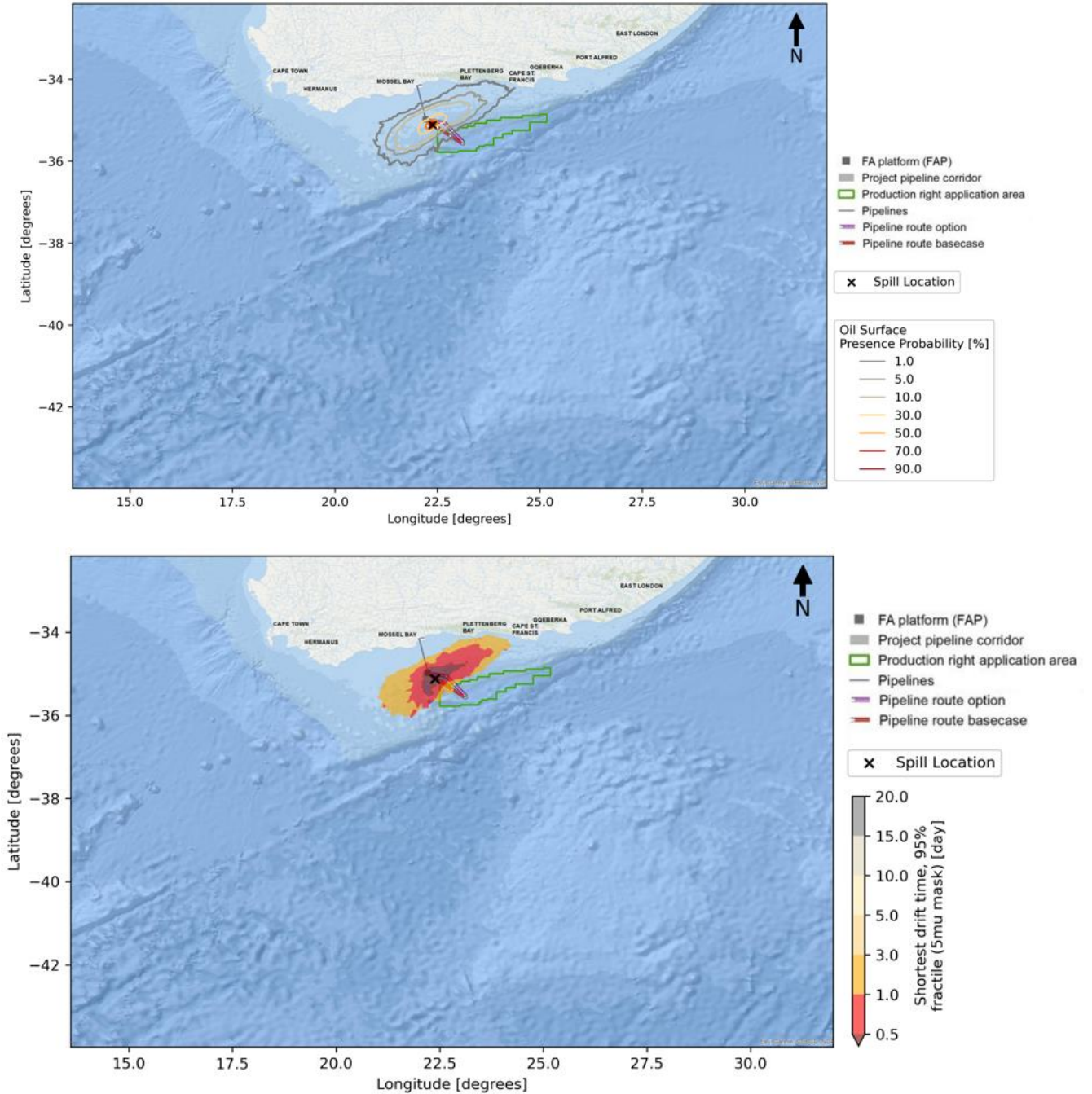


Figure 5.19 Scenario 2 model results statistics, all simulations (all seasons): Probability of surface oil presence (top) and minimum time to oil slick exposure (bottom)

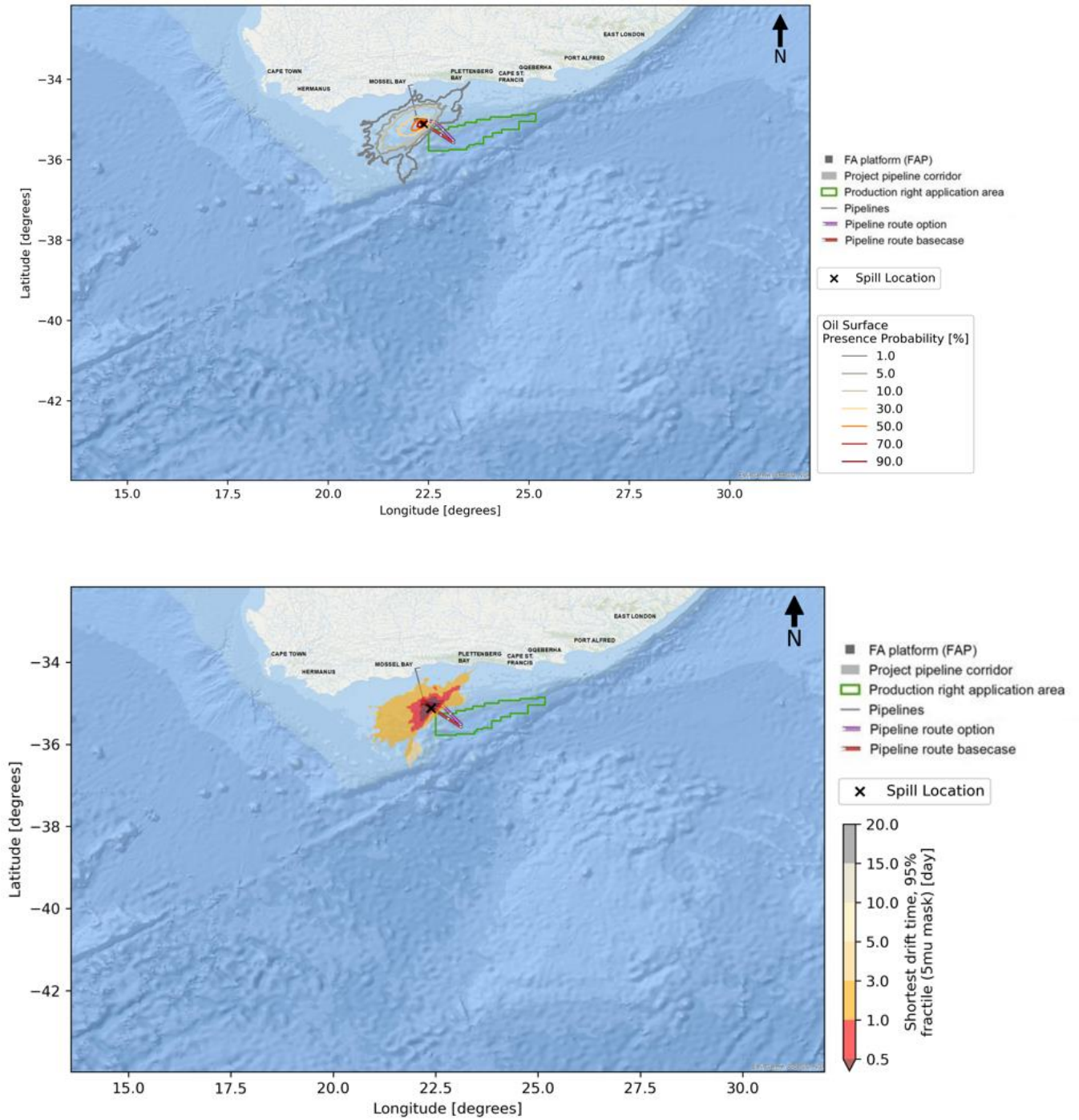


Figure 5.20 Scenario 2 model results statistics, all simulations that start in Season 1 (December-February): Probability of surface oil presence (top) and minimum time to oil slick exposure (bottom)

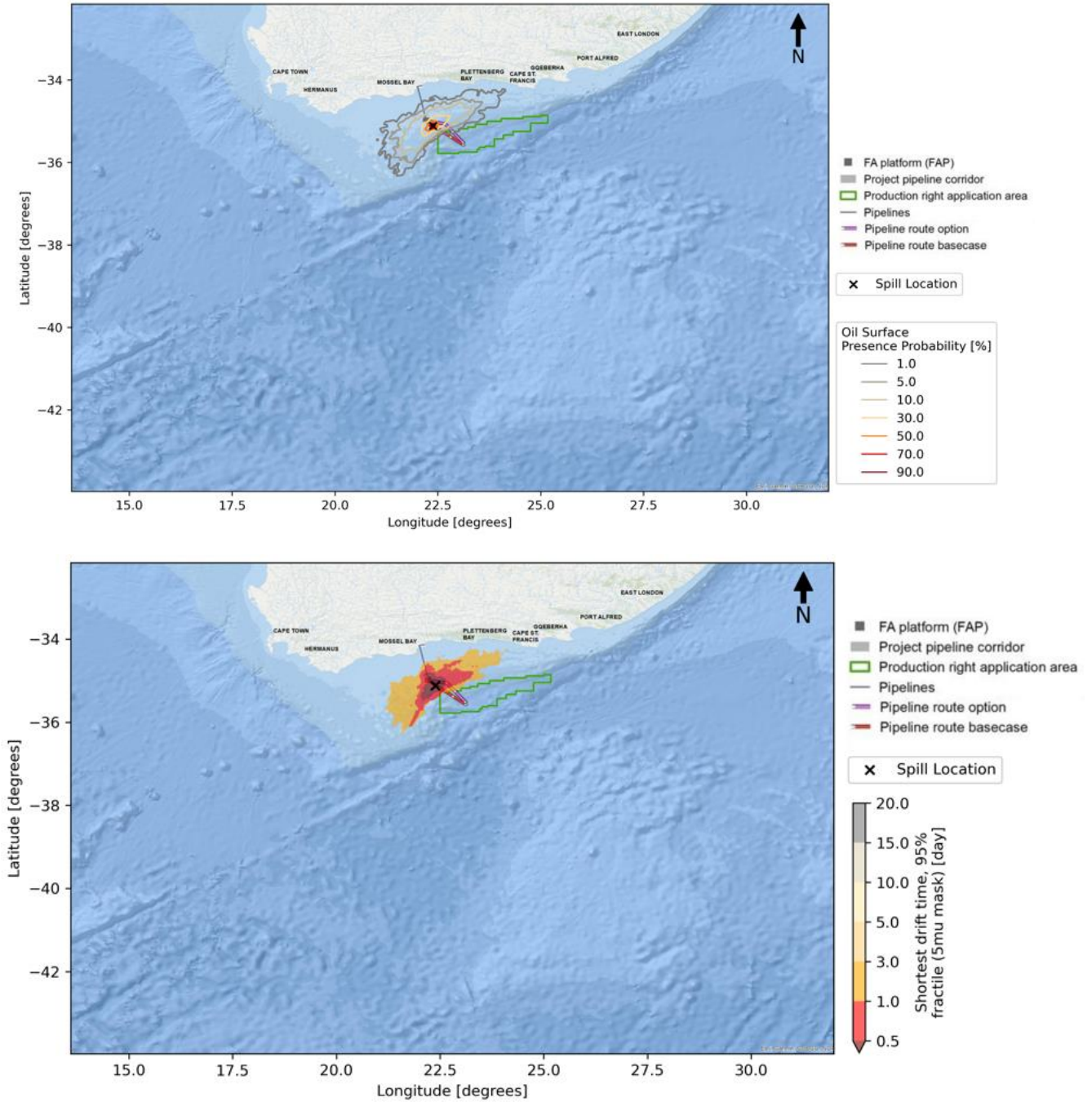


Figure 5.21 Scenario 2 model results statistics, all simulations that start in Season 2 (March - May): Probability of surface oil presence (top) and minimum time to oil slick exposure (bottom)

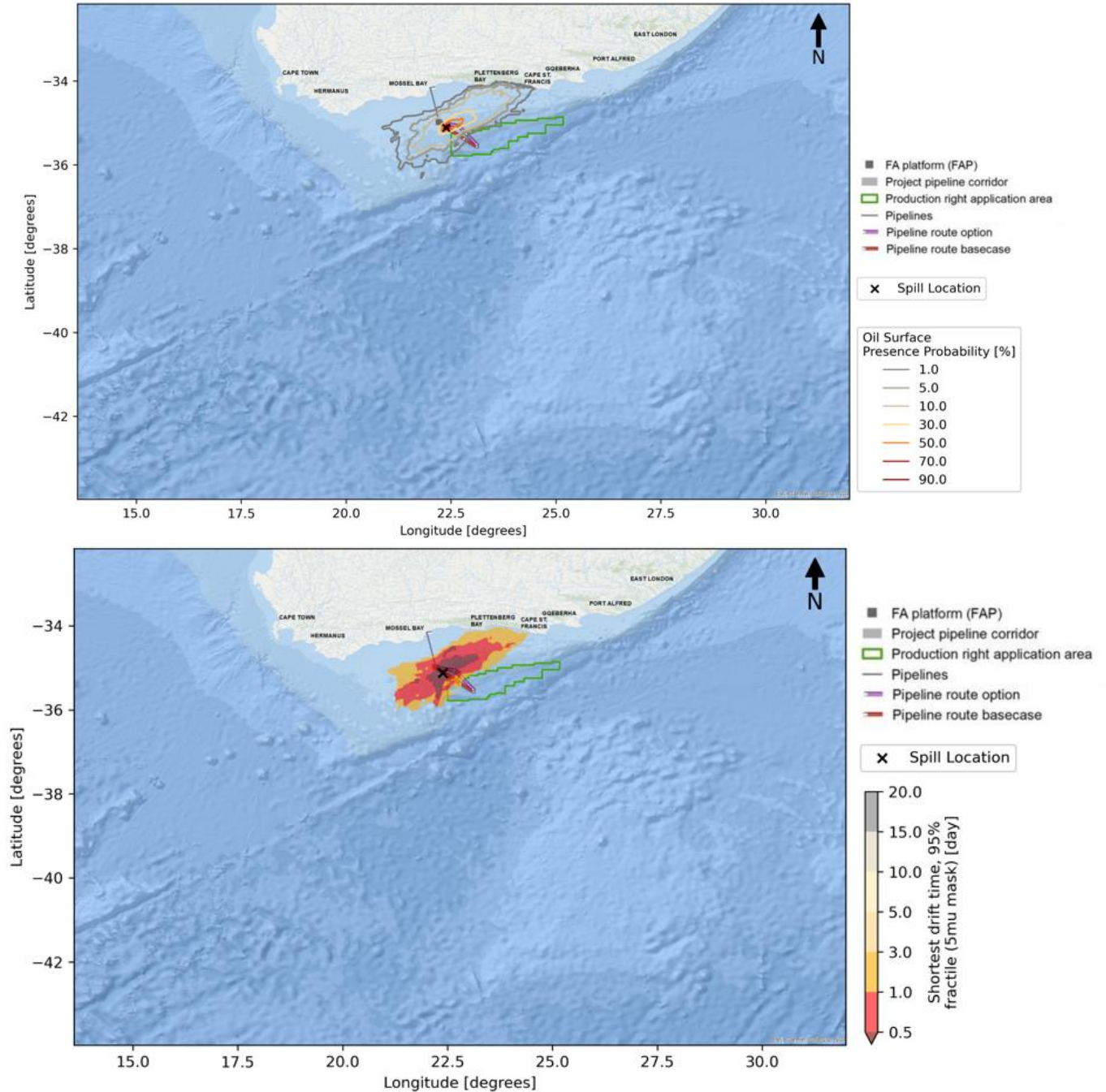


Figure 5.22 Scenario 2 model results statistics, all simulations that start in Season 3 (June - August): Probability of surface oil presence (top) and minimum time to oil slick exposure (bottom)

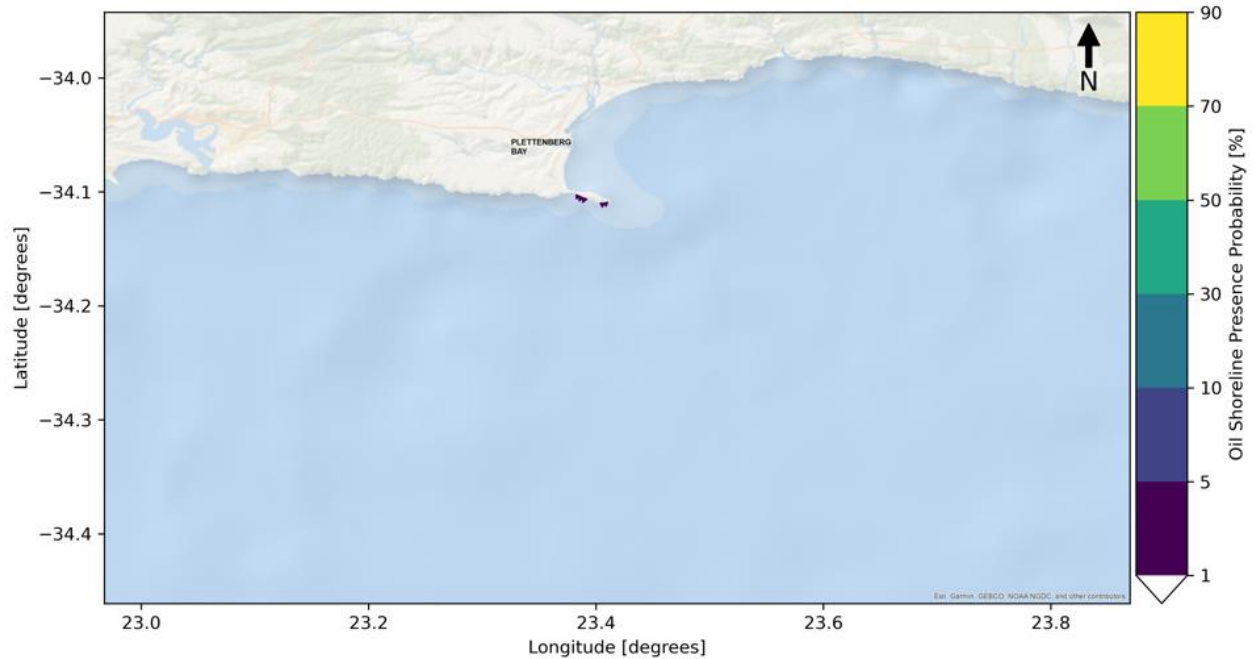


Figure 5.23 Scenario 2 model results statistics, all simulations that start in Season 3 (June - August): Shoreline oiling probability, zoomed-in on the impacted shoreline

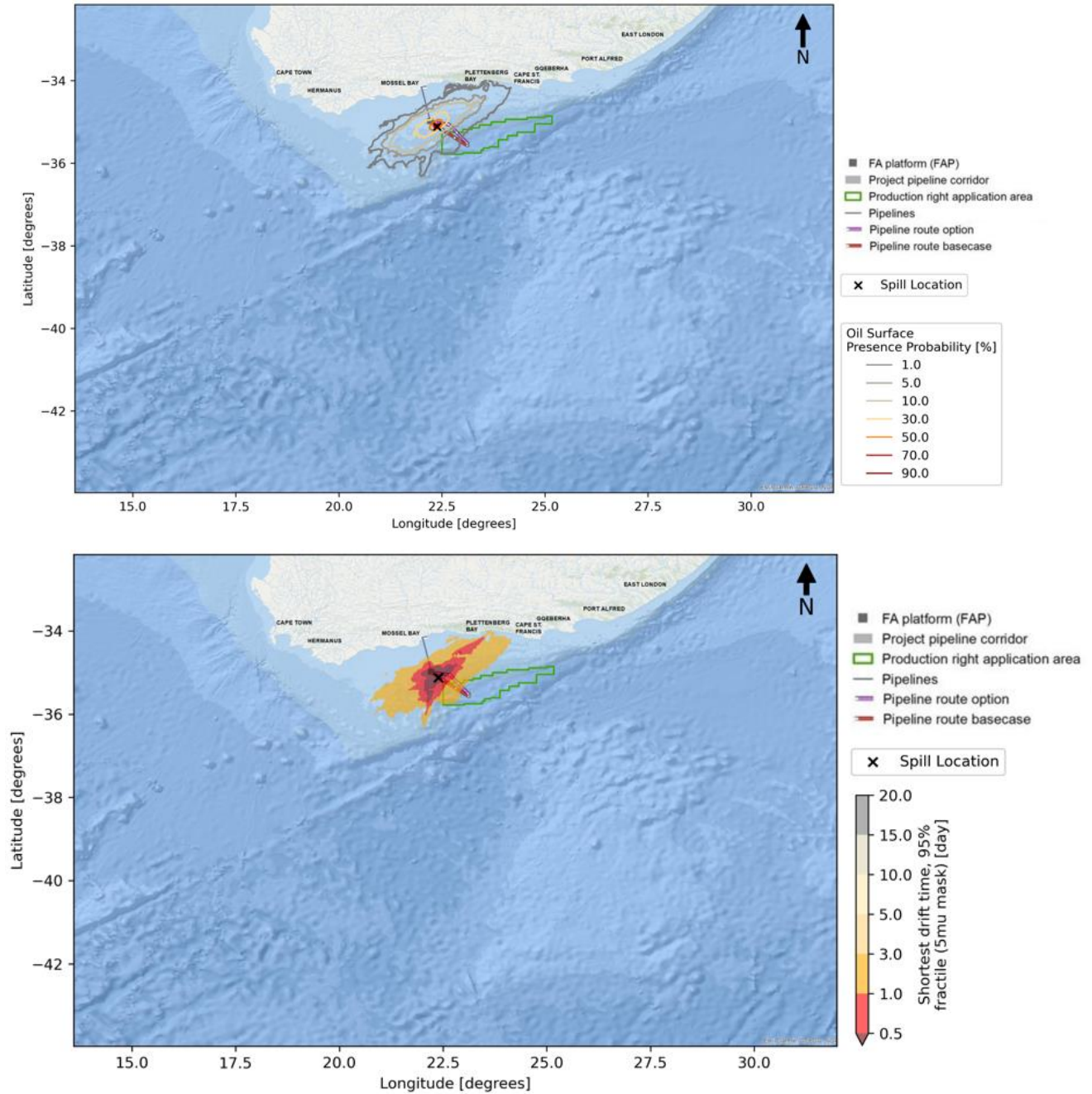


Figure 5.24 Scenario 2 model results statistics, all simulations that start in Season 4 (September - November): Probability of surface oil presence (top) and minimum time to oil slick exposure (bottom)

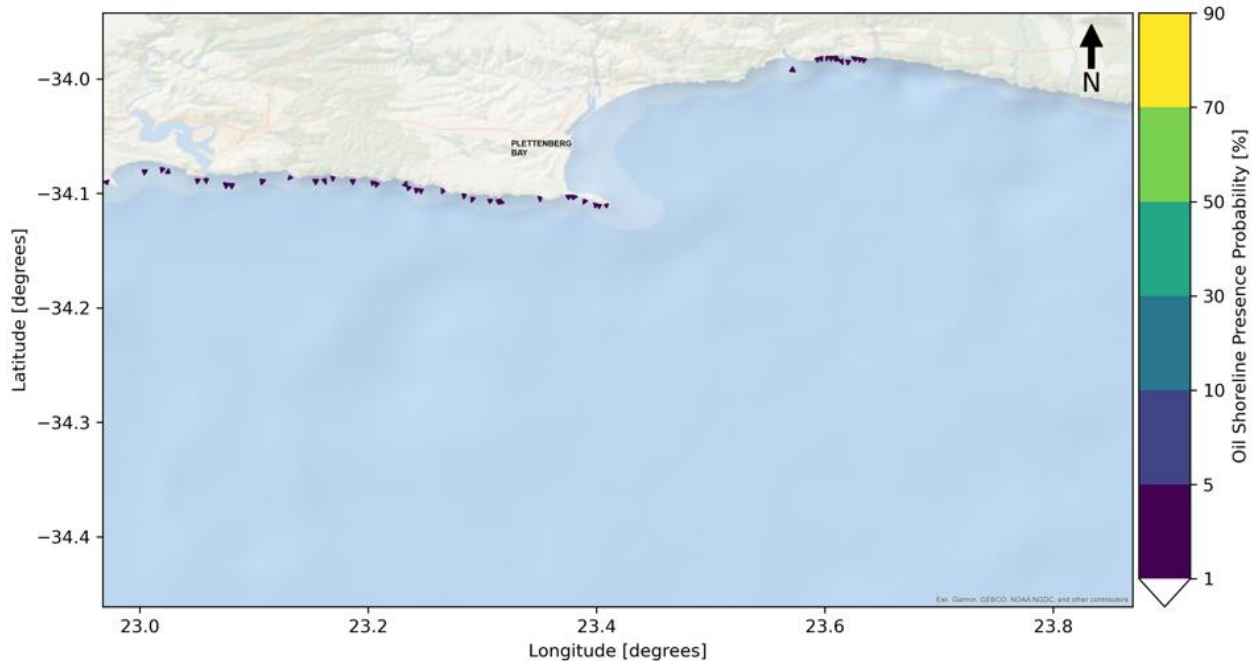


Figure 5.25 Scenario 2 model results statistics, all simulations that start in Season 4 (September - November): Shoreline oiling probability, zoomed-in on the impacted shoreline

5.3.2 Deterministic Model Result

The worst-case simulations from stochastic simulations were re-simulated and further analysed to illustrate mass balance as well as drift evolution. The worst-case was selected from those that produced the longest impacted shoreline. The worst-case simulations can be seen from Table 5.3.

Table 5.3 Starting Date of Deterministic Simulations

Season	Starting Date
S1	01-02-2012
S2	03-03-2014
S3	07-06-2012
S4	27-09-2013

Figure 5.26 - Figure 5.30 show the mass balance from the worst-case model result from 'all seasons' and from each season. The mass balance plot, illustrating oil from the surface slick, dispersed oil, and sedimented oil, is provided in a zoomed-out plot (i.e., consisting of all components), as well as a zoomed-in plot (i.e., consisting of only low value components). From 'all seasons' results, one can again conclude that the most important weathering process for condensate is evaporation. Figure 5.31 - Figure 5.35 are particle track maps that apply thin lines to show drift evolution. Light blue lines show a snapshot of the spill particle trajectory on day 1, whereas the green, yellow and black lines show the snapshot of the spill particle trajectory on days 3, 5 and 10, respectively. It should be noted that the particle track maps only show oil at the surface with slick thickness > 5 μm .

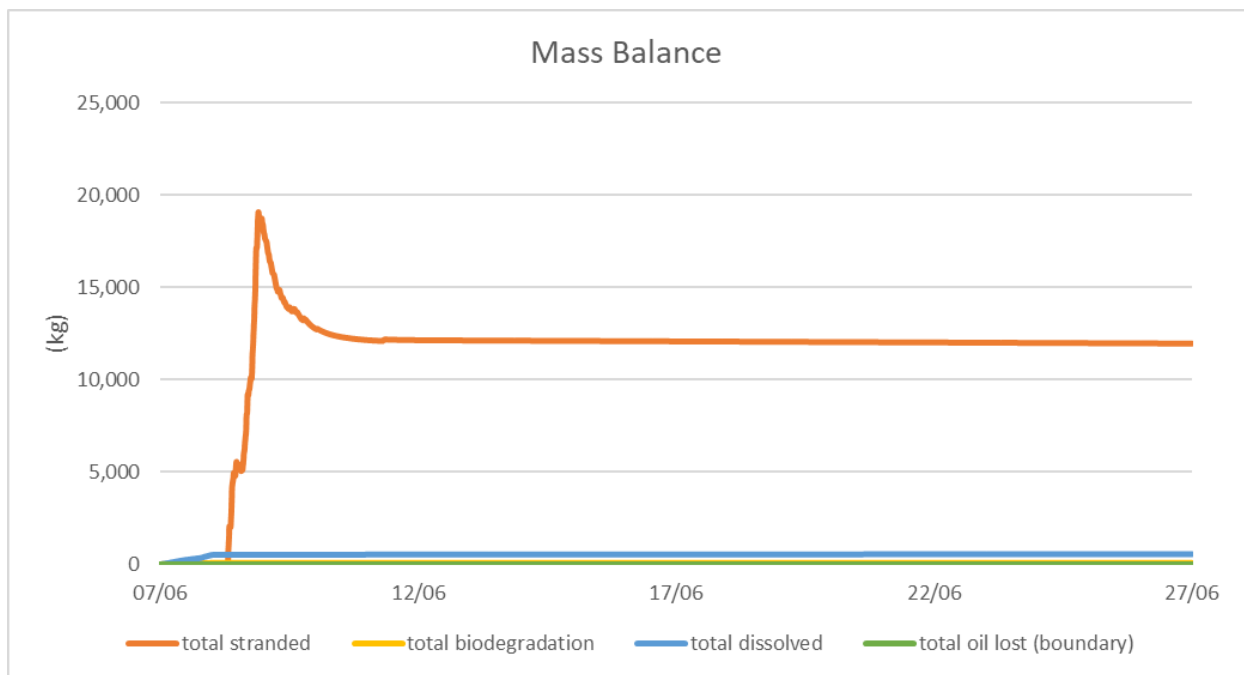
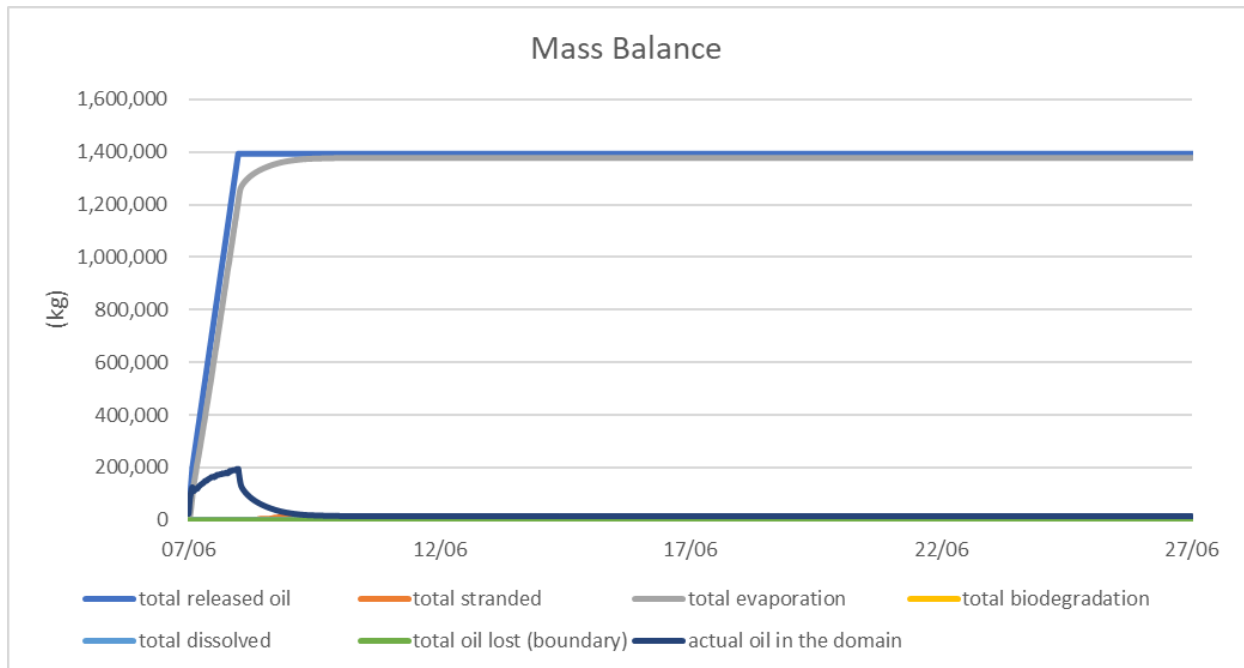


Figure 5.26 Scenario 2 model results mass balance, the worst-case from all simulations (all seasons). Top - all components

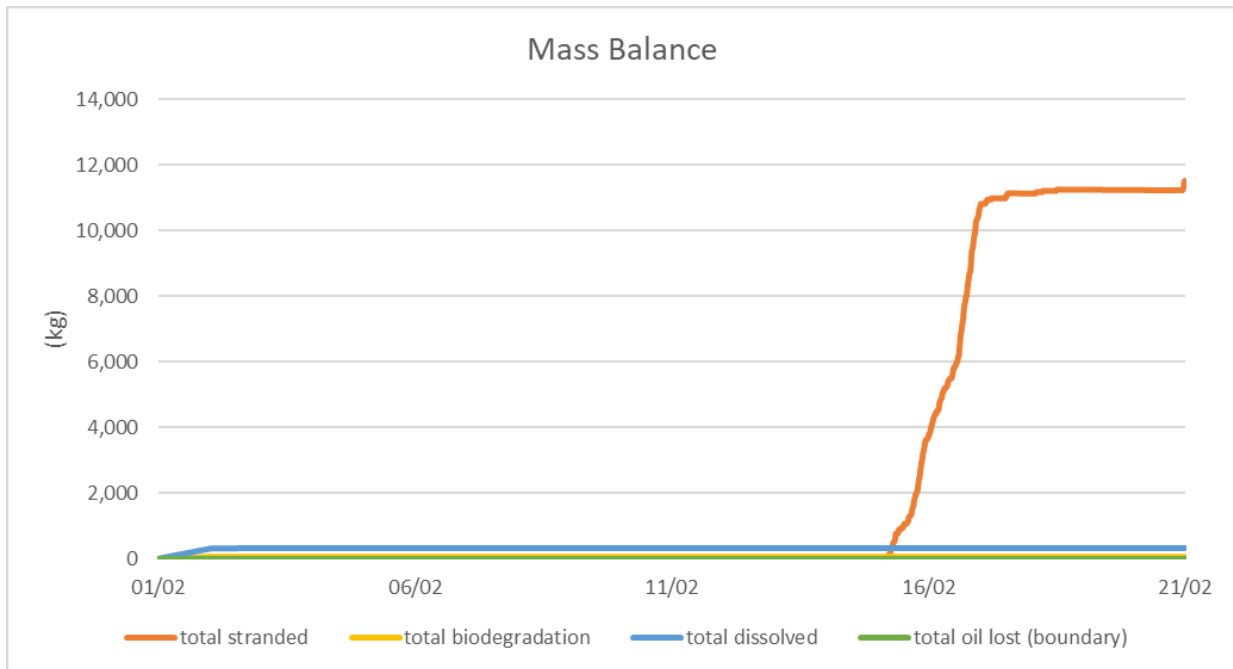
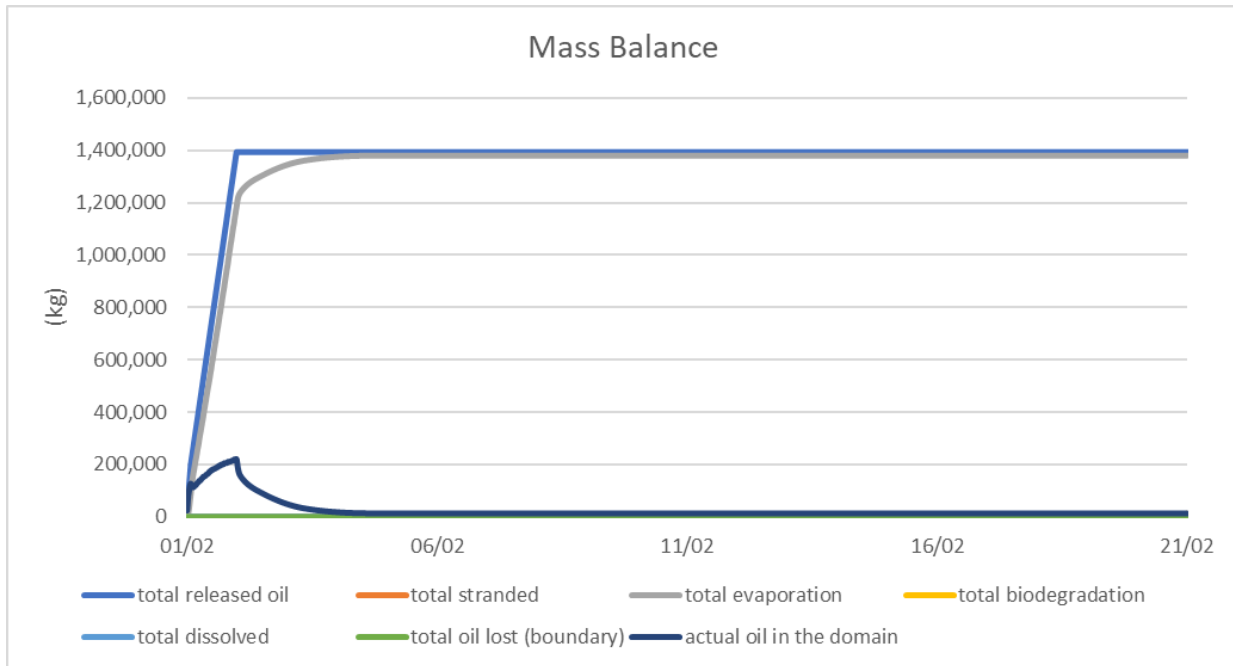


Figure 5.27 Scenario 2 model results mass balance, the worst-case from all simulations that start in Season 1 (December – February). Top - all components; bottom - zoomed-in for low value components

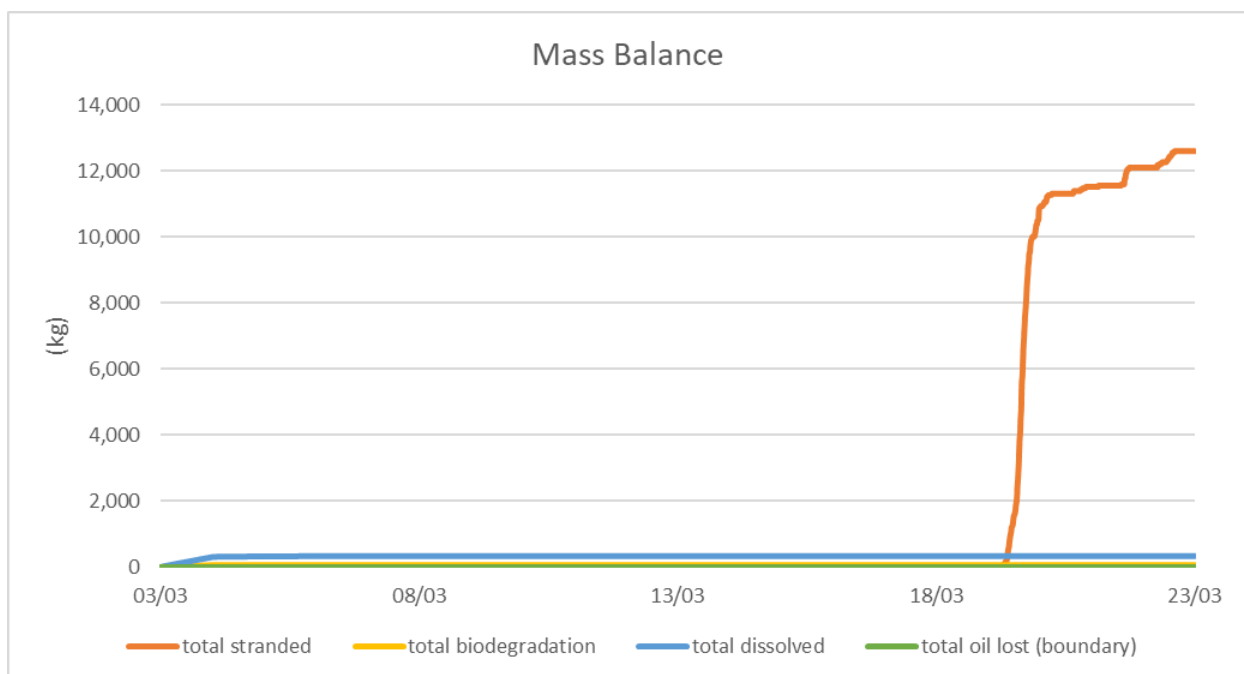
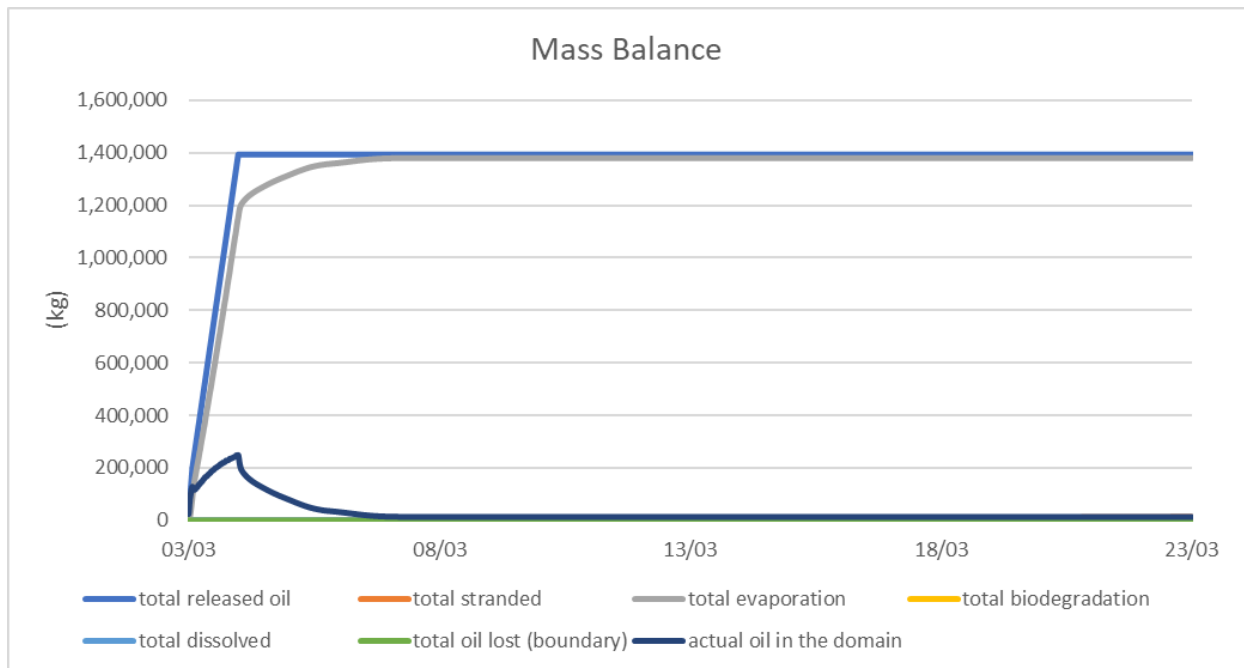


Figure 5.28 Scenario 2 model results mass balance, the worst-case from all simulations that start in Season 2 (March – May). Top - all components; bottom - zoomed-in for low value components

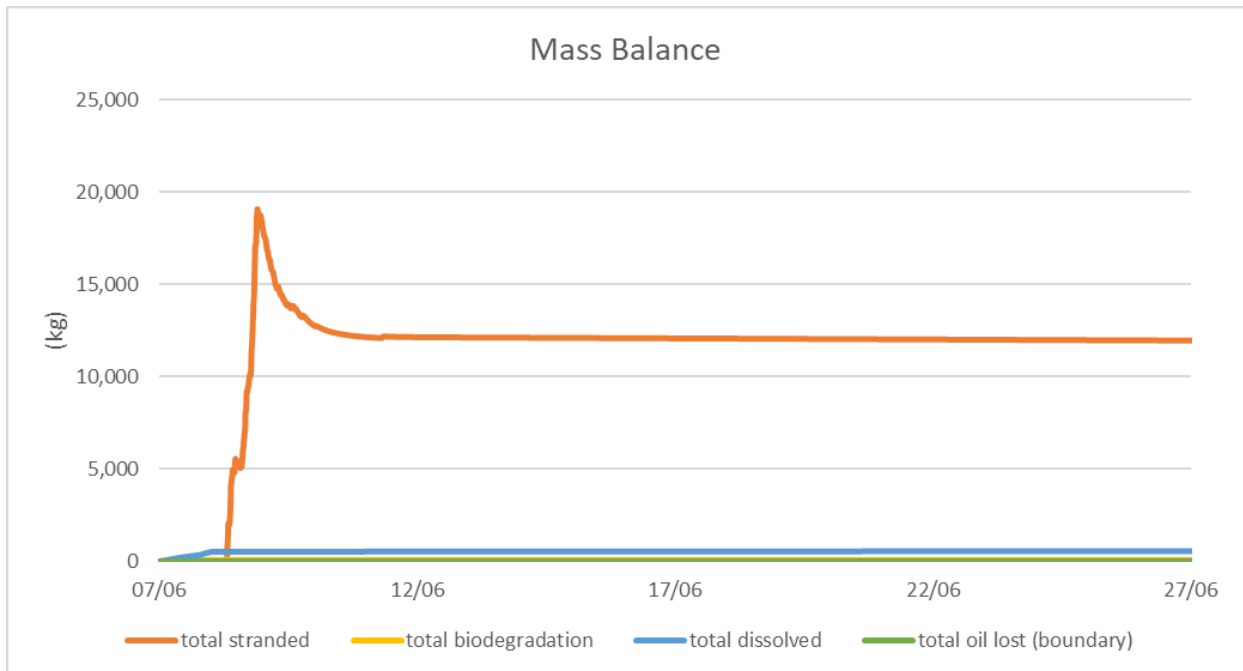
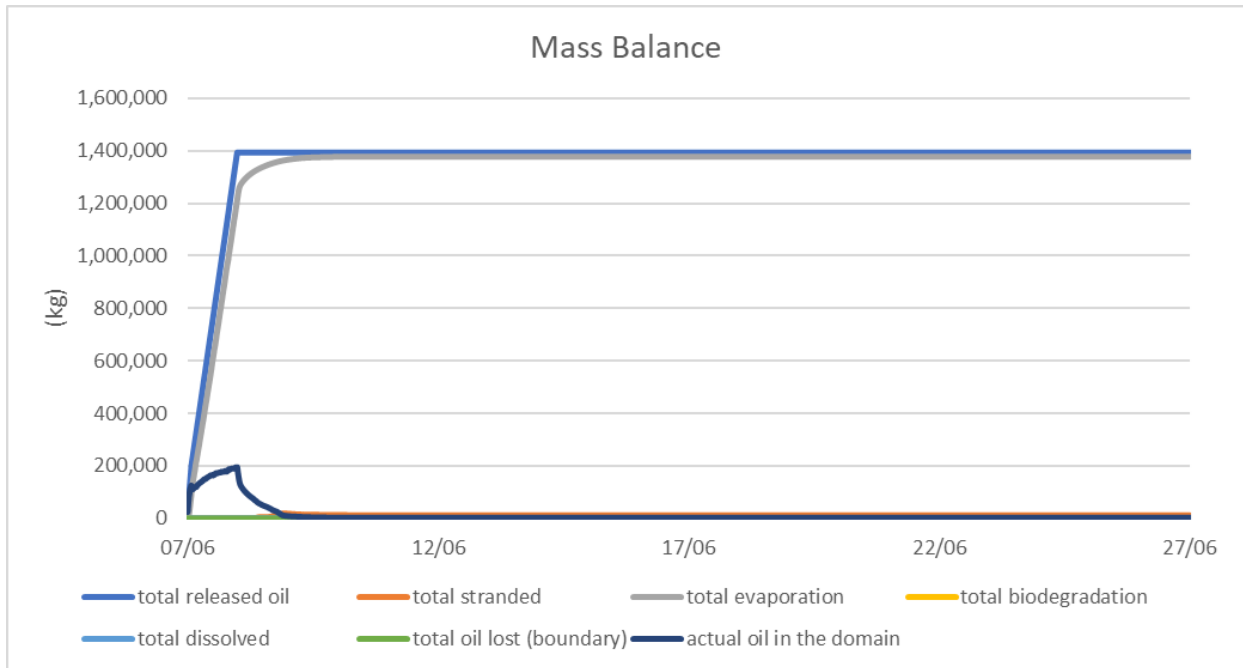


Figure 5.29 Scenario 2 model results mass balance, the worst-case from all simulations that start in Season 3 (June – August). Top - all components; bottom - zoomed-in for low value components

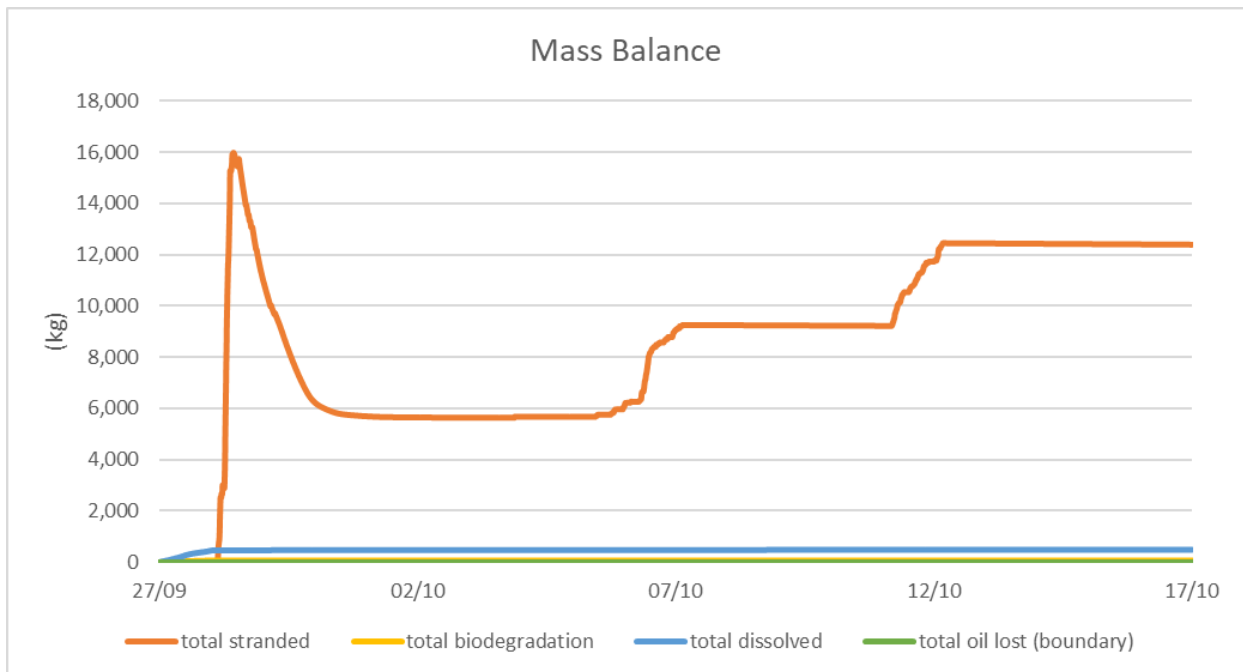
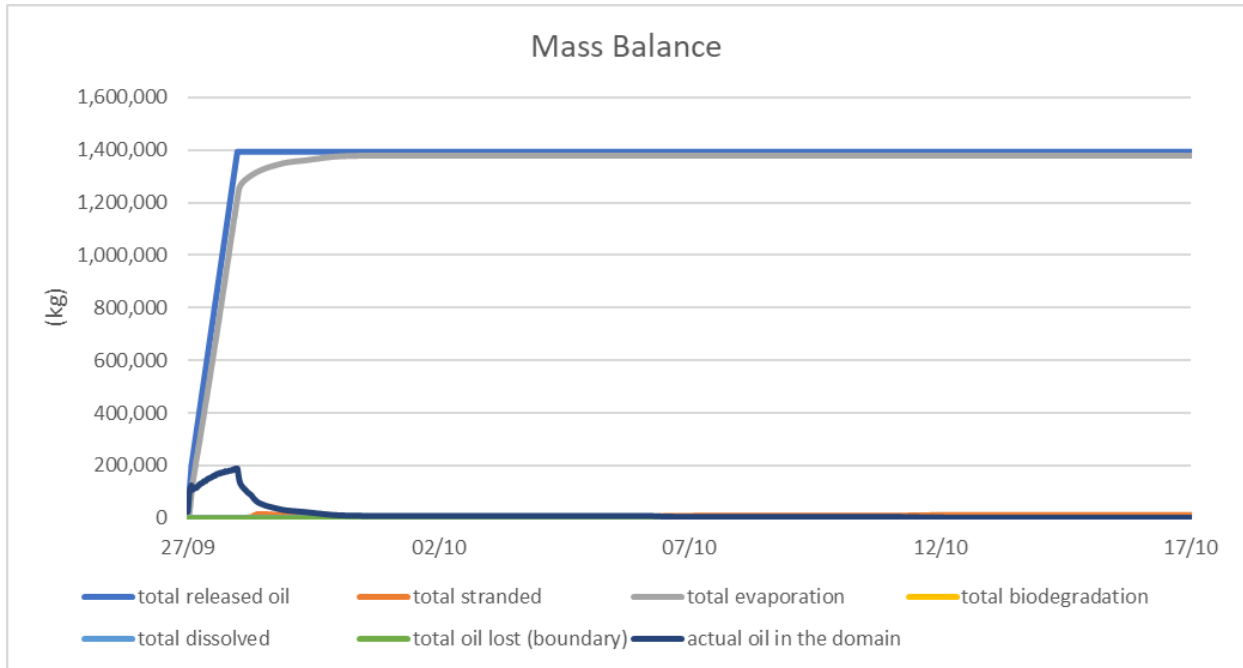


Figure 5.30 Scenario 2 model results mass balance, the worst-case from all simulation that start in Season 4 (September – November). Top - all components; bottom - zoomed-in for low value components

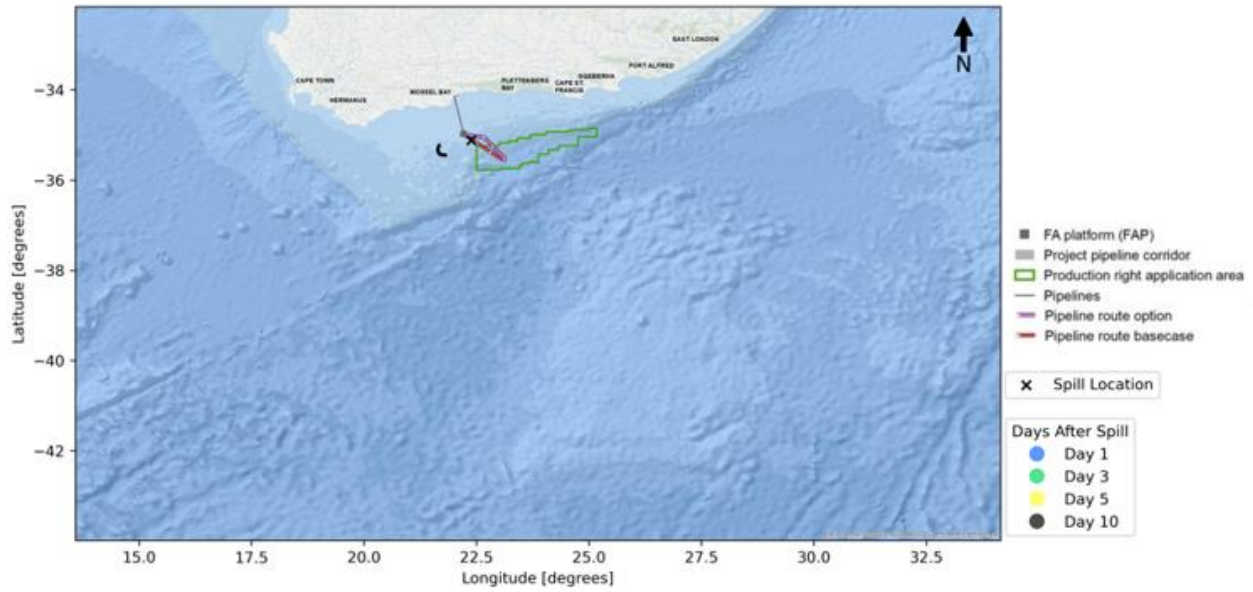


Figure 5.31 Scenario 2 model result drift evolution, the worst-case from all simulations

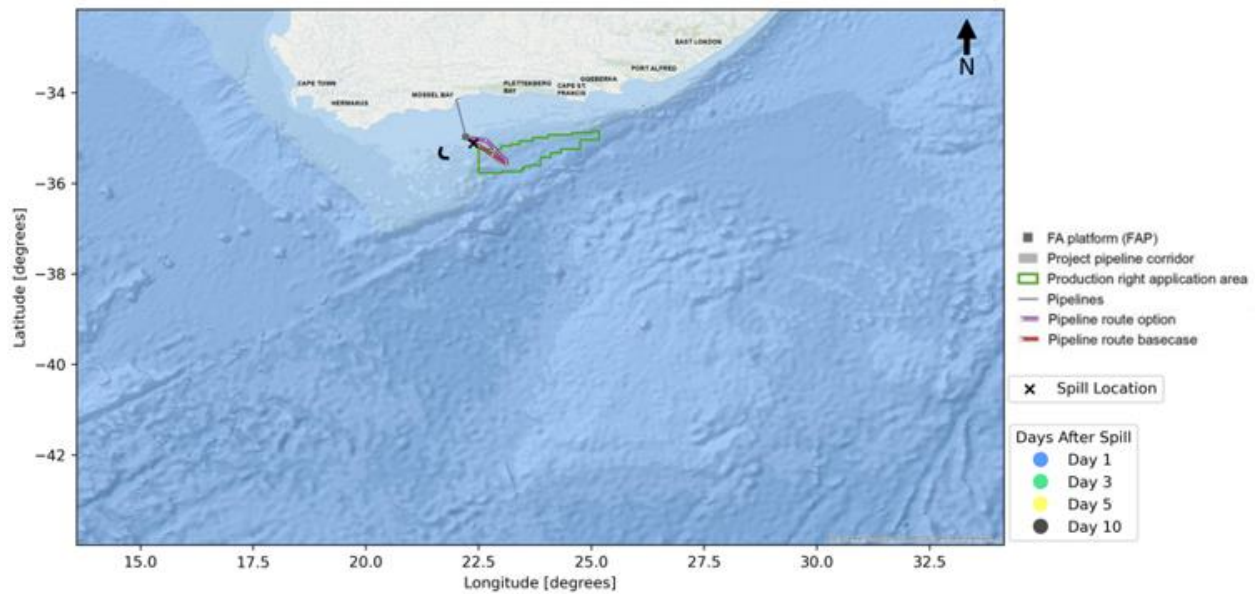


Figure 5.32 Scenario 2 model result drift evolution, the worst-case from all simulations that start in Season 1 (December – February)

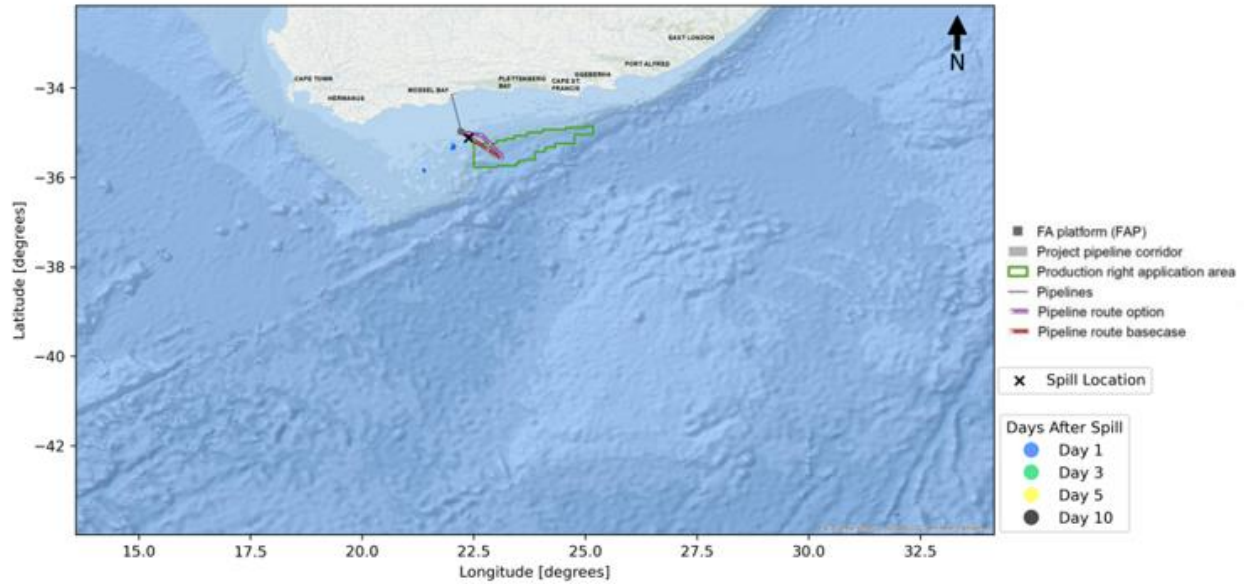


Figure 5.33 Scenario 2 model result drift evolution, the worst-case from all simulations that start in Season 2 (March – May)

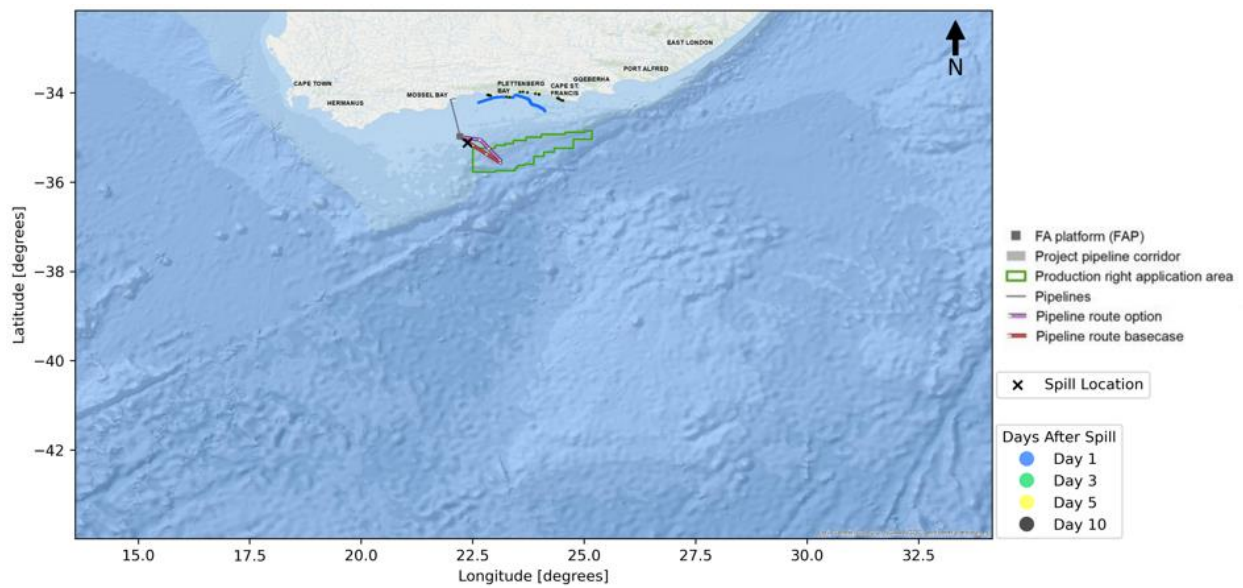


Figure 5.34 Scenario 2 model result drift evolution, the worst-case from all simulations that start in Season 3 (June – August)

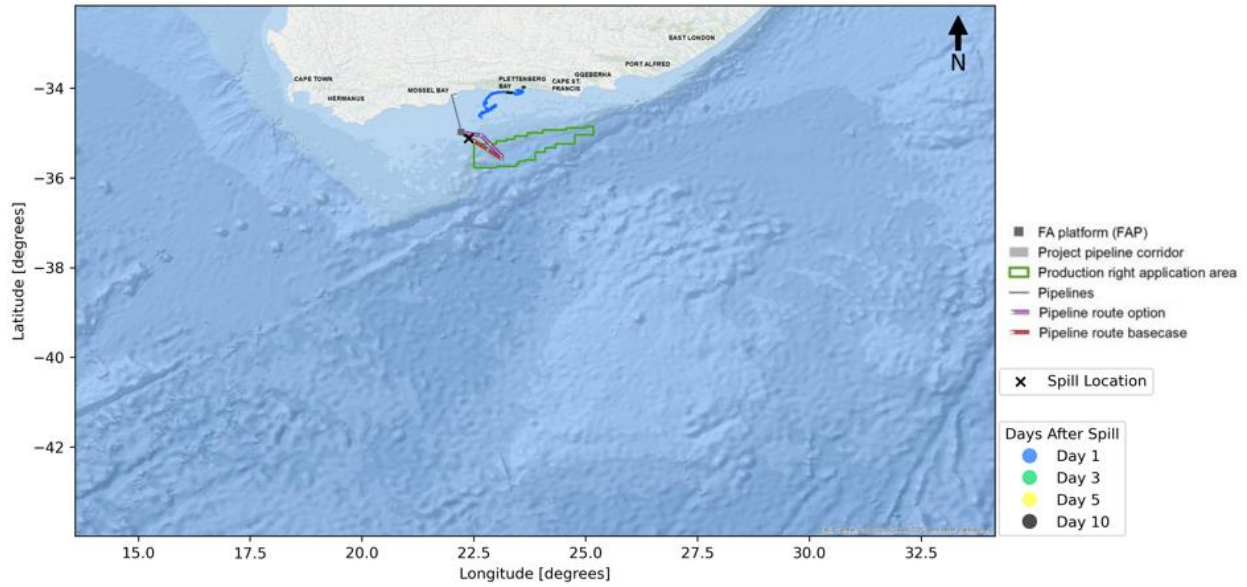


Figure 5.35 Scenario 2 model result drift evolution, the worst-case from all simulations that start in Season 4 (September – November)

5.3.3 Results Summary

The key points of interest identified for the study were Bird Island, De Hoop MPA, Knysna Lagoon, Klein Brak Estuary, Stilbaai Estuary, Tsitsikamma MPA, and Walker Bay. Results were derived for provided coordinates associated with each locale and a 500m buffer around them. Table 5.4 summarizes the model results for the affected points of interest for each of the four seasons. In all seasons, the main direction of the spill drift is southwest – northwest, with the maximum distance to the 90%-oil-surface-probability contour reaching up to 10 km from the release point.

The shoreline length with oil amounts $> 10\text{g/m}^2$ can reach 19 km, with impacted shoreline comprising of Huisklip Nature Reserve, Nature Valley Beach, Robberg Nature Reserve, Kranshoek, Knoetzie Beach, Knysna Lagoon. The maximum worst-case scenario shore fouling i.e., based on deterministic simulation, can reach up to 0.2-1.3 tons (in one cell with cell area around 0.1 km^2), with the worst-case (from deterministic) shoreline length impacted is around 0.2-1.3km. The minimum arrival time of spilled oil on shore from all stochastic simulation result is expected to be around 1-1.5 days.

With respect to the focus areas, only Knysna Lagoon experience oil concentrations larger than 10 g/m^2 . The probability of the shoreline oiling at Knysna Lagoon can reach 0.25-0.5% from all simulations, and 1% from simulations that started in Season 3 and 4.

Table 5.4 Summary of Scenario 2 Results- Pipeline Rupture

Pipeline Rupture (Closure well)	All Simulations	Season 1 (Dec-Feb)	Season 2 (Mar-May)	Season 3 (Jun -Aug)	Season 4 (Sep-Nov)
Spill	Blow out – Closure Well				
Flow Rate / Amount	Coil: 19320 bbl/d (0-2h), 10728 bbl/d (2-24h), Qgas: 6170000 Sm3/d (0-2h), 1415000 Sm3/d (2-24h),				
Main Direction of the Spill Drift	Toward SW or NE	Toward SW or NE	Toward SW or NE	Toward SW or NE	Toward SW or NE
MAX. Distance of the 90%-oil-surface-Probability Contour	10 km from Release Point (RP)	10 km from RP	10 km from RP	10 km from RP	10 km from RP
MAX. Distance of the 1%-oil-surface-Probability Contour	195 km NE and 165 km SW from RP	145 km NE and 485 km SW from RP	210 km NE and 155 km SW from RP	230 km NE and 140 km SW from RP	205 km NE and 165 km SW from RP
Offshore Surface Waters Possibly Reached by a Spill	South African	South African	South African	South African	South African
Shoreline Length that could Receive Oil >10 g/m² (considering all the simulations)	35 km	0 km	0 km	20.5 km	18.4 km
Shoreline possibly impacted (by oil >10 g/m²)	Huisklip Nature Reserve, Nature Valley Beach, Robberg Nature Reserve, Kranshoek, Knoetzie Beach, Knysna Lagoon	-	-	Huisklip Nature Reserve, Nature Valley Beach, Robberg Nature Reserve, Kranshoek, Knoetzie Beach, Knysna Lagoon	Nature Valley Beach, Robberg Nature Reserve, Kranshoek, Knoetzie Beach, Knysna Lagoon
Deterministic Worst-case Shoreline Length Impacted (>10g/m²)	19 km	0 km	0 km	19 km	18 km
MAX. % Shoreline Impact Probability (>10g/m²)	0.75%	0%	0%	1.9%	1%
MAX. Oil Amount Onshore (tons)*	1	0.2	0.5	1	1.3
Probability of Shoreline Oiling > 10 g/m²:					
Bird Island	0%	0%	0%	0%	0%
De Hoop MPA	0%	0%	0%	0%	0%
Knysna Lagoon	0.25-0.5%	0%	0%	1%	1%
Klein Brak Estuary	0%	0%	0%	0%	0%
Stilbaai Estuary	0%	0%	0%	0%	0%
Tsitsikamma MPA	0%	0%	0%	0%	0%
Walker Bay	0%	0%	0%	0%	0%
Minimum Shoreline Arrival Time	1-1.5 days	-	-	1-1.5 days	1-1.5 days

*The maximum oil amount onshore corresponds to the deterministic simulation part of the stochastic scenario. The maximum oil amount onshore does not have a threshold.

NOTE: all the table content are based on stochastic model, except the deterministic Worst-case Shoreline Length Impacted and MAX. oil amount onshore

6 Bibliographic References

- /1/ Beal, L.M., Bryden, H.L., 1997. Observations of an Agulhas undercurrent. *Deep Sea Res. Oceanogr. Res. Pap.* 44, 1715–1724.
- /2/ Beal, L.M., 2009. A time series of Agulhas Undercurrent transport. *J. Phys. Oceanogr.* 39, 2436–2450.
- /3/ Beal, L.M., Elipot, S., Houk, A., Leber, G.M., 2015. Capturing the transport variability of a western boundary jet: results from the Agulhas current time-series experiment (ACT). *J. Phys. Oceanogr.* 45, 1302–1324.
- /4/ French, D., M. Reed, K. Jayko, S. Feng, H. Rines, S. Pavignano, T. Isaji, S. Puckett, A. Keller, F. W. French III, D. Gifford, J. McCue, G. Brown, E. MacDonald, J. Quirk, S. Natzke, R. Bishop, M. Welsh, M. Phillips and B.S. Ingram. *The CERCLA Type A Natural Resource Damage Assessment Model for Coastal and Marine Environments (NRDAM/CME), Technical Documentation, Vol. I -VI*, Final Report, submitted to the Office of Environmental Policy and Compliance, U.S. Dept. of the Interior, Washington, D.C., Contract No. 14-0001-91-C-11. April, 1996.
- /5/ French-McCay D., Z. Li, M. Horn, D. Crowley, M. Spaulding, D. Mendelsohn, C. Turner Modeling oil fate and subsurface exposure concentrations from the Deepwater Horizon oil spill Proceedings of the 39th AMOP Technical Seminar on Environmental Contamination and Response, Emergencies Science Division, Environment Canada, Ottawa, ON, Canada, 39 (2016), pp. 115-150.
- /6/ French McCay, D., “State-of-the-Art and Research Needs for Oil Spill Impact Assessment Modeling.” *Proceedings of the 32nd AMOP Technical Seminar on Environmental Contamination and Response*, Jan. 2009, pp. 601–653.
- /7/ HES Expertise Services, 2022, Block 5/6/7 - Release Points 1 & 2 Oil Spill Drift Modelling Technical Report
- /8/ Naval Research Laboratory. (2014–2021). *Global Ocean Forecast System (GOFS) 3.1* [Dataset]. <https://www.hycom.org/dataserver/gofs-3pt1/analysis>.
- /9/ OLF [Norwegian Oil Industry Association]. 2008. Guideline for risk assessment of effects on fish from acute oil pollution. The Norwegian Oil Industry Association. Norway.
- /10/TotalEnergies. 2022. "Drilling Discharge Modeling Technical Report."
- /11/Walker, J.D., L. Petrakis, and R.R. Colwell. 1976. Comparison of the biodegradability of crude and fuel oils. *Can. J. Microbiol.* 22:598-602.

Appendix A: MIKE 21 & MIKE 3 Flow Model FM, Oil Spill Module - Short Description



MIKE 21 & MIKE 3 Flow Model FM

Oil Spill Module

Short Description



DHI headquarters

Agern Allé 5
DK-2970 Hørsholm
Denmark

+45 4516 9200 Telephone
+45 4516 9333 Support
+45 4516 9292 Telefax

mike@dhigroup.com
www.mikepoweredbydhi.com

MIKE 21 & MIKE 3 Flow Model FM – Oil Spill Module

Accidental oil spills remind us of the dramatic impacts that oil can have on the environment. They also bring into focus, the importance of efficient emergency planning. Oil spills pose serious threats to the marine environment. They also put a lot of pressure on the entities that are responsible for the emergency response and clean-up operations, such as oil companies and national authorities.

This is the background for the Oil Spill Module. The module simulates the weathering and movement of oil represented by discrete particles in a flow field using a so-called Lagrangian approach. It may also simulate the spreading of dissolved oil using advection-dispersion calculations, which are based on the Eulerian approach.

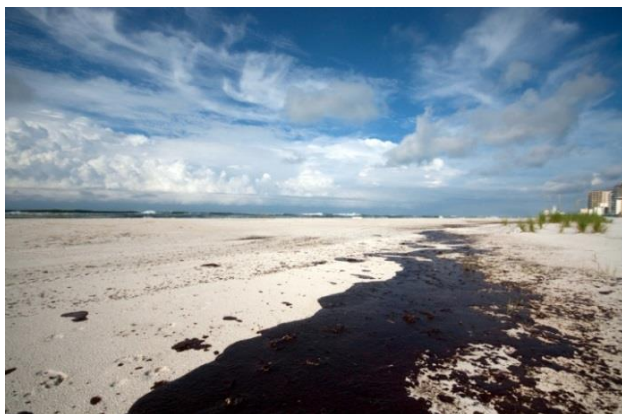
The Oil Spill Module is an add-on module to MIKE 21 & MIKE 3 Flow Model FM. It requires a coupling to the hydrodynamic solver and to the transport solver for passive components (Advection Dispersion module). The hydrodynamic basis is obtained with the MIKE 21 HD FM or MIKE 3 HD FM module.

Application Areas

The Oil Spill Module can be applied in the open sea, coastal areas, estuaries, rivers and lakes. It can be applied in two or three dimensions. However, when considering dissolved oil three dimensions are recommended.

The Oil Spill Module can be applied in studies of e.g.

- environmental impact assessment
- single spill impacts
- clean-up operations
- emergency response systems
- assessment of required amounts of dispersants

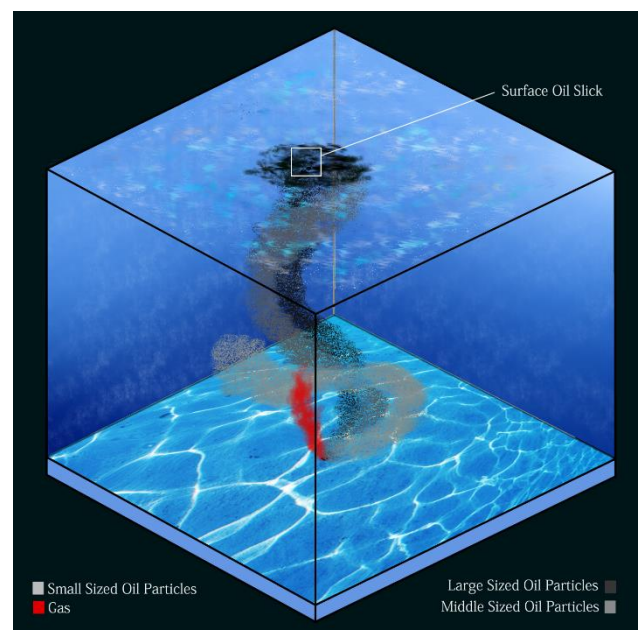


© Whirler

Features

The Oil Spill Module in MIKE 21 & MIKE 3 Flow Model FM includes the following features:

- all weathering processes
- movement of the oil on the surface and in the water column
- movement of dissolved oil independently of non-dissolved oil
- jet from a sub-sea blowout (oil and gas mix)
- the effects of dispersants
- clean-up using booms and skimmers
- stranding with the possibility of re-entering the water
- ice edge interaction with the possibility of re-entering the water



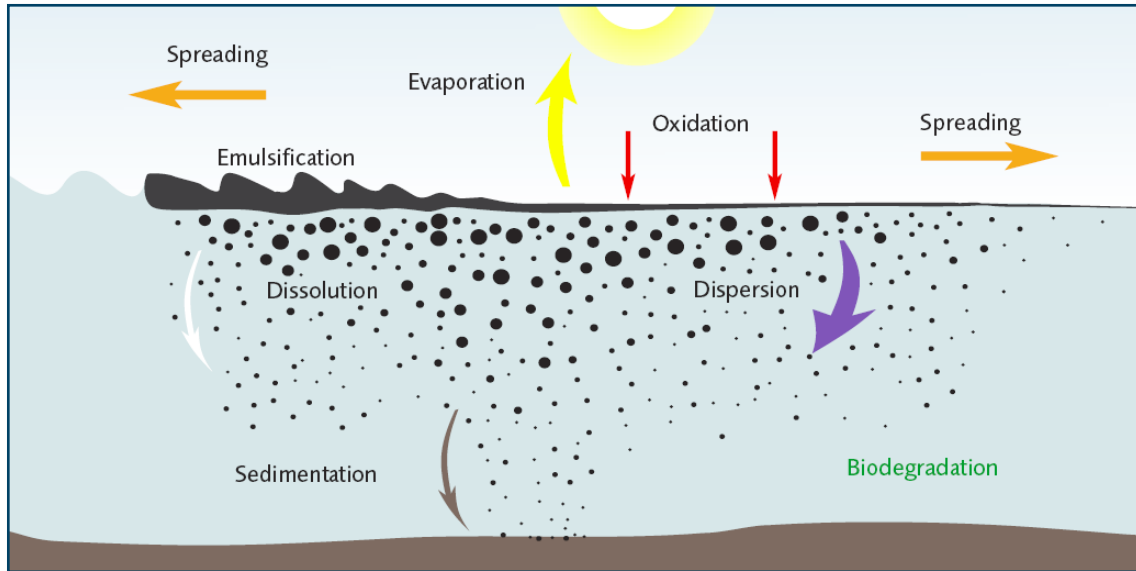
Jet from sub-sea blowout with mix of oil and gas. © DHI

Oil Characterisation

The different types of oil are characterised through a number of key parameters including e.g. density, viscosity, pour point and maximum water content. Additionally, the oil is divided into the following five fractions:

- heavy fraction
- semi-volatile fraction
- volatile fraction
- wax
- asphaltene

Each of these are described through a number of key parameters and weathering constants.



Weathering processes (from Fate of Marine Oil Spills, 2002)

Weathering Processes

The following weathering processes are included in the Oil Spill Module:

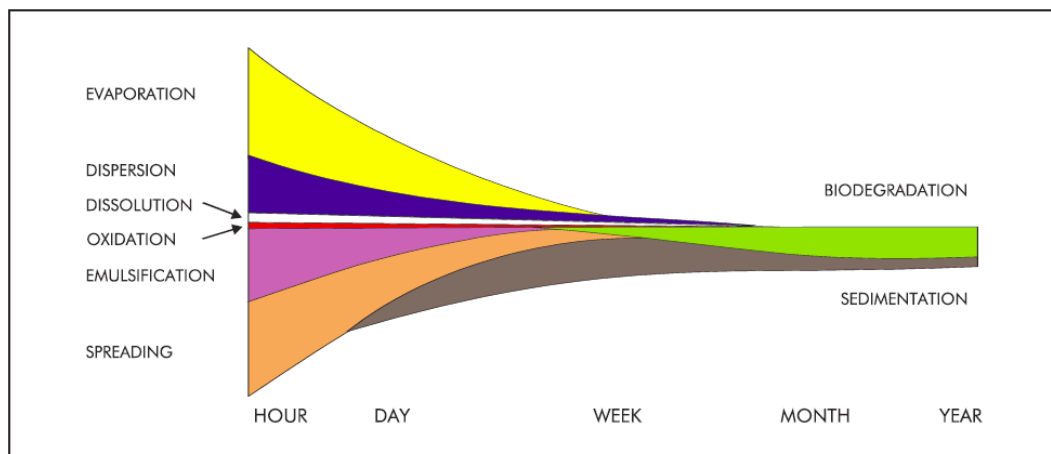
- spreading (viscous, gravity based)
- evaporation
- emulsification
- vertical dispersion (by waves)
- dissolution
- biodegradation
- photo-oxidation

All of these processes and the other features in the Oil Spill Module are handled by a MIKE ECO Lab template. This means that all processes/features may be inspected (and updated if so desired) using the MIKE ECO Lab editor (a MIKE ECO Lab license is required to use the MIKE ECO Lab editor). An illustration of the weathering processes and their time scales is shown above and below.

Environmental Data Requirements

The following environmental data are required for an oil spill simulation:

- Current data in 2D or 3D. These will normally come from a coupled or de-coupled MIKE 21 or MIKE 3 FM simulation.
- Wind data. These are used for calculation of the surface layer drift. The wind data are also applied in e.g. the evaporation process.
- Wave data. These are used for the vertical dispersion of the oil. Note that when oil particles are dispersed into the water column no evaporation will take place. This may have an important effect on the amount of oil hitting e.g. a coast.
- Ice data (optional). Oil drifting in ice-infested waters will follow the ice. Also, the weathering processes will be adjusted.



Time scales for weathering processes (from Fate of Marine Oil Spills, 2002)

Solution Technique

The oil spill simulation is executed using the MIKE ECO Lab engine and a MIKE ECO Lab oil spill template. The execution comprises both Lagrangian particle tracking (including weathering processes) and Eulerian advection-dispersion computations of dissolved oil (optional).

An oil spill simulation may either be run as a coupled model together with the MIKE 21 or MIKE 3 Flow Model FM or in the de-coupled mode. In order to save time the de-coupled mode, where flow data from a previous MIKE 21 or MIKE 3 FM simulation are re-used, is normally used.

The spreading of an oil spill is calculated by dividing the oil spill into discrete parcels, termed particles.

The movements of the particles are given as a sum of a displacement determined by the hydrodynamic flow field (and optionally the wind) and a dispersive component as a result of random processes (e.g. turbulence in the water).

The movement of dissolved oil is calculated using the advective-dispersion formulation in the transport solver in MIKE 21 & MIKE3 FM.

Input

Input data to the Oil Spill Module is divided into a number of groups:

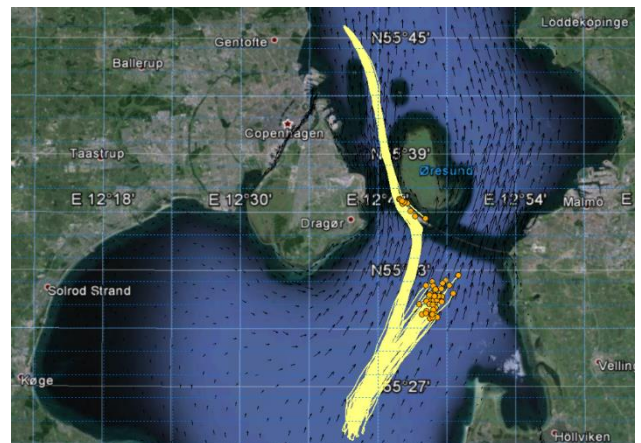
- environmental data (currents, wind, wave and ice)
- current profile specification near surface and bottom (optional)
- dispersion coefficients
- oil characteristics for the five fractions including weathering constants
- gas characteristics, if sub-sea blowout
- spill location, depth, duration and amount
- blowout characteristics
- boom and skimmer specifications
- possibility of oil re-entering the water after being stranded (depending on type of coast, e.g. sandy beach or vertical rocks)
- initial conditions
- boundary conditions

The oil spill may be specified as an instantaneous spill (at the outset of the simulation) or as a spill continuing for some time. The location may be fixed or moving.

Output

A number of output types are available:

- 2D-maps or 3D maps (the latter only when running the Oil Spill Module in a 3D domain) containing the instantaneous value (as mass, area concentration of volume concentration) or the statistical value (min, mean, max, time average or cell average) of all oil parameters. These parameters include (among many):
 - total mass excluding water
 - total mass including water
 - oil slick thickness (2D only)
 - amount stranded incl. and excl. water (2D only)
 - time of first arrival (2D only)
- Mass budget as a time series. This is useful for identifying how the weathering processes affects the oil.
- Particle tracks and particle properties. These are useful for illustrating the spreading of the oil spill. An example is shown below.

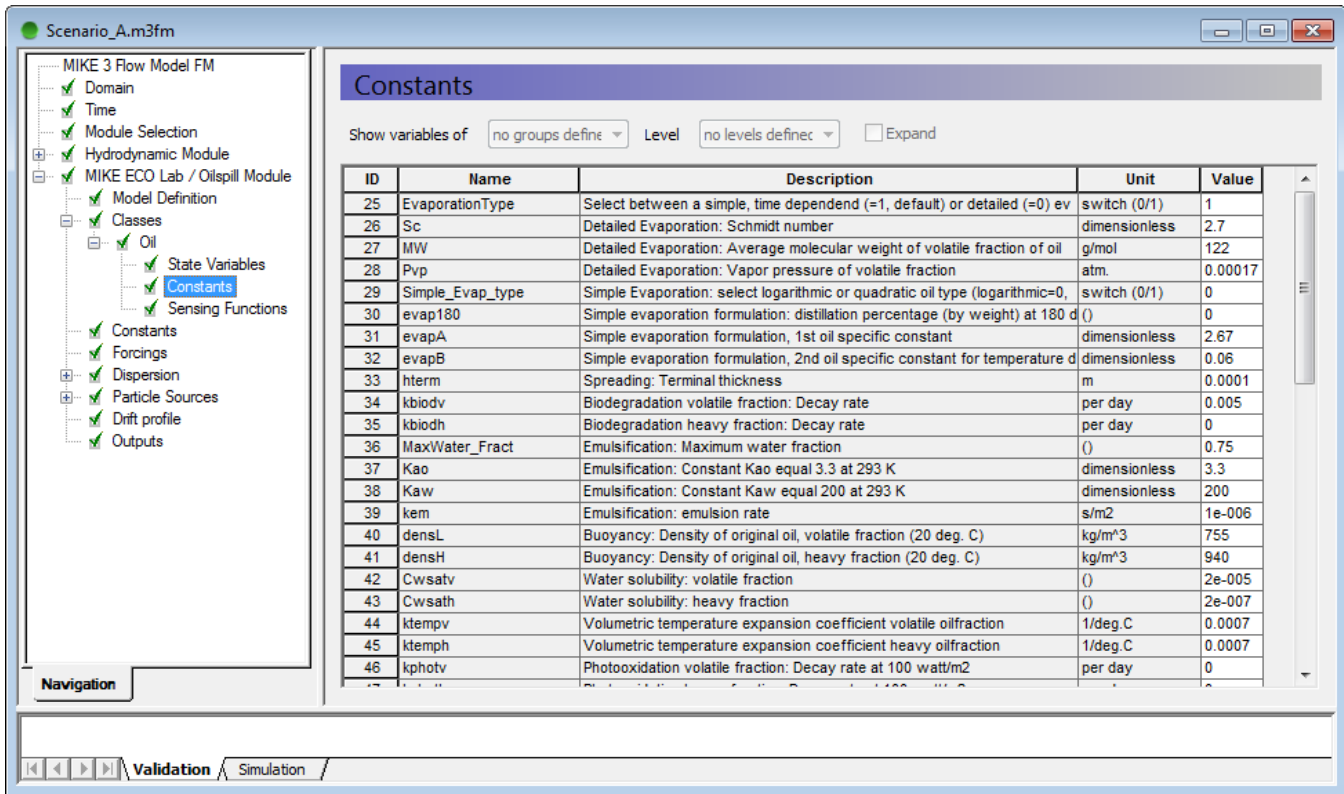


Visualisation of oil trajectories and current field on Google Earth background

Pre- and post-processing tools

The Oil Spill/Particle Track toolbox contains facilities aimed for pre- and post processing of oil spill and particle tracking simulation output:

The Oil Spill Boom and Skimmer tool enables the user to quickly define the input for the boom and skimmer feature of the extended DHI oil spill model. The toolbox tools can also be used to reverse flow fields for subsequent backtracking of spill events, to process and convert large quantities of data in XML files and to calculate connectivity between grid cells in a user-specified Cartesian grid.

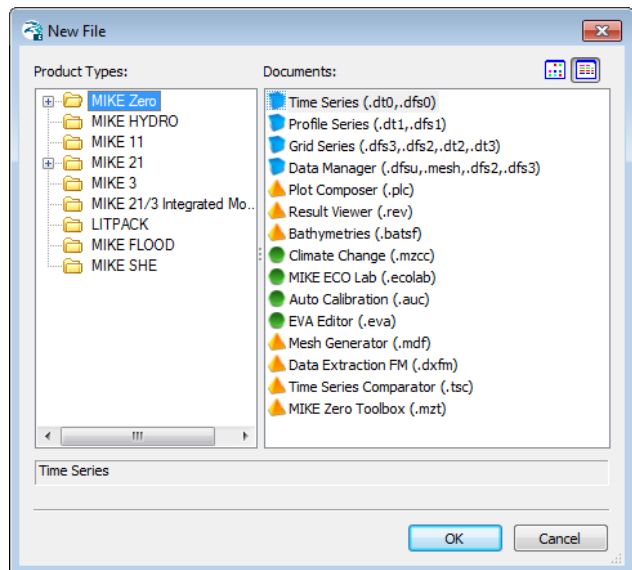


Graphical user interface of the Oil Spill Module showing weathering constants

Graphical User interface

The MIKE 21 & MIKE 3 Flow Model FM, Oil Spill Module is operated through a fully Windows integrated Graphical User Interface (GUI) and is compiled as a true 64-bit application. Support is provided at each stage by an Online Help System. A screen shot of the GUI is shown on the next page.

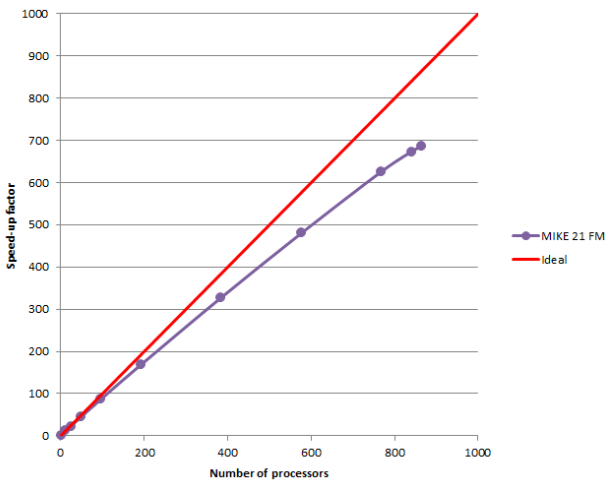
The common MIKE Zero shell provides entries for common data file editors, plotting facilities and a toolbox with utilities as the Mesh Generator and Data Viewer.



Overview of the common MIKE Zero utilities

Parallelisation

The computational engines of the MIKE 21/3 FM series are available in versions that have been parallelised using both shared memory as well as distributed memory architecture. The latter approach allows for domain decomposition. The result is much faster simulations on systems with many cores. It could be feasible to carry out OS modelling using decoupled result files from a HD simulation.



Example of MIKE 21 HD FM speed-up using a HPC Cluster with distributed memory architecture (purple)

Hardware and Operating System Requirements

The MIKE Zero Modules support Microsoft Windows 7 Professional Service Pack 1 (64 bit), Windows 10 Pro (64 bit), Windows Server 2012 R2 Standard (64 bit) and Windows Server 2016 Standard (64 bit).

Microsoft Internet Explorer 9.0 (or higher) is required for network license management. An internet browser is also required for accessing the web-based documentation and online help.

The recommended minimum hardware requirements for executing the MIKE Zero modules are:

Processor:	3 GHz PC (or higher)
Memory (RAM):	2 GB (or higher)
Hard disk:	40 GB (or higher)
Monitor:	SVGA, resolution 1024x768
Graphics card:	64 MB RAM (256 MB RAM or higher is recommended)

Support

News about new features, applications, papers, updates, patches, etc. are available here:

www.mikepoweredbydhi.com/Download/DocumentsAndTools.aspx

For further information on MIKE 21 & MIKE 3 Flow Model FM software, please contact your local DHI office or the support centre:

MIKE Powered by DHI Client Care
 Agern Allé 5
 DK-2970 Hørsholm
 Denmark

Tel: +45 4516 9333
 Fax: +45 4516 9292

mike@dhigroup.com
www.mikepoweredbydhi.com

Documentation

The MIKE 21 & MIKE 3 Flow Model FM models are provided with comprehensive user guides, online help, scientific documentation, application examples and step-by-step training examples.



Further reading

- Al-Rabeh, A., 1994. *Estimating surface oil spill transport due to wind in the Arabian Gulf*. Ocean Engineering 21:461-465. doi: 10.1016/0029-8018(94)90019-1.
- Betancourt F., A. Palacio, and A. Rodriguez, 2005. *Effects of the Mass Transfer Process in Oil Spill*. American Journal of Applied Science 2:939-946.
- Delvigne, G., and C. Sweeney, 1988. *Natural dispersion of oil*. Oil and Chemical Pollution 4:281-310. doi: 10.1016/S0269-8579(88)80003-0.
- Fate of Marine Oil Spills*, 2002. Page 8. Technical Reports, The International Tanker Owners Pollution Federation Limited (ITOPF), London.
- Fingas, M. F., 1996. *The evaporation of oil spills: Prediction of equations using distillation data*. Spill Science & Technology Bulletin 3:191-192. doi: 10.1016/S1353-2561(97)00009-1.
- Fingas, M. F., 1997. *Studies on the evaporation of crude oil and petroleum products: I. the relationship between evaporation rate and time*. Journal of Hazardous Materials 56:227-236. doi: 10.1016/S0304-3894(97)00050-2.
- Fingas, M.F., 2004. *Modeling evaporation using models that are not boundary-layer regulated*. Journal of Hazardous Materials, Volume 107, 2004, pp. 27-36.
- French-McCay, D. P., 2004. *Oil spill impact modeling: Development and validation*. Environmental Toxicology and Chemistry 23:2441-2456. doi: 10.1897/03-382.
- Mackay, D., I. Buist, R. Mascarenhas, and S. Paterson, 1980. *Oil spill processes and models*. Environmental Emergency Branch, Department of Fisheries and Environment, Environment Canada, Ottawa, ON.
- Mackay, D., and W. Zagorski, 1982. *Water-in-oil emulsions: a stability hypothesis*. Proceedings of the Fifth Annual Arctic Marine Oilspill Program Technical Seminar:61-74.
- Reed, M., 1989. *The physical fates component of the natural resource damage assessment model system*. Oil and Chemical Pollution 5:99-123. doi: 10.1016/S0269-8579(89)80009-7.
- Rugbjerg, M. 2009. *Hydrodynamic and environmental modelling in the vicinity of Scott Reef*, Coasts & Ports 2009, Wellington, New Zealand, 16-18 September 2009
- Sebastião, P., and C. Guedes Soares, 1995. *Modeling the fate of oil spills at sea*. Spill Science & Technology Bulletin 2:121-131. doi: 10.1016/S1353-2561(96)00009-6.
- Xie, H., P. D. Yapa, and K. Nakata, 2007. *Modeling emulsification after an oil spill in the sea*. Journal of Marine Systems 68:489-506. doi: 10.1016/j.jmarsys.2007.02.016.

Appendix B: Offshore Production Right and Environmental Authorisation Applications for Block 11B/12B – Analysis of Metocean Data for Oil Spill and Drilling Discharge Modelling



TotalEnergies E&P South Africa BV

OFFSHORE PRODUCTION RIGHT AND ENVIRONMENTAL AUTHORISATION APPLICATIONS FOR BLOCK 11B/12B

Analysis of Metocean Data for Oil Spill and
Drilling Discharge Modelling.





TotalEnergies E&P South Africa BV

OFFSHORE PRODUCTION RIGHT AND ENVIRONMENTAL AUTHORISATION APPLICATIONS FOR BLOCK 11B/12B

Analysis of Metocean Data for Oil Spill and Drilling Discharge
Modelling.

TYPE OF DOCUMENT (VERSION) PUBLIC

PROJECT NO. .41105306

OUR REF. NO. 41105306-358665-9

DATE: JULY 2023



TotalEnergies E&P South Africa BV

OFFSHORE PRODUCTION RIGHT AND ENVIRONMENTAL AUTHORISATION APPLICATIONS FOR BLOCK 11B/12B

Analysis of Metocean Data for Oil Spill and Drilling Discharge
Modelling.

WSP

Building 1, Maxwell Office Park
Magwa Crescent West, Waterfall City
Midrand, 1685
South Africa

Phone: +27 11 254 4800

WSP.com



QUALITY CONTROL

Issue/revision	Final
Date	04 July 2023
Prepared by	Ashwin Gadgil
Signature	
Checked by	Sundar Prasad
Signature	
Authorised by	Roy van Ballegooyen
Signature	
Project number	41105306
Report number	41105306-358665-9

CONTENTS

1	INTRODUCTION	1
1.1	DISCHARGE LOCATIONS AND OVERVIEW OF METOCEAN CONDITIONS	1
1.2	ENVIRONMENTAL DATA	6
1.3	DISPERSION MODELLING SIMULATION PERIODS	7
2	DISCHARGE 4	8
2.1	SELECTION OF DRILLING DISCHARGE SIMULATION PERIODS FOR DISCHARGE 4	14
2.1.1	SEASON 1- DECEMBER TO FEBRUARY	16
2.1.2	SEASON 2- MARCH TO MAY	17
2.1.3	SEASON 3- JUNE TO AUGUST	19
2.1.4	SEASON 4- SEPTEMBER TO NOVEMBER	20
3	DISCHARGE 5	22
3.1	SELECTION OF DRILLING DISCHARGE SIMULATION PERIODS FOR DISCHARGE 5	28
3.1.1	SEASON 1- DECEMBER TO FEBRUARY	28
3.1.2	SEASON 2- MARCH TO MAY	29
3.1.3	SEASON 3- JUNE TO AUGUST	31
3.1.4	SEASON 4- SEPTEMBER TO NOVEMBER	32
4	CONDENSATE PIPE LEAK LOCATION	34
5	STUDY LIMITATIONS	40
6	REFERENCES	41
7	CLOSURE	43

TABLES

Table 1-1 - Discharge location characteristics	6
Table 1-2 - Environmental average data (Discharge 4 & 5 PARTRACK Modelling SRF, TEEPSA, 2022)	6
Table 1-3 - Overview of metocean conditions by season at Discharge 4, 5, and Pipe Leak for 2012 - 2016	7
Table 2-1 - Yearly and monthly surface current speed and direction statistics at Discharge 4	9
Table 2-2 - Yearly and monthly seabed current speed and direction statistics at Discharge 4	12
Table 2-3 - Yearly and monthly wind speed and direction statistics at Discharge 4	12
Table 3-1 - Yearly and monthly surface current speed and direction statistics at Discharge 5	23
Table 3-2 - Yearly and monthly seabed current speed and direction statistics at Discharge 5	26
Table 3-3 - Table 4: Yearly and monthly wind speed and direction statistics at Discharge 5	26
Table 4-1 - Yearly and monthly surface current speed and direction statistics at Pipe Leak location	35
Table 4-2 - Yearly and monthly seabed current speed and direction statistics at Pipe Leak location	38
Table 4-3 - Yearly and monthly wind speed and direction statistics at Pipe Leak location	38

FIGURES

Figure 1-1 - Locations of Discharge 4, Discharge 5, and condensate Pipe Leak in the study area	2
Figure 1-2 - Mean ocean surface velocities derived from satellite-tracked drifters following the ocean at 15 m depth (https://oceancurrents.rsmas.miami.edu/atlantic/agulhas_2.html)	3
Figure 1-3 - Satellite-derived sea surface temperature (°C) for 4 June 2014 showing the main features of the Agulhas Current, including the shear edge features on the inner edge of the Agulhas Current and early evidence of an upstream Natal Pulse that will propagate	

downstream resulting in a major perturbation of flows in Block 11B/12B. The black lines represent the 200, 1000, and 3000 m isobaths (Source: Tedesco <i>et al.</i> , 2019)	4
Figure 1-4 - Daily composite of SEVIRI SST on 13 May 2009, during the passage of a Natal Pulse. Overlaid vectors represent the cross-track absolute geostrophic current velocities derived from the high resolution along-track altimetry (Source: Krug and Dufois, 2014).	5
Figure 2-1 - Average annual current and wind speed roses at Discharge 4 for 2012-2016	8
Figure 2-2 - Average monthly surface current roses at Discharge 4 for 2012 – 2016 (colour bar represents current speed in m/s)	10
Figure 2-3 - Average monthly seabed current roses at Discharge 4 for 2012 – 2016 (colour bar represents current speed in m/s)	11
Figure 2-4 - Average monthly wind roses at Discharge 4 for 2012 – 2016 (colour bar represents wind speed in m/s)	13
Figure 2-5 - Locations of Discharge 4 and Discharge 5 relative to Southwest Indian Seamount MPA	14
Figure 2-6 - Typical sequence and duration of mud and cuttings discharges	15
Figure 2-7 - Variation of discharged mud and cuttings quantity with time at drilling location	15
Figure 2-8 - Bottom current mean and maximum speed, and primary direction at Discharge 4 for Season 1 (2012 – 2016)	16
Figure 2-9 - Seabed and surface current vectors at Discharge 4 from 17 Dec 2015 to 30 Jan 2016 with boxes showing the period selected for drilling discharge simulation in Season 1	17
Figure 2-10 - Bottom current mean and maximum speed, and primary direction at Discharge 4 for Season 2 (2012 – 2016)	18
Figure 2-11 - Seabed and surface current vectors at Discharge 4 from 3 Mar 2013 to 16 Apr 2013 with boxes showing the period selected for drilling discharge simulation in Season 2	18
Figure 2-12 - Bottom current mean and maximum speed, and primary direction at Discharge 4 for Season 3 (2012 – 2016)	19
Figure 2-13 - Seabed and surface current vectors at Discharge 4 from 5 Aug 2016 to 18 Sep 2016 with boxes showing the period selected for drilling discharge simulation in Season 3	20
Figure 2-14 - Bottom current mean and maximum speed, and primary direction at Discharge 4 for Season 4 (2012 – 2016)	21
Figure 2-15 - Seabed and surface current vectors at Discharge 4 from 10 Oct 2014 to 23 Nov 2014 with boxes showing the period selected for drilling discharge simulation in Season 4	21
Figure 3-1 - Average annual current and wind speed roses at Discharge 5 for 2012-2016	22

Figure 3-2 - Average monthly surface current roses at Discharge 5 for 2012 – 2016 (colour bar represents current speed in m/s)	24
Figure 3-3 - Average monthly seabed current roses at Discharge 5 for 2012 – 2016 (colour bar represents current speed in m/s)	25
Figure 3-4 - Average monthly wind roses at Discharge 5 for 2012 – 2016 (colour bar represents wind speed in m/s)	27
Figure 3-5 - Bottom current mean and maximum speed, and primary direction at Discharge 5 for Season 1 (2012 – 2016)	28
Figure 3-6 - Seabed and surface current vectors at Discharge 5 from 14 Dec 2015 to 27 Jan 2016 with boxes showing the period selected for drilling discharge simulation in Season 1	29
Figure 3-7 - Bottom current mean and maximum speed, and primary direction at Discharge 5 for Season 2 (2012 – 2016)	30
Figure 3-8 - Seabed and surface current vectors at Discharge 5 from 3 Mar 2013 to 16 Apr 2013 with boxes showing the period selected for drilling discharge simulation in Season 2	30
Figure 3-9 - Bottom current mean and maximum speed, and primary direction at Discharge 5 for Season 3 (2012 – 2016)	31
Figure 3-10 - Seabed and surface current vectors at Discharge 5 from 2 Aug 2015 to 15 Sep 2015 with boxes showing the period selected for drilling discharge simulation in Season 3	32
Figure 3-11 - Bottom current mean and maximum speed, and primary direction at Discharge 5 for Season 4 (2012 – 2016)	33
Figure 3-12 - Seabed and surface current vectors at Discharge 5 from 5 Oct 2015 to 18 Nov 2015 with boxes showing the period selected for drilling discharge simulation in Season 4	33
Figure 4-1 - Average annual current and wind speed roses at Pipe Leak location for 2012-2016	34
Figure 4-2 - Average monthly surface current roses at Pipe Leak for 2012 – 2016 (colour bar represents current speed in m/s)	36
Figure 4-3 - Average monthly seabed current roses at Pipe Leak for 2012 – 2016 (colour bar represents current speed in m/s)	37
Figure 4-4 - Average monthly wind roses at Pipe Leak for 2012 – 2016 (colour bar represents wind speed in m/s)	39



APPENDICES

APPENDIX A

SATOCHEAN HYDRODYNAMIC DATABASE: CALIBRATION AND VALIDATION

APPENDIX B

DOCUMENT LIMITATIONS

1 INTRODUCTION

A statistical assessment of wind and current data was carried out at three locations within License Block 11B/12B, located off the Southern Cape Coast of South Africa. The area of interest is approximately 12,000 km² and lies between Mossel Bay and Cape St. Francis in waters of depths of between 500 m and 2,300 m. The data was sourced from a SAT-OCEAN (TotalEnergies, 2022) hindcast model covering a 5-year period (Jan 2012 – Dec 2016). The SAT-OCEAN model has a resolution of 1/32 degree (about 3.5 km) in the study area. Model output is provided at 3-hour time steps. The vertical z-coordinates of the model (m) are 0, 5, 10, 20, 30, 40, 50, 75, 100, 125, 150, 200, 300, 400, 500, 750, 1000, 1250, 1500, 1750, 2000, 2250, 2500, 2750, 3000, 3250, 3500, 4000, 5000, and 5500. The calibration and validation of these data are reported in Appendix A. See also Russo *et al.* (2022) that has undertaken an intercomparison of re-analysis products (including HYCOM upon which the SATOCEAN data is based) for southern African Waters.

1.1 DISCHARGE LOCATIONS AND OVERVIEW OF METOCEAN CONDITIONS

Metocean statistics have been compiled to support the numerical modelling of condensate dispersion from a subsea blowout and a submarine pipeline leak, and dispersion of drilling mud and cuttings discharges at the seabed and near the water surface. Three locations, Discharge 4 and Discharge 5, on the southwest end of Block 11B/12B, and Pipe Leak on the shallower continental shelf and approximately 87 km northwest of Discharge 5, are considered for the present assessment, and are shown in Figure 1-1.

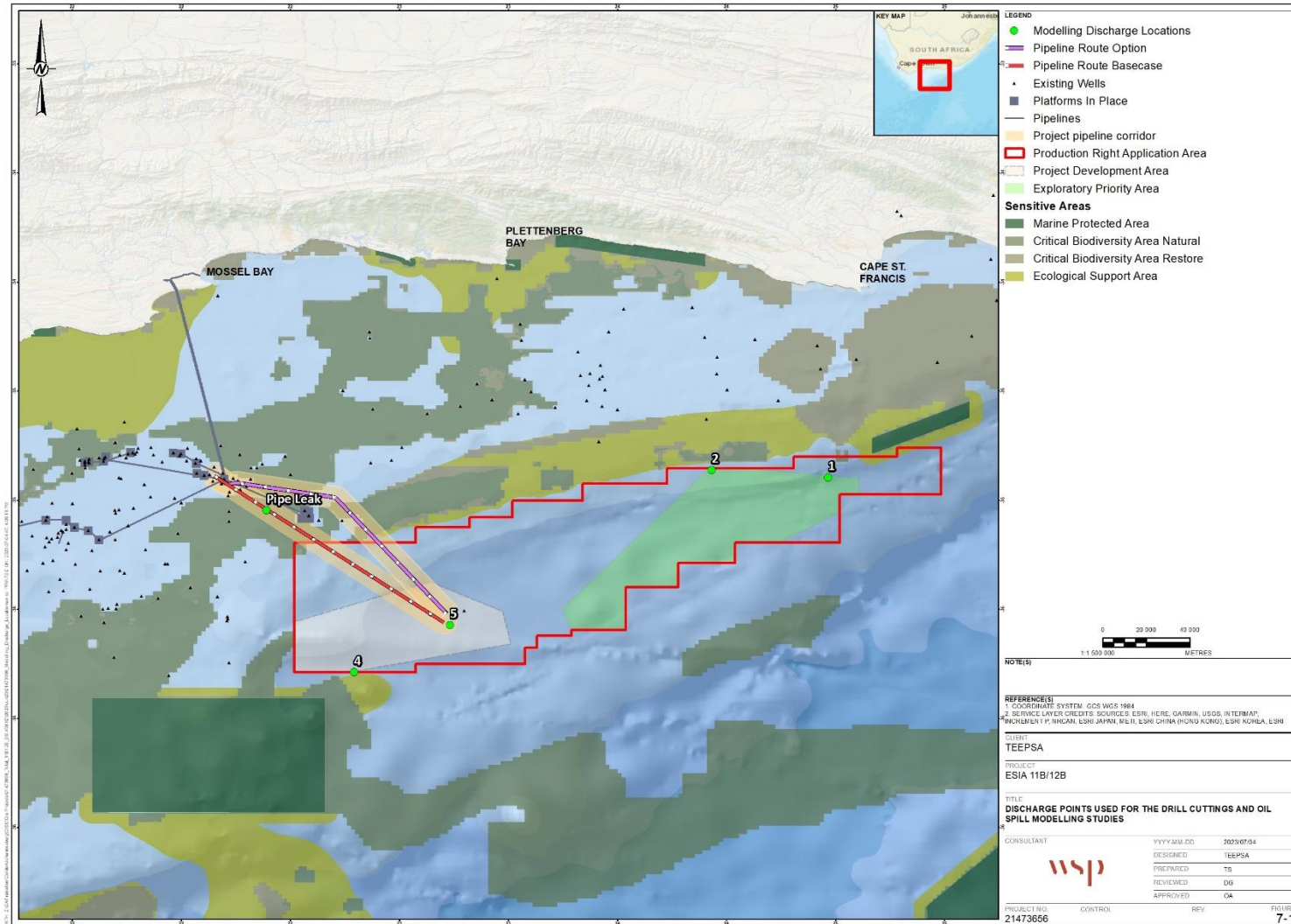


Figure 1-1 - Locations of Discharge 4, Discharge 5, and condensate Pipe Leak in the study area

The primary driver of ocean dynamics in Block 11B/12B is the strong Agulhas Current which flows southward along the east coast of Africa from 27°S to 40°S and is estimated to transport 70 million cubic metres of water per second. Figure 1-2 shows drifter derived surface current velocities and spatial extent of the flow. The eastward Agulhas Return Current at approximately 40°S can also be seen.

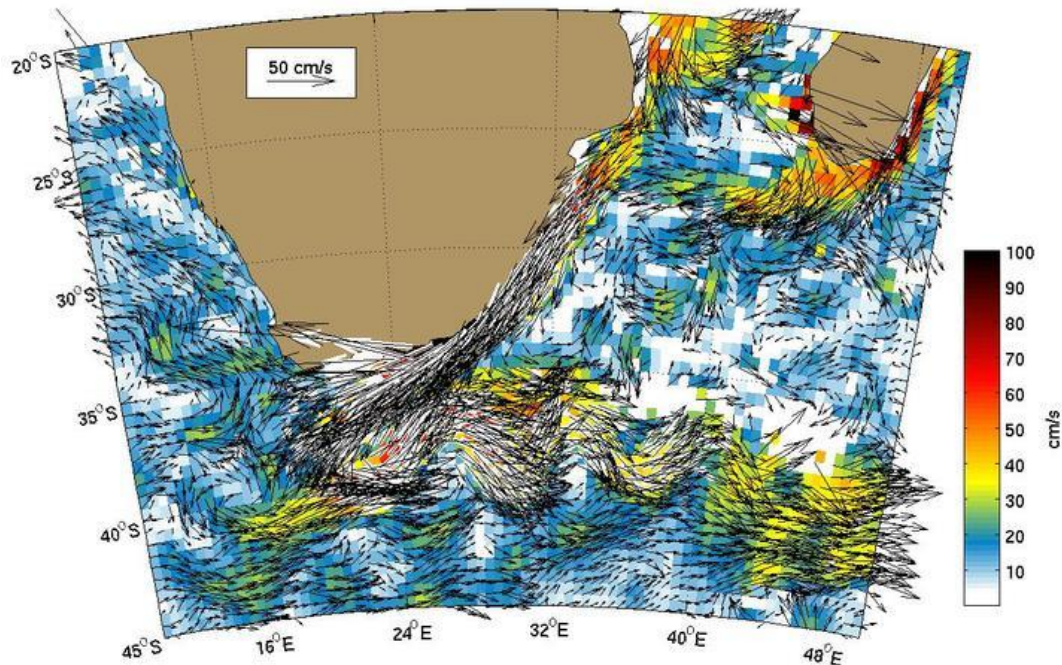


Figure 1-2 - Mean ocean surface velocities derived from satellite-tracked drifters following the ocean at 15 m depth
(https://oceancurrents.rsmas.miami.edu/atlantic/agulhas_2.html)

The licence block 11B/12B is located on the inner edge of the Agulhas Current that is subject mainly to strong steady south-westward Agulhas Current flows but also flow reversals associated with:

- shear edge features (e.g., Lutjeharms *et al.*, 1988, 2003; Krug *et al.*, 2014; Tedesco *et al.*, 2019), and
- larger-scale variability due to occasional large-scale perturbations of the Agulhas Current such as the passing of Natal Pulses (e.g., Lutjeharms and Roberts, 1988; Roualt and Penven, 2011) that are evidenced throughout the depth of the water column (Lutjeharms *et al.*, 2001).

Such perturbations (Figure 1-3 and Figure 1-4) strongly influence the largely wind-driven flows and associated water column structures of the adjacent Agulhas Bank (Boyd and Shillington, 1994; Largier and Swart, 1987; Swart and Largier, 1987; Largier *et al.*, 1992; Bailey *et al.*, 2022); . This influence extends into coastal embayments of the eastern Agulhas Bank (Schumann *et al.*, 1988; Goschen and Schumann, 1990).

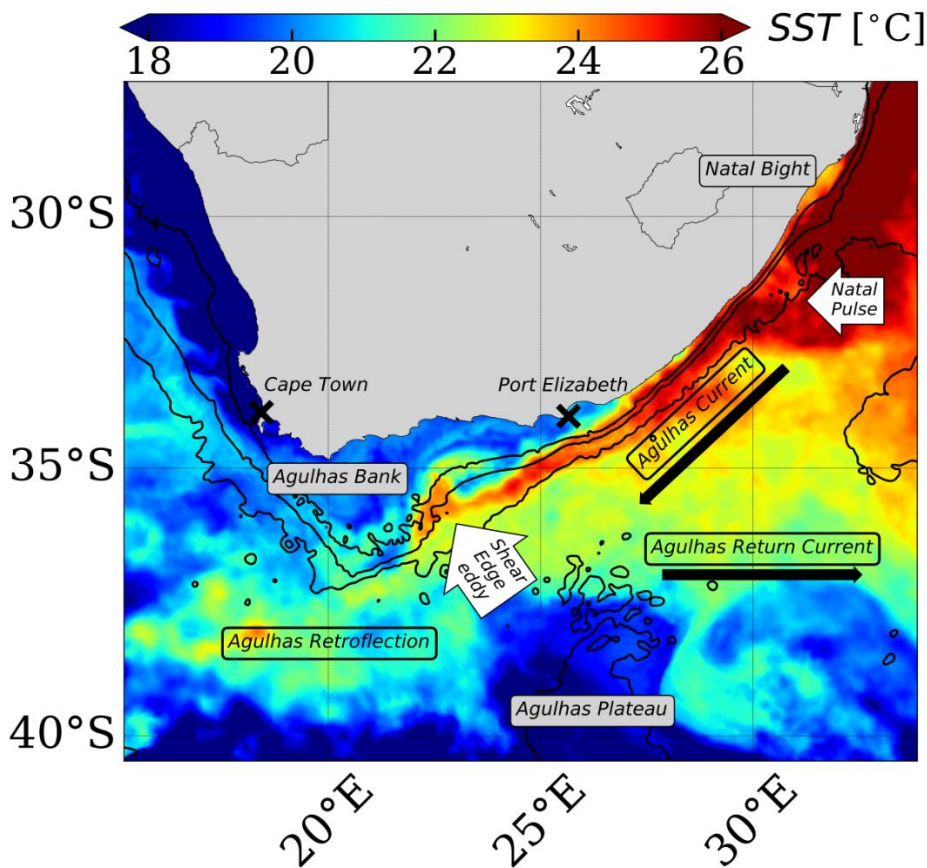


Figure 1-3 - Satellite-derived sea surface temperature (°C) for 4 June 2014 showing the main features of the Agulhas Current, including the shear edge features on the inner edge of the Agulhas Current and early evidence of an upstream Natal Pulse that will propagate downstream resulting in a major perturbation of flows in Block 11B/12B. The black lines represent the 200, 1000, and 3000 m isobaths (Source: Tedesco *et al.*, 2019)

Discharge locations 4 and 5 are situated on the inner edge of the Agulhas Current that is strongly influenced by the predominantly strong south-westerly surface flows of the Agulhas Currents. These flows are significantly weaker at depth and more prone to current reversals. There is evidence of a more persistent current reversals in the deeper waters (> 1 500 m) on the inshore edge of the upstream regions of the Agulhas Current (Beal and Bryden, 1997; Beal, 2009; Beal *et al.*, 2015), an influence that could extend into licence Block 11B/12B but at slightly greater depths (~ 1 800m).

The Pipe Leak (rupture) discharge location, in the shallower waters (~ 140 m to 150 m water depth) of the adjacent Agulhas Bank is more strongly influenced by wind driven flows, particularly in the surface waters where there is evidence of more persistent north-easterly wind-driven flows in the surface waters associated with the strong westerly winds associated with passing mid-latitude cyclones (“cold fronts”) that occur during the winter months.

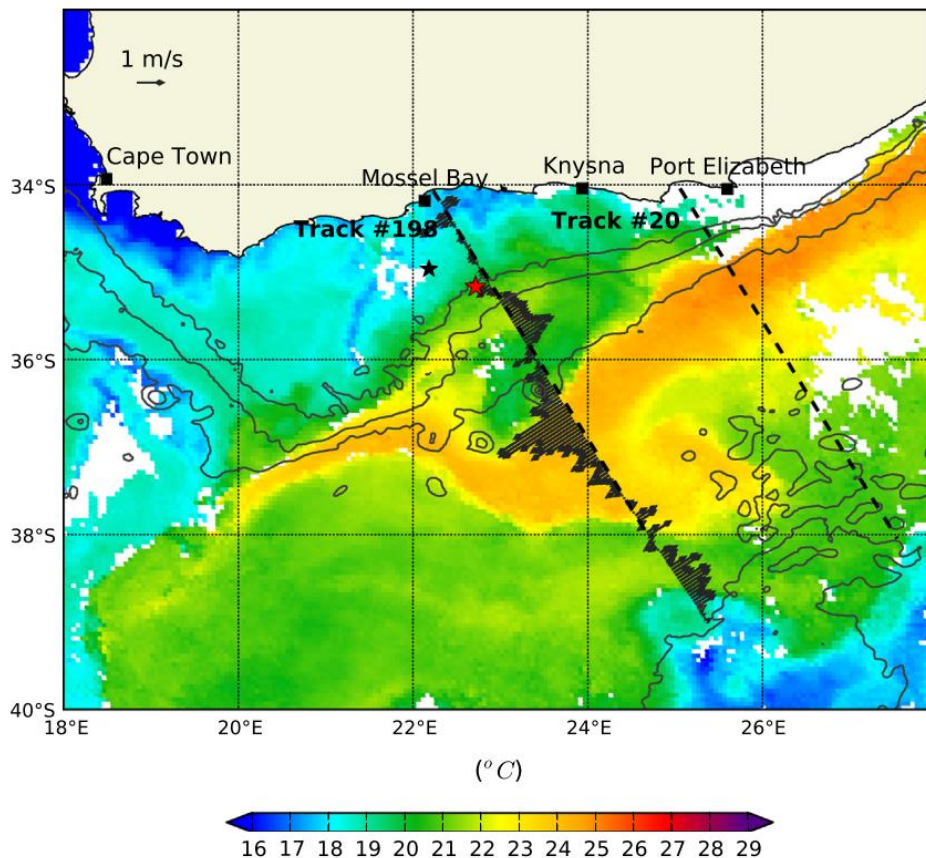


Figure 1-4 - Daily composite of SEVIRI SST on 13 May 2009, during the passage of a Natal Pulse. Overlaid vectors represent the cross-track absolute geostrophic current velocities derived from the high resolution along-track altimetry (Source: Krug and Dufois, 2014).

Early studies suggested based on limited data suggested a lack of seasonality in the surface core speeds of the Agulhas Current (Pearce and Gründlingh, 1982). More recent studies have indicated a seasonality in the volume fluxes of the Agulhas Current (Beal *et al.*, 2015; Hutchinson, 2018), however it is not clear how this would influence current speeds in the region of interest to the drilling discharge and oil spill modelling studies. Despite this limited evidence of seasonality in the Agulhas Current speeds, it is rather the major changes in current speeds expected for the offshore discharge locations due to the onshore-offshore movement of the Agulhas Current, shear edge features and major episodic perturbations such as the passing of a Natal Pulse (Lutjeharms *et al.*, 1989; 2003; Krug *et al.*, 2014), that are of greatest relevance. However, as noted above, there is an increasing seasonality in the current flows upon moving further inshore into the increasingly shallow waters of the Agulhas Bank and coastal embayments, this being particularly true for the surface waters.

The drilling cutting discharge modelling is strongly influenced by the Agulhas Currents flows occurring throughout the water column. Given that the influences of drilling discharges mainly are confined to deeper waters, it is not expected that there will be evidence of significant seasonal variability in such influences. The major variability will be due to shear edge features (that have a greater influence in surface waters) and major perturbations of the of the Agulhas Current such as those due to Natal Pulses (that typically influence the full water column). The transport and fate of the condensate

in the oil spill modelling, although influenced by deeper flows as the condensate rises through the water column, is predominantly determined by surface flows (whether those of the Agulhas Current in deeper waters or those of the mainly wind-driven flows in the shallower waters of the adjacent Agulhas Bank). The capturing of seasonal effects in the oil spill modelling therefore is important. This is adequately achieved by the use stochastic simulations undertaken throughout the year.

The key characteristics of wind and current at the three discharge locations are presented in Table 1-1. Note that oceanographic convention is used for current direction which indicates the direction *towards* which the current flows. Meteorological convention is used for wind direction and signifies the direction *from* which the wind blows. The wind speed is reported at the standard elevation of 10 m above MSL and corresponds to a 10-minute average.

Table 1-1 - Discharge location characteristics

Location	Longitude (Deg WGS 84)	Latitude (Deg WGS 84)	Depth (m)	Current - primary direction (to)	Wind - primary direction (from)
4	22.745542° E	35.782903° S	~1600	SW to WSW	WSW to WNW
5	23.141025° E	35.588141° S	~1815	SW to WSW	WSW to WNW
Pipe leak	22.383794° E	35.116225° S	~146	SW to WSW	WSW to W, E

1.2 ENVIRONMENTAL DATA

Environmental data at Discharge 4 and 5 are summarized in Table 1-2.

Table 1-2 - Environmental average data (Discharge 4 & 5 PARTRACK Modelling SRF, TEEPSEA, 2022)

Environmental Parameter	Value	
Upper water column temperature (°C)	20.9	
Middle water column temperature (°C)	6.3	
Lower water column temperature (°C)	3.1	
Air Temperature (°C)	19.3	
Salinity (PSU)	Surface (0 m)	35.4
	Middle (1250 m)	34.6
	Bottom (2500 m)	34.8
Seawater oxygen content (mg/l)	Upper	7.7
	Lower	6.9
Median grain size (mm)	0.3	
Suspended sediment (mg/l)	0	

1.3 DISPERSION MODELLING SIMULATION PERIODS

Metocean data was analysed for four seasons: Season 1 (December – February (Summer)); Season 2 (March – May (Fall)); Season 3 (June – August (Winter)); Season 4 (September – November (Spring)). Average metocean conditions for each discharge location and season are presented in Table 1-3. Sections 2 and 3 of this report provide the detailed results derived from data at Discharge 4 and Discharge 5, respectively.

Table 1-3 - Overview of metocean conditions by season at Discharge 4, 5, and Pipe Leak for 2012 - 2016

		Discharge 4				Discharge 5				Pipe Leak			
		S1	S2	S3	S4	S1	S2	S3	S4	S1	S2	S3	S4
Surface Current	Average (m/s)	1.4	1.2	1.1	1.4	1.5	1.4	1.2	1.5	0.4	0.4	0.6	0.5
	Maximum (m/s)	3.1	3.4	4.8	3.8	3.1	3.6	4.9	3.8	2.6	2.7	5.0	3.5
	Most frequent Direction	SW	SW	SW	SW	SW	SW	SW	SW	SW	SW	NE	SW
Winds	Average (m/s)	7.7	8.2	9.9	9.1	7.6	8.2	9.8	9.1	6.8	7.0	8.6	8.2
	Maximum (m/s)	23.2	24.1	27.8	23.5	21.9	24.1	27.8	23.7	21.0	19.9	24.5	22.5
	Most frequent Direction	E	W	W	W	E	ENE	W	W	E	W	W	WSW

2 DISCHARGE 4

The average metocean data at the Discharge 4 location over the five-year dataset is presented in Figure 2-1.

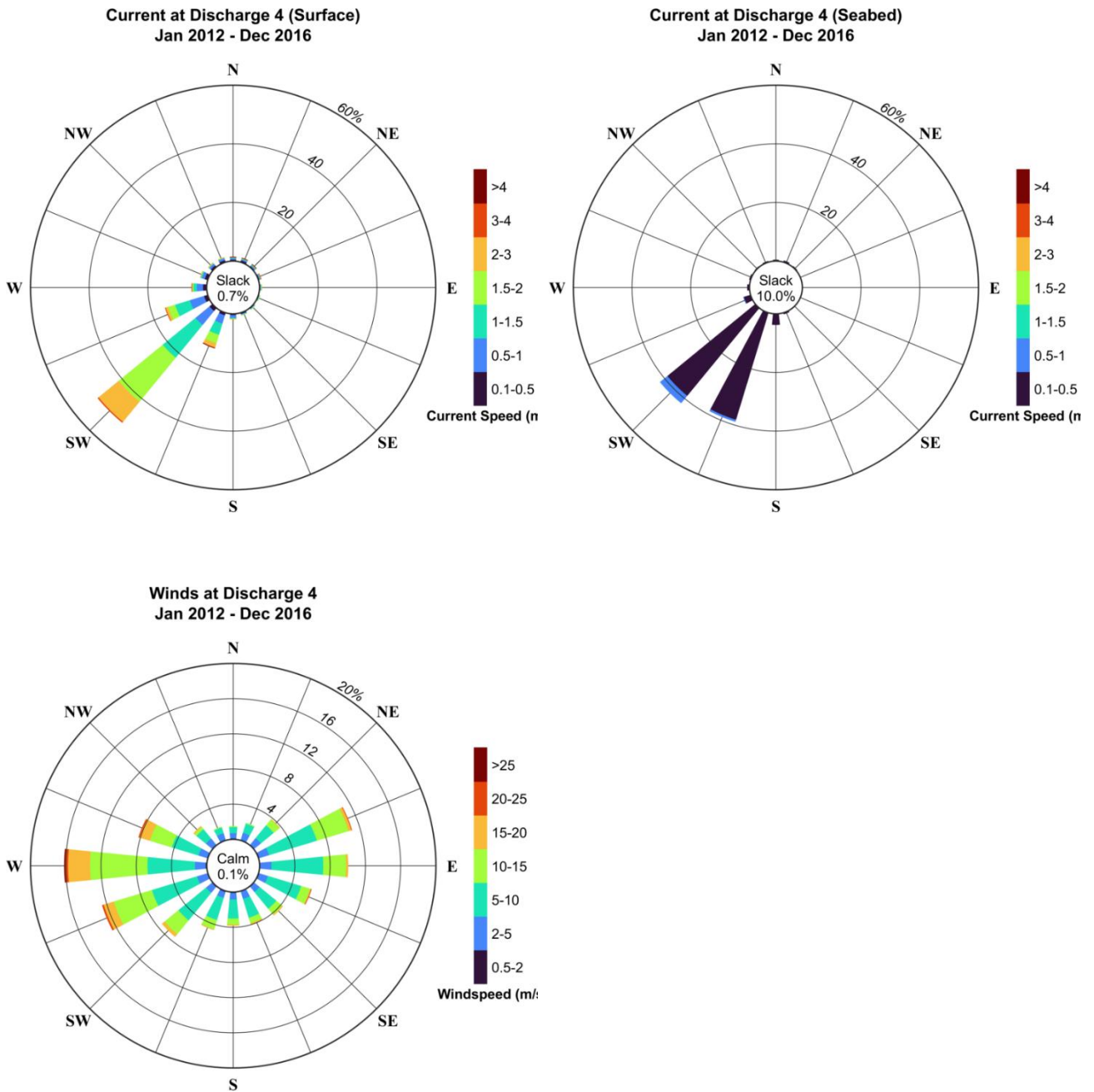


Figure 2-1 - Average annual current and wind speed roses at Discharge 4 for 2012-2016



The dominant direction for surface current at Discharge 4 is towards SW for the 2012 to 2016 period with an occurrence probability greater than approximately 50%. Current speeds can reach up to 4 m/s at the surface.

Dominant current direction at the seabed is towards SSW and SW for approximately 80% of the time. Part of the drill cuttings are discharged at the seabed, which makes seabed currents an important factor in drilling discharge modelling.

Dominant wind directions are from between WSW and WNW (approximately 36% of the time), and ENE and ESE (approximately 27% of the time). Wind speeds are mostly in the 5 m/s to 20 m/s range.

Figure 2-2 and Table 2-1 present the average monthly current roses at the surface for 2012 to 2016 and the associated statistics, respectively. The surface current at Discharge 4 is predominantly directed to the southwest in all months. There are periods of the year (Feb, May and June) when occurrences of flow towards the north are also observed. The peak monthly surface current speed of 4.8 m/s to NNE, and 4.2 m/s to SSW occur in June and July, respectively. These comprise strong wind-driven flows associated with the passing “cold fronts” that occur during the winter season. The nearest coastal regions lie to the north and NNE of Discharge 4.

Table 2-1 - Yearly and monthly surface current speed and direction statistics at Discharge 4

SPEED (M/S)	YRLY	JAN	FEB	MAR	APR	MAY	JUN	JUL	AUG	SEP	OCT	NOV	DEC
Median	1.2	1.5	0.7	1.4	1.3	0.8	1.0	1.1	1.1	1.3	1.2	1.6	1.8
Mean	1.3	1.6	0.9	1.4	1.3	0.9	1.1	1.1	1.2	1.3	1.2	1.6	1.7
Std. deviation	0.0	0.5	0.6	0.6	0.6	0.6	0.6	0.6	0.6	0.6	0.6	0.5	0.5
Minimum	0.0	0.1	0.0	0.1	0.1	0.0	0.0	0.0	0.1	0.0	0.1	0.1	0.1
Maximum	4.8	3.1	2.9	3.4	3.0	3.0	4.8	4.2	3.1	3.6	3.8	3.0	3.1
Most frequent direction	SW	SW	SW	SW	SW	SW	SW	SW	SW	SW	SW	SW	SW
Strongest current direction	NNE	SSW	SSW	SW	SW	SW	NNE	SSW	SW	SW	NNE	SW	WSW

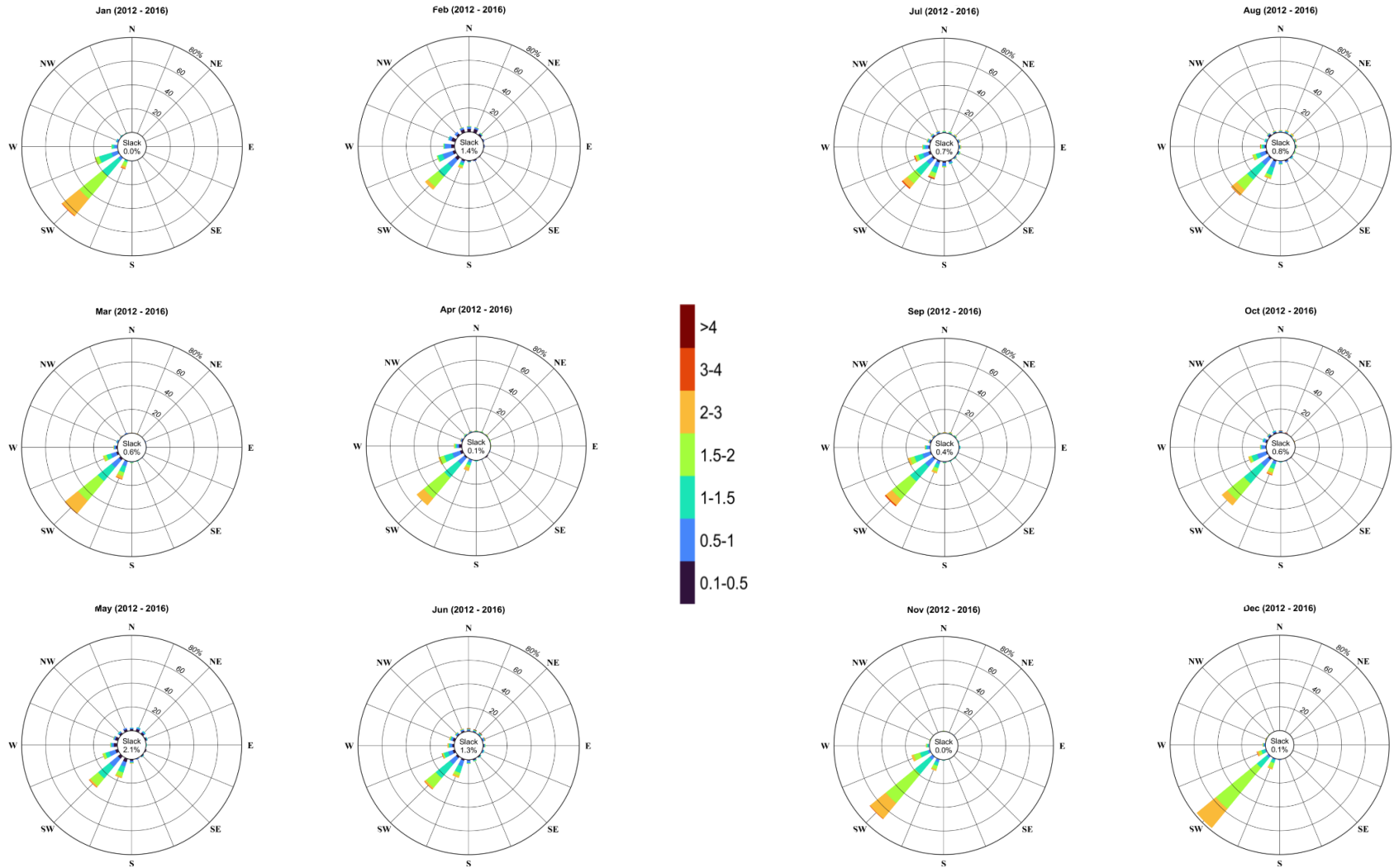


Figure 2-2 - Average monthly surface current roses at Discharge 4 for 2012 – 2016 (colour bar represents current speed in m/s)

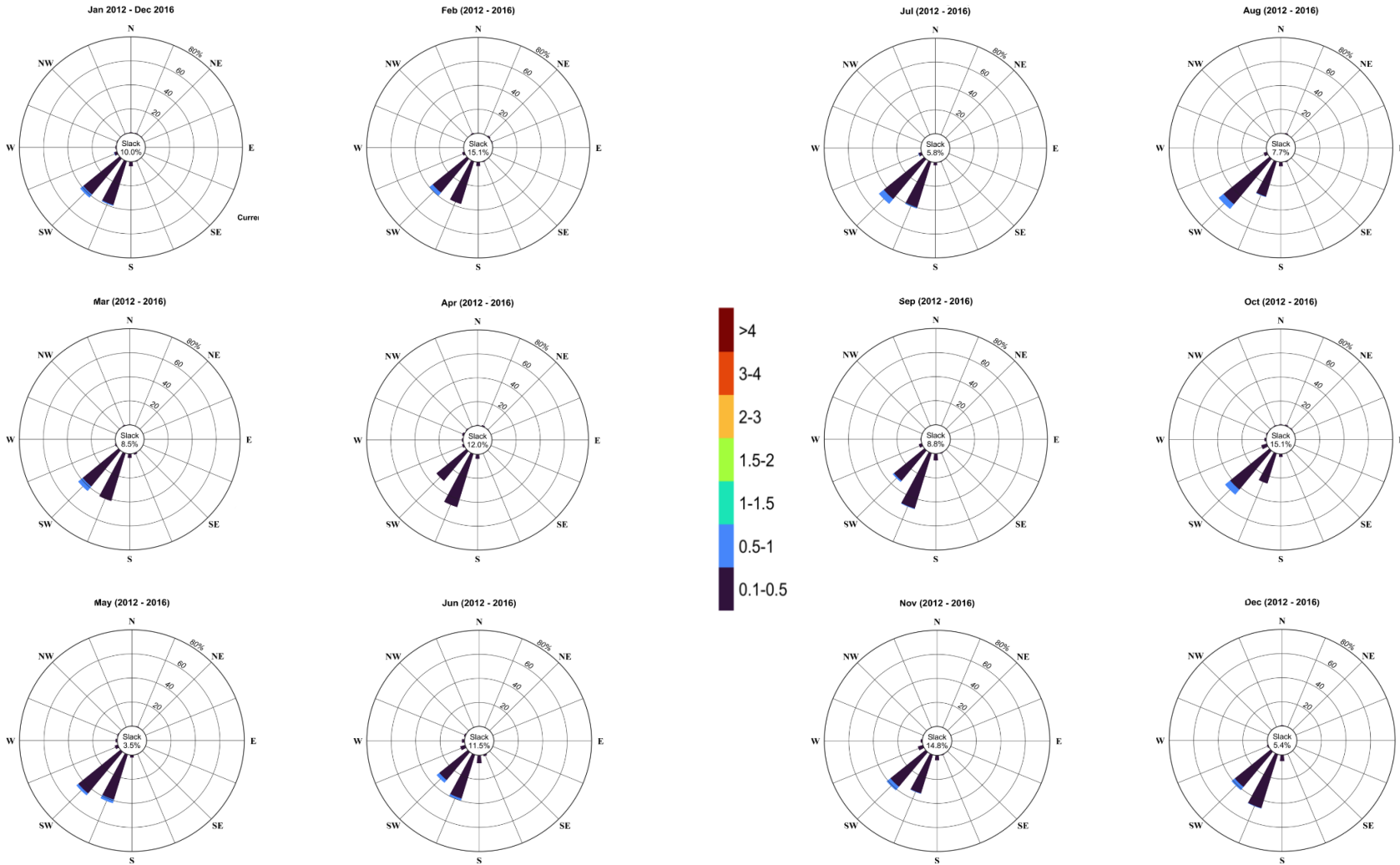


Figure 2-3 - Average monthly seabed current roses at Discharge 4 for 2012 – 2016 (colour bar represents current speed in m/s)

Figure 2-3 and Table 2-2 present the monthly current roses at the seabed for 2012 to 2016 and their associated statistics, respectively. The seabed currents present a low directional variability compared to the surface currents (Figure 2-3) and the dominant flow direction is to the southwest. Table 2-2 shows that the current speed is higher in the period from May to September (end of Q2 and Q3), and the dominant direction is largely SW.

Table 2-2 - Yearly and monthly seabed current speed and direction statistics at Discharge 4

SPEED (M/S)	YRLY	JAN	FEB	MAR	APR	MAY	JUN	JUL	AUG	SEP	OCT	NOV	DEC
Median	0.2	0.2	0.3	0.2	0.2	0.3	0.2	0.2	0.2	0.2	0.2	0.2	0.2
Mean	0.2	0.2	0.3	0.3	0.2	0.3	0.2	0.3	0.3	0.2	0.3	0.2	0.3
Std. deviation	0.0	0.1	0.1	0.1	0.1	0.1	0.1	0.1	0.1	0.1	0.1	0.1	0.1
Minimum	0.0	0.0	0.0	0.0	0.0	0.0	0.0	0.0	0.0	0.0	0.0	0.0	0.0
Maximum	0.9	0.6	0.6	0.6	0.5	0.7	0.7	0.9	0.6	0.5	0.6	0.7	0.6
Most frequent direction	SW	SW	SW	SSW	SSW	SW	SW	SW	SW	SSW	SW	SW	SSW
Strongest current direction	SW	SW	SW	SW	SW	SSW	SW	SW	SW	SW	SW	SW	SW

Figure 2-4 and Table 2-3 present the average monthly wind speed and direction statistics at 10 m elevation above sea level. Winds mainly occur in the east and west quadrants. The most frequent direction for stronger winds (>15 m/s) is from W over the five-year analysis period. The period from May to September also experiences mostly westerly winds.

Table 2-3 - Yearly and monthly wind speed and direction statistics at Discharge 4

SPEED (M/S)	YRLY	JAN	FEB	MAR	APR	MAY	JUN	JUL	AUG	SEP	OCT	NOV	DEC
Median	8.3	7.5	7.5	8.2	7.8	7.8	9.7	9.7	9.2	9.7	9.0	8.4	7.7
Mean	8.7	7.5	7.7	8.2	8.0	8.3	10.0	10.1	9.7	9.9	8.9	8.6	7.8
Std. deviation	0.6	3.1	3.1	3.1	3.6	3.9	4.7	4.6	4.5	3.9	3.3	3.5	3.1
Minimum	0.2	0.3	0.3	0.5	0.6	0.3	0.5	0.2	0.6	0.8	0.4	0.3	0.3
Maximum	27.8	19.4	19.4	24.1	20.5	19.7	27.8	23.8	24.9	23.5	22.1	23.0	23.2
Most frequent direction	W	E	ENE	ENE	ENE	W	W	W	W	W	ENE	WSW	E
Strongest wind direction	W	W	W	W	W	W	W	W	W	W	W	WSW	WSW

In summary, the current data at Discharge 4 for the years 2012 to 2016 indicates flow at the sea surface mostly towards the SW for all months with some variability in speed, and mostly constant SW flow direction and speed at the seabed for all months. There are periods of the year (Feb, May and June) when occurrences of surface flow towards the north are also observed. The months of May to September also see an increase in the frequency and strength of winds from the west compared to other times in the year

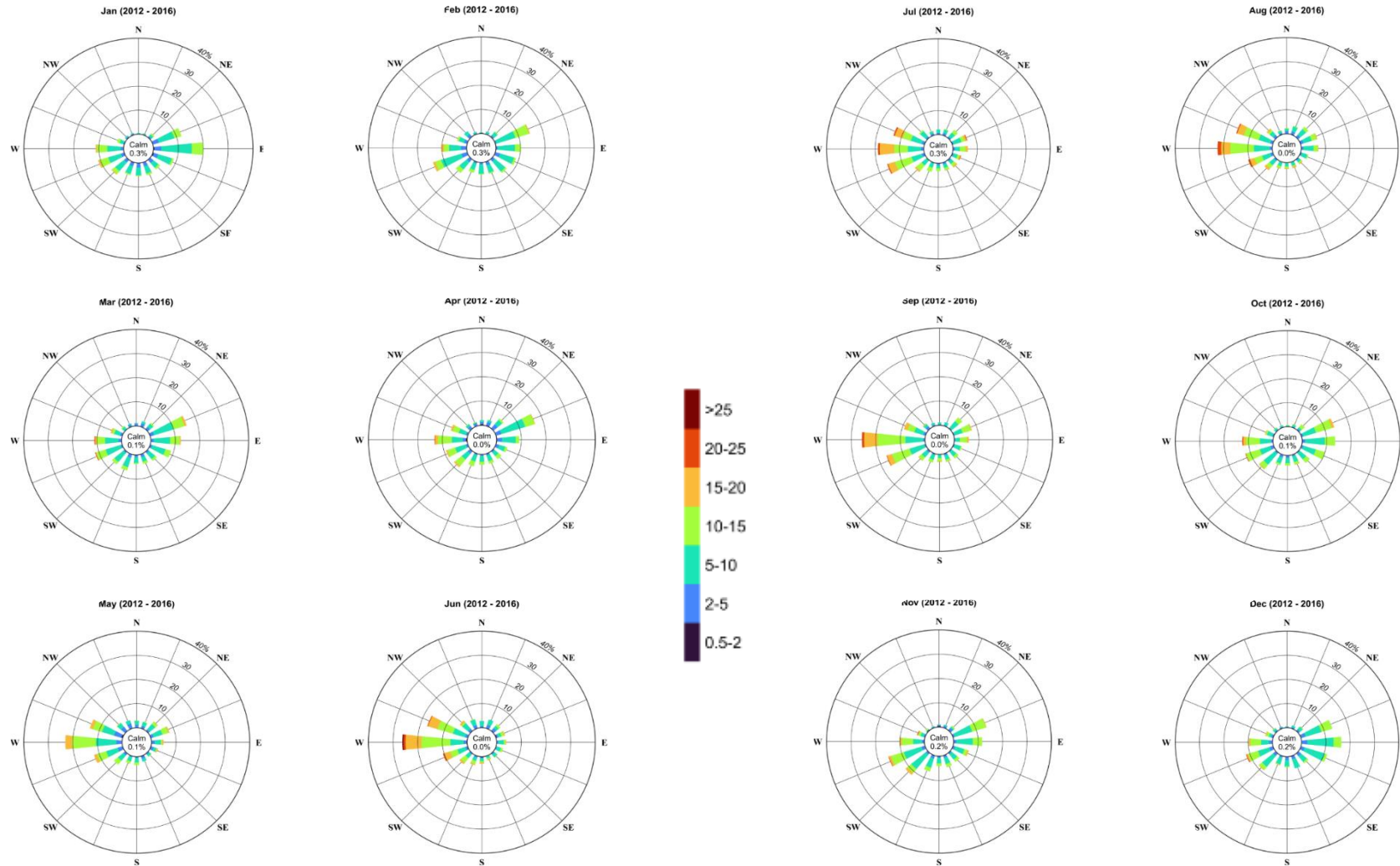


Figure 2-4 - Average monthly wind roses at Discharge 4 for 2012 – 2016 (colour bar represents wind speed in m/s)

2.1 SELECTION OF DRILLING DISCHARGE SIMULATION PERIODS FOR DISCHARGE 4

Simulations for the dispersion of drill cuttings and drilling muds from well drilling operations at Discharge 4 require the selection of a suitable model start time in each season. The methodology to identify the start time for each season in the present study involved an examination of the near-seabed and surface current speed and direction which would lead to maximum transport of drilling discharges towards the nearest Marine Protected Area (MPA). For Discharge 4, the nearest MPA is the Southwest Indian Seamount Marine Protected Area, whose NE corner lies approximately 18.1 km to the SW as shown in Figure 2-5.

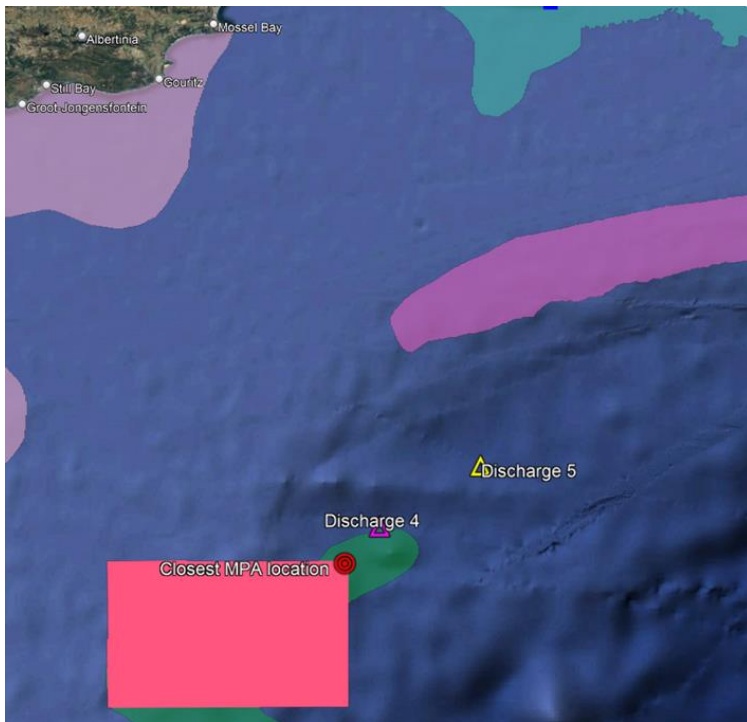


Figure 2-5 - Locations of Discharge 4 and Discharge 5 relative to Southwest Indian Seamount MPA

Based on information provided by Total, there are two distinct discharge phases over the course of drilling a well:

- Riserless phase – representing the first 270 hrs of operations, which includes 54 hrs of discharge at the seabed and 216 hrs (9 days) of no discharge. The total mass of cuttings and drilling mud released at the seabed during this phase is 1127 tonnes and 2326 tonnes, respectively.
- Riser phase – representing the next 344 hrs of drilling operations, which includes 200 hrs of discharge at 10 m below the water surface and 144 hrs (6 days) of no discharge. The total mass of cuttings and drilling mud released during this phase is 478 tonnes and 4100 tonnes, respectively.

Figure 2-6 illustrates the sequence of drilling discharge operations and the time spent for each operation. Figure 2-7 shows the quantity (mass in tonnes) of the drilling muds and cuttings discharged from the commencement of drilling to the final HPWBM mud discharge at the end of the 8.5” diameter section of the well.

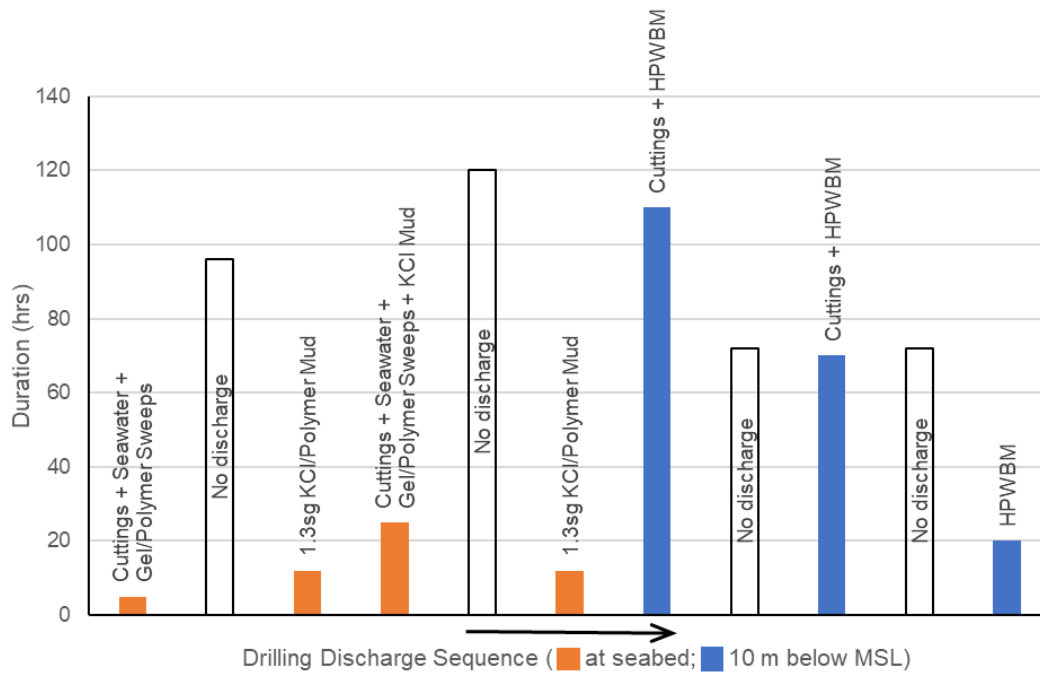


Figure 2-6 - Typical sequence and duration of mud and cuttings discharges

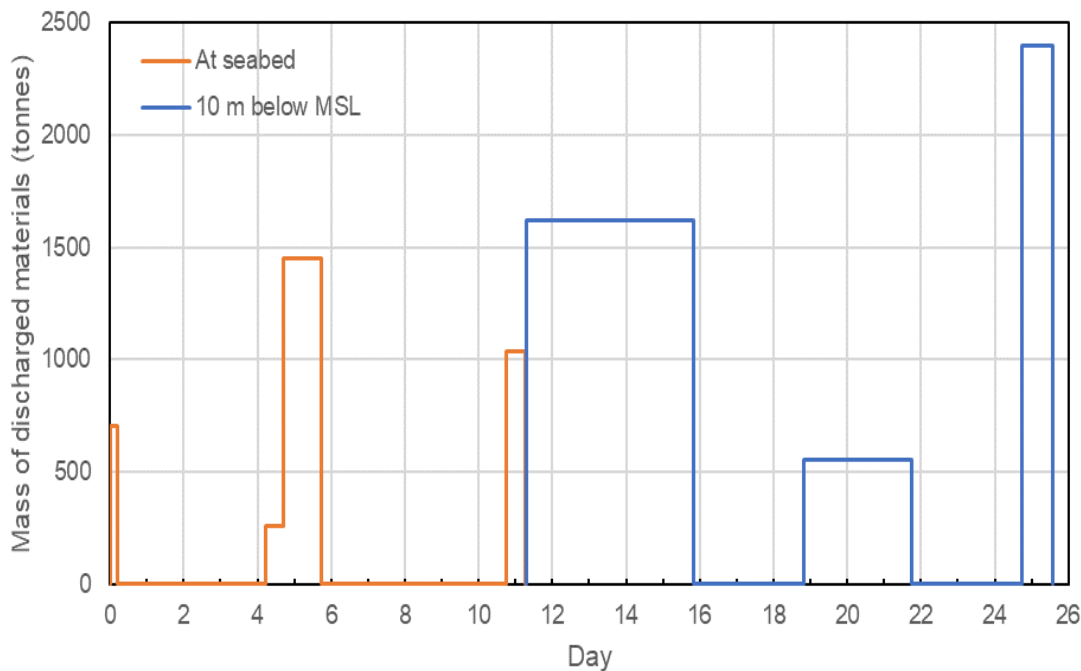


Figure 2-7 - Variation of discharged mud and cuttings quantity with time at drilling location

Since discharges at both the seabed and close to the water surface have the potential to reach the MPA, the current speed and direction data at these elevations were analysed to estimate the periods of time when the maximum combined seabed and surface transport of seawater towards the MPA occurred during each season in the 5-year metocean dataset. It is these periods that were used for the model simulations.

2.1.1 SEASON 1- DECEMBER TO FEBRUARY

Figure 2-8 presents summary statistics of current speed and direction at the seabed for each month of Season 1. Maximum current speed tends to mostly remain in the range of 0.4 m/s to 0.6 m/s, while average speed mostly lies in the 0.2 m/s to 0.3 m/s range. The most frequently occurring flow direction for the strongest 10% of the seabed currents is almost always to the southwest with a couple of months in 2016 showing stronger flows to the SSW. These observations are most probably related to large-scale perturbation of the Agulhas Currents due to the passing of a Natal Pulse.

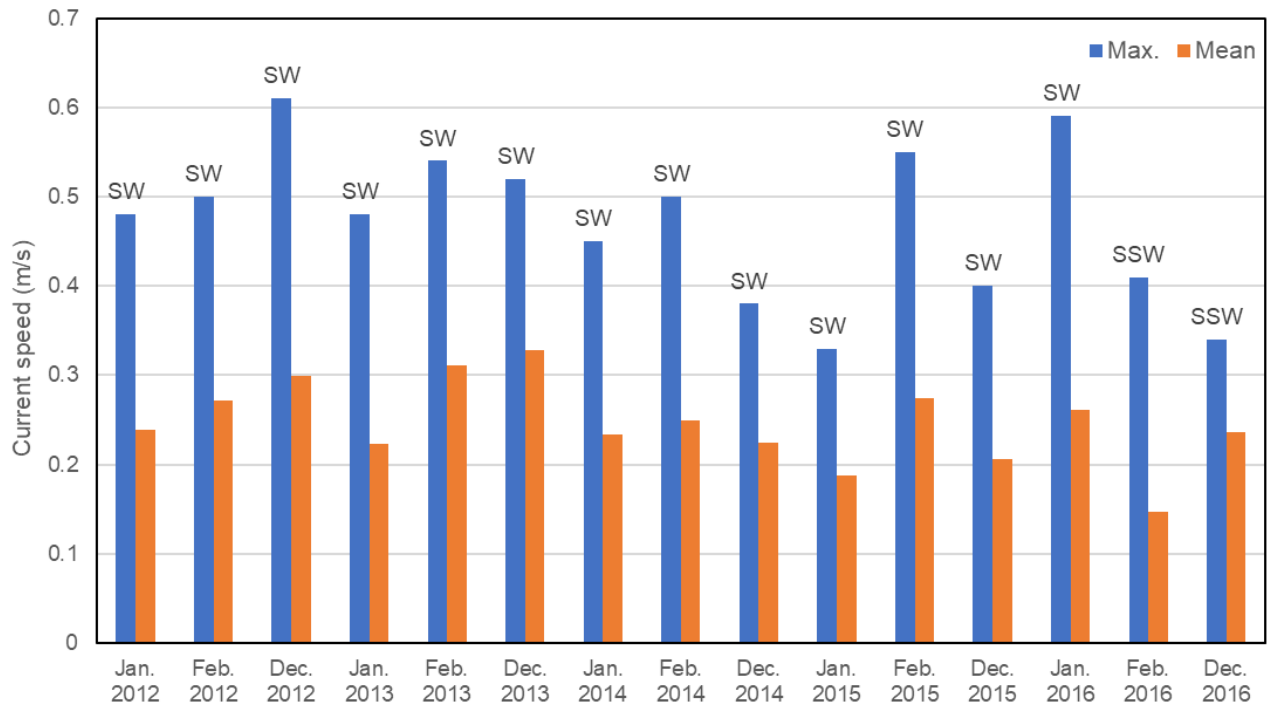


Figure 2-8 - Bottom current mean and maximum speed, and primary direction at Discharge 4 for Season 1 (2012 – 2016)

Figure 2-9 shows the current vectors at the seabed and surface at Discharge 4 for a 45-day period from 17 Dec 2015 to 30 Jan 2016. For clarity, the seabed and surface current vectors are scaled independently. The selected start time for the drilling discharge simulation in **Season 1 is 26 Dec 2015 at 1500 hrs**, as it yields the maximum combined seabed and surface transport of seawater towards the nearest MPA. The simulation periods for the riserless and riser phases of the well drilling are shown in Figure 2-9.

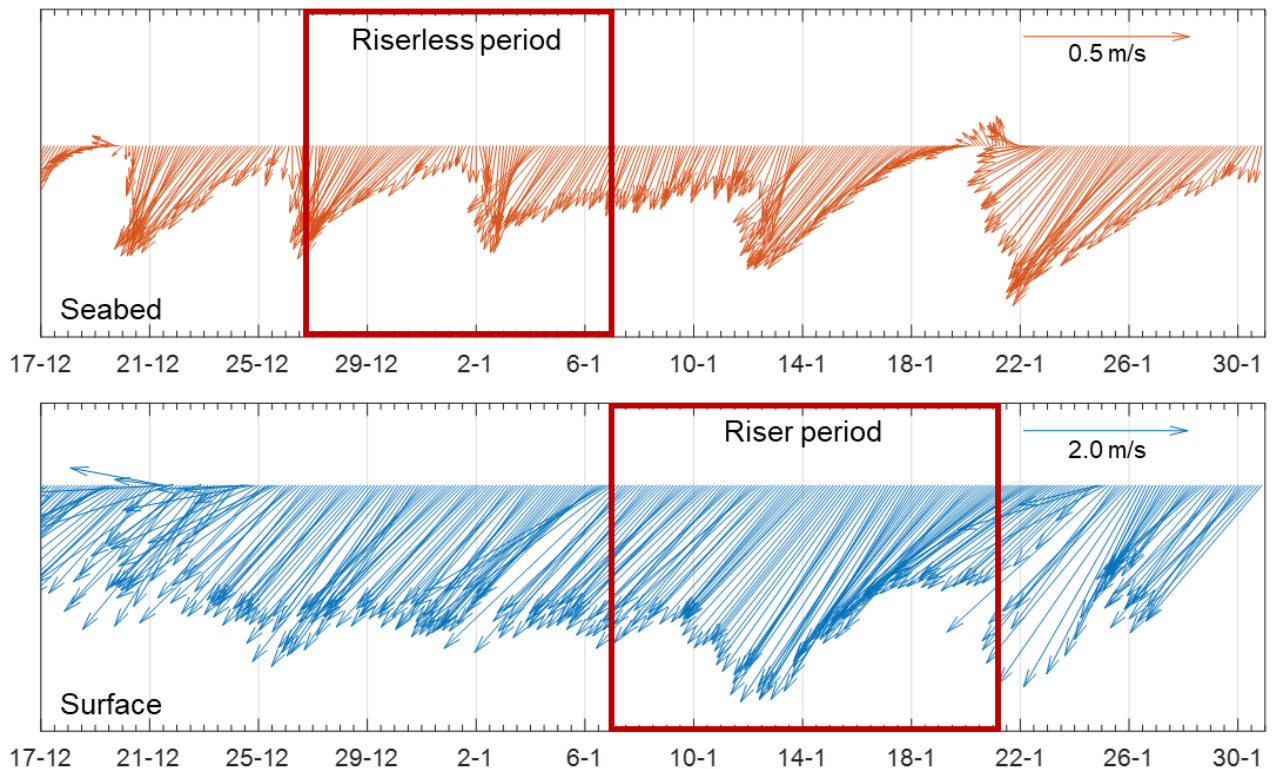


Figure 2-9 - Seabed and surface current vectors at Discharge 4 from 17 Dec 2015 to 30 Jan 2016 with boxes showing the period selected for drilling discharge simulation in Season 1

2.1.2 SEASON 2- MARCH TO MAY

Figure 2-10 presents summary statistics of current speed and direction at the seabed for each month of Season 2. In comparison with Season 1, there is a wider range in the maximum current speed which typically varies between 0.3 m/s to 0.6 m/s. The maximum speed of approximately 0.7 m/s occurs in May 2012. Average current speed is like Season 1 and mostly lies in the 0.2 m/s to 0.3 m/s range. The most frequently occurring flow direction for the strongest 10% of the seabed currents is almost always to the southwest although 2012 and April 2016 had stronger flows to the SSW.

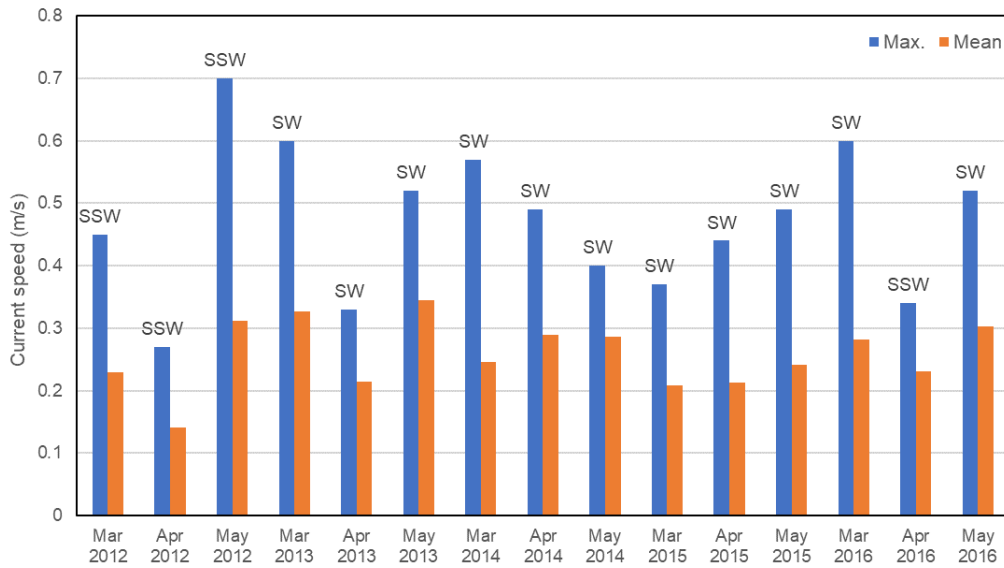


Figure 2-10 - Bottom current mean and maximum speed, and primary direction at Discharge 4 for Season 2 (2012 – 2016)

Figure 2-11 shows the current vectors at the seabed and surface at Discharge 4 for a 45-day period from 3 Mar 2013 to 16 Apr 2013. For clarity, the seabed and surface current vectors are scaled independently. The selected start time for the drilling discharge simulation in **Season 2 is 12 Mar 2013 at 0900 hrs**, as it yields the maximum combined seabed and surface transport of seawater towards the nearest MPA. The simulation periods for the riserless and riser phases of the well drilling are shown in Figure 2-11.

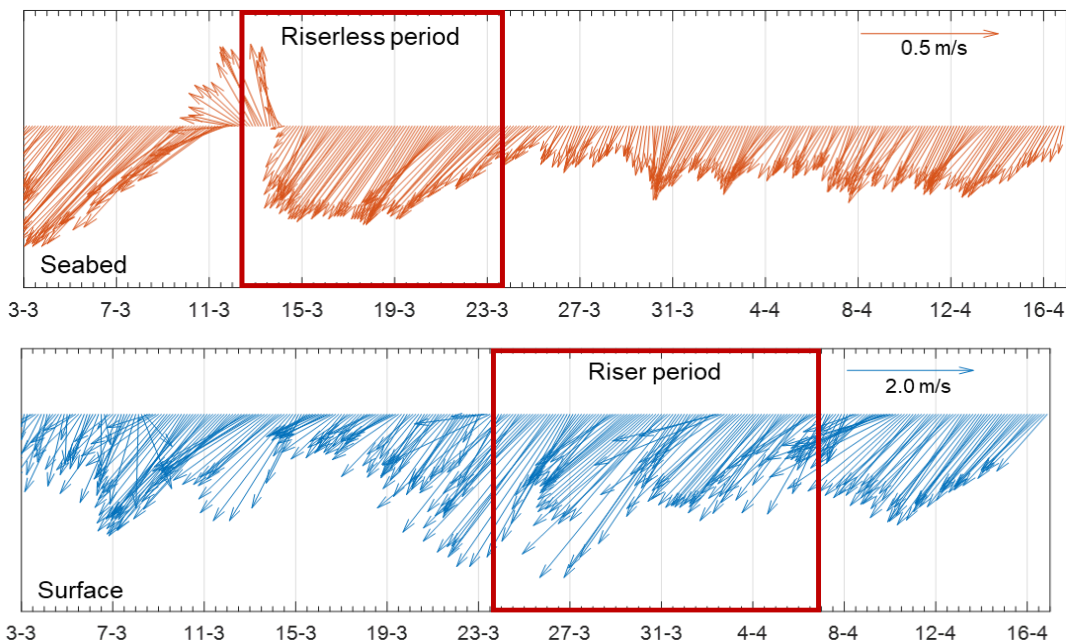


Figure 2-11 - Seabed and surface current vectors at Discharge 4 from 3 Mar 2013 to 16 Apr 2013 with boxes showing the period selected for drilling discharge simulation in Season 2

2.1.3 SEASON 3- JUNE TO AUGUST

Figure 2-12 presents summary statistics of current speed and direction at the seabed for each month of Season 3. The maximum current speed typically varies between 0.4 m/s to 0.6 m/s with a notable outlier of approximately 0.85 m/s occurring in July 2016. Average current speed mainly lies between 0.2 m/s and 0.3 m/s. The most frequently occurring flow direction for the strongest 10% of the seabed currents is almost always to the southwest except in July 2012 when this direction was to the SSW.

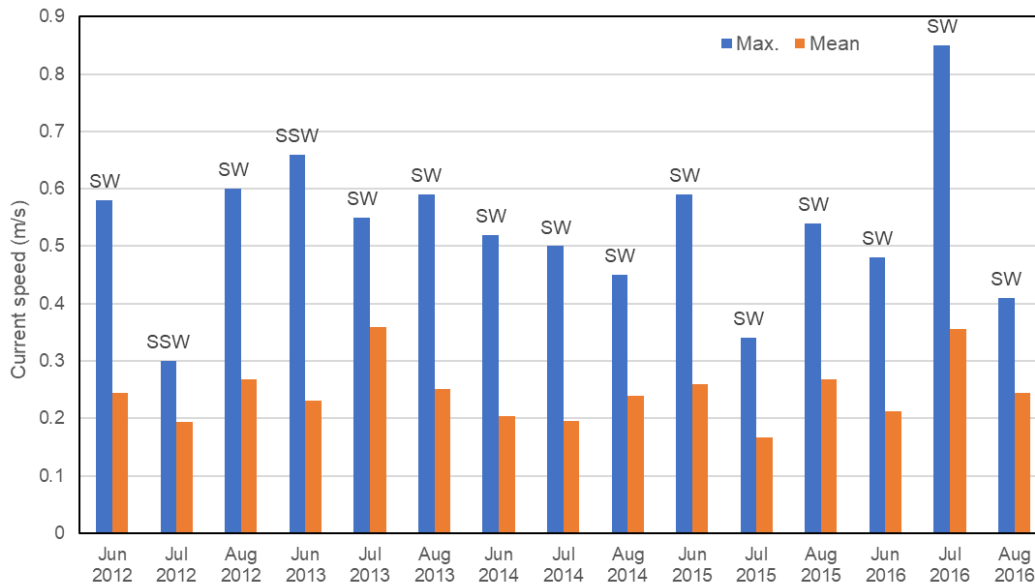


Figure 2-12 - Bottom current mean and maximum speed, and primary direction at Discharge 4 for Season 3 (2012 – 2016)

Figure 2-13 shows the current vectors at the seabed and surface at Discharge 4 for a 45-day period from 5 Aug 2016 to 18 Sep 2016. For clarity, the seabed and surface current vectors are scaled independently. The selected start time for the drilling discharge simulation in **Season 3 is 14 Aug 2016 at 0900 hrs**, as it yields the maximum combined seabed and surface transport of seawater towards the nearest MPA. The simulation periods for the riserless and riser phases of the well drilling are shown in Figure 2-13.

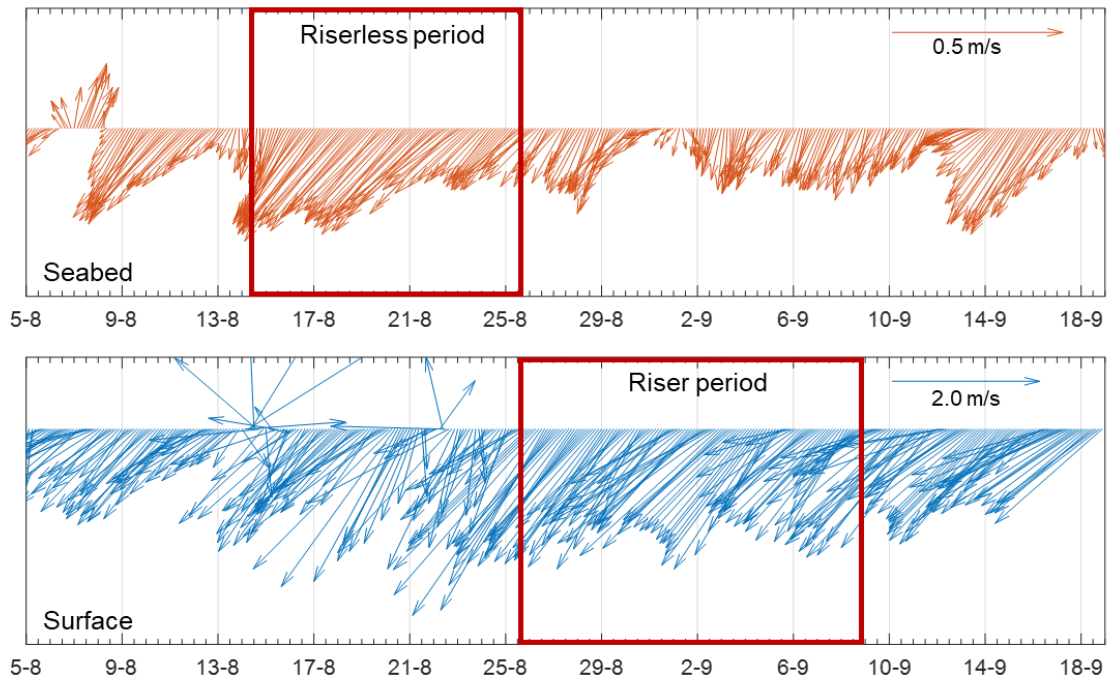


Figure 2-13 - Seabed and surface current vectors at Discharge 4 from 5 Aug 2016 to 18 Sep 2016 with boxes showing the period selected for drilling discharge simulation in Season 3

2.1.4 SEASON 4- SEPTEMBER TO NOVEMBER

Figure 2-14 presents summary statistics of current speed and direction at the seabed for each month of Season 4. The maximum current speed typically varies between 0.4 m/s to 0.5 m/s although Oct and Nov 2012 contain maximum speeds exceeding 0.6 m/s. Average current speed mainly lies between 0.2 m/s and 0.3 m/s. The most frequently occurring flow direction for the strongest 10% of the seabed currents is almost always to the southwest except in Sep and Nov 2016 when this direction was to the SSW.

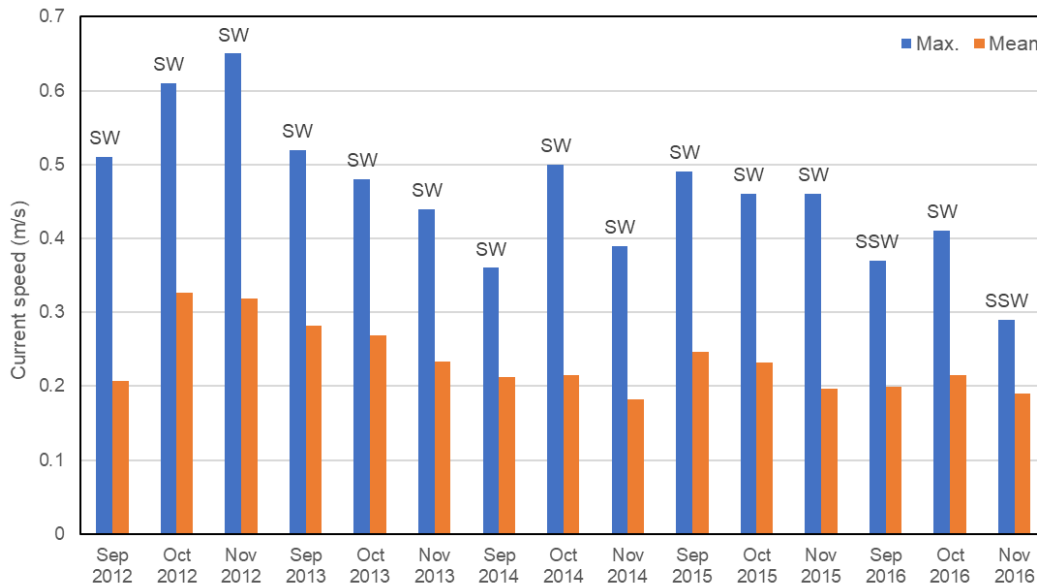


Figure 2-14 - Bottom current mean and maximum speed, and primary direction at Discharge 4 for Season 4 (2012 – 2016)

Figure 2-15 shows the current vectors at the seabed and surface at Discharge 4 for a 45-day period from 10 Oct 2014 to 23 Nov 2014. For clarity, the seabed and surface current vectors are scaled independently. The selected start time for the drilling discharge simulation in **Season 4 is 19 Oct 2014 at 1200 hrs**, as it yields the maximum combined seabed and surface transport of seawater towards the nearest MPA. The simulation periods for the riserless and riser phases of the well drilling are shown in Figure 2-15.

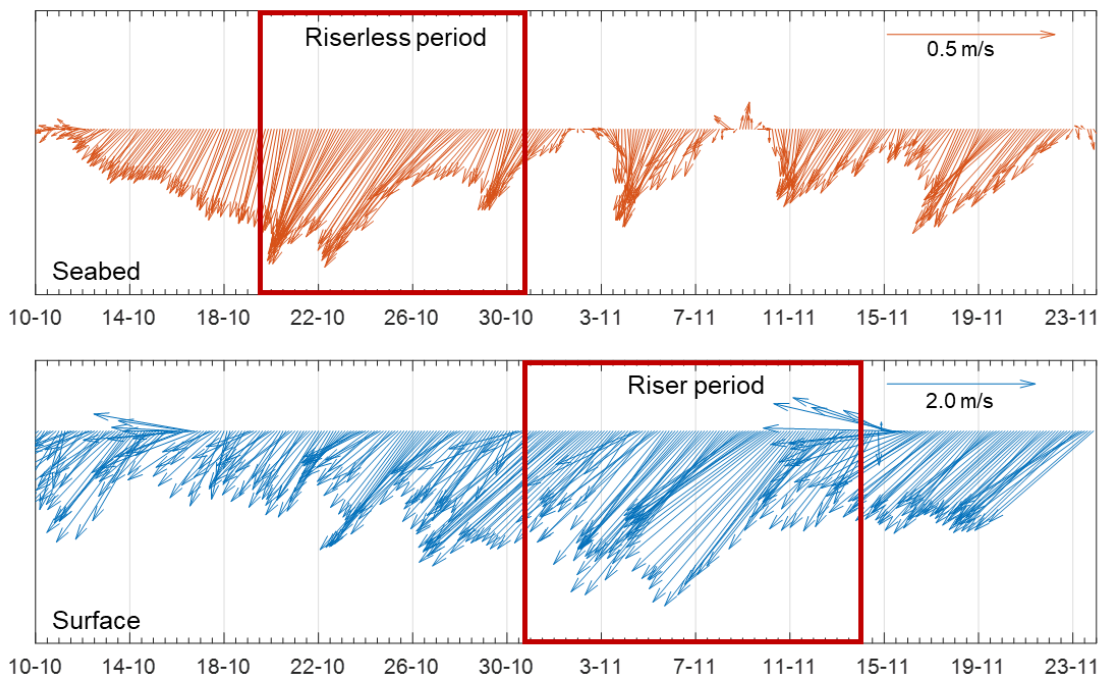


Figure 2-15 - Seabed and surface current vectors at Discharge 4 from 10 Oct 2014 to 23 Nov 2014 with boxes showing the period selected for drilling discharge simulation in Season 4

3 DISCHARGE 5

The average metocean data at the Discharge 5 location over the five-year data is presented in Figure 3-1

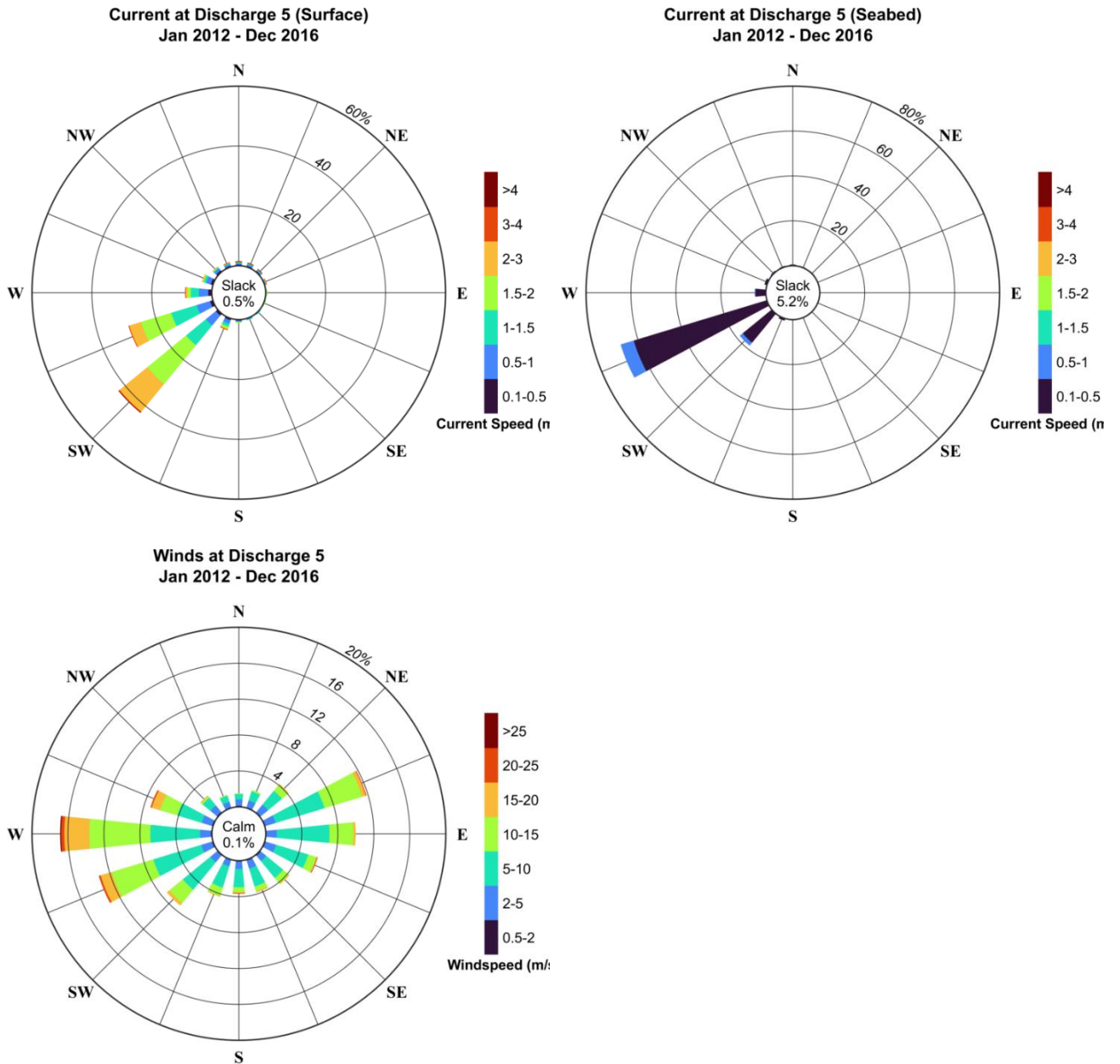


Figure 3-1 - Average annual current and wind speed roses at Discharge 5 for 2012-2016

The dominant direction for surface current at Discharge 5 is towards SW and WSW for the 2012 to 2016 period with an occurrence probability greater than approximately 70%. Current speeds can reach up to 4 m/s at the surface.



Dominant current direction at the seabed is towards WSW and SW for approximately 80% of the time. Part of the drill cuttings are discharged at the seabed, which makes seabed currents an important factor in drilling discharge modelling.

Dominant wind directions are from between WSW and WNW (approximately 36% of the time), and ENE and ESE (approximately 28% of the time). Wind speeds are mostly in the 5 m/s to 20 m/s range.

Figure 3-2 and Table 3-1 present the average monthly current roses at the surface for 2012 to 2016 and the associated statistics, respectively. The surface current at Discharge 5 is predominantly directed to the southwest in all months. There are periods of the year (Feb, May and June) when occurrences of flow towards the north are also observed. The peak monthly surface current speed of 4.9 m/s to N, and 4.4 m/s to SW occur in June and July, respectively. The nearest coastal regions lie to the north of Discharge 5.

Table 3-1 - Yearly and monthly surface current speed and direction statistics at Discharge 5

SPEED (M/S)	YRLY	JAN	FEB	MAR	APR	MAY	JUN	JUL	AUG	SEP	OCT	NOV	DEC
Median	1.4	1.6	0.9	1.7	1.4	1.1	1.2	1.1	1.3	1.4	1.4	1.8	1.9
Mean	1.4	1.6	1.0	1.6	1.4	1.1	1.2	1.2	1.3	1.4	1.4	1.8	1.9
Std. deviation	0.1	0.6	0.6	0.6	0.6	0.6	0.6	0.7	0.6	0.6	0.6	0.5	0.4
Minimum	0.0	0.1	0.0	0.1	0.1	0.0	0.0	0.0	0.0	0.1	0.1	0.1	0.4
Maximum	4.9	3.0	2.6	3.6	3.1	2.8	4.9	4.4	4.1	3.5	3.8	3.1	3.1
Most frequent direction	SW	SW	SW	SW	SW	SW	SW	SW	SW	WSW	SW	SW	SW
Strongest current direction	N	SW	SW	SW	WSW	SW	N	SW	SW	SW	NNE	WSW	W

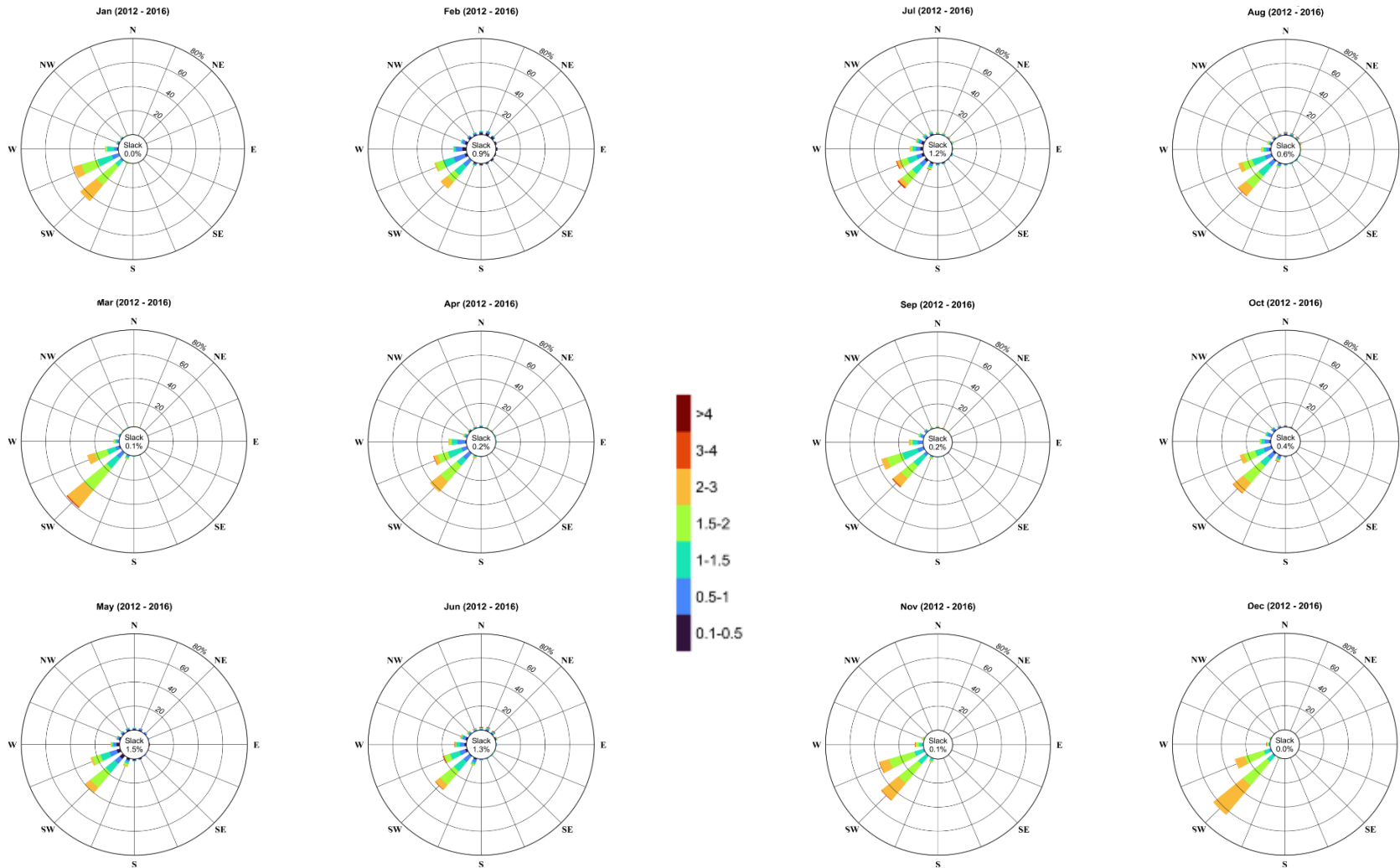


Figure 3-2 - Average monthly surface current roses at Discharge 5 for 2012 – 2016 (colour bar represents current speed in m/s)

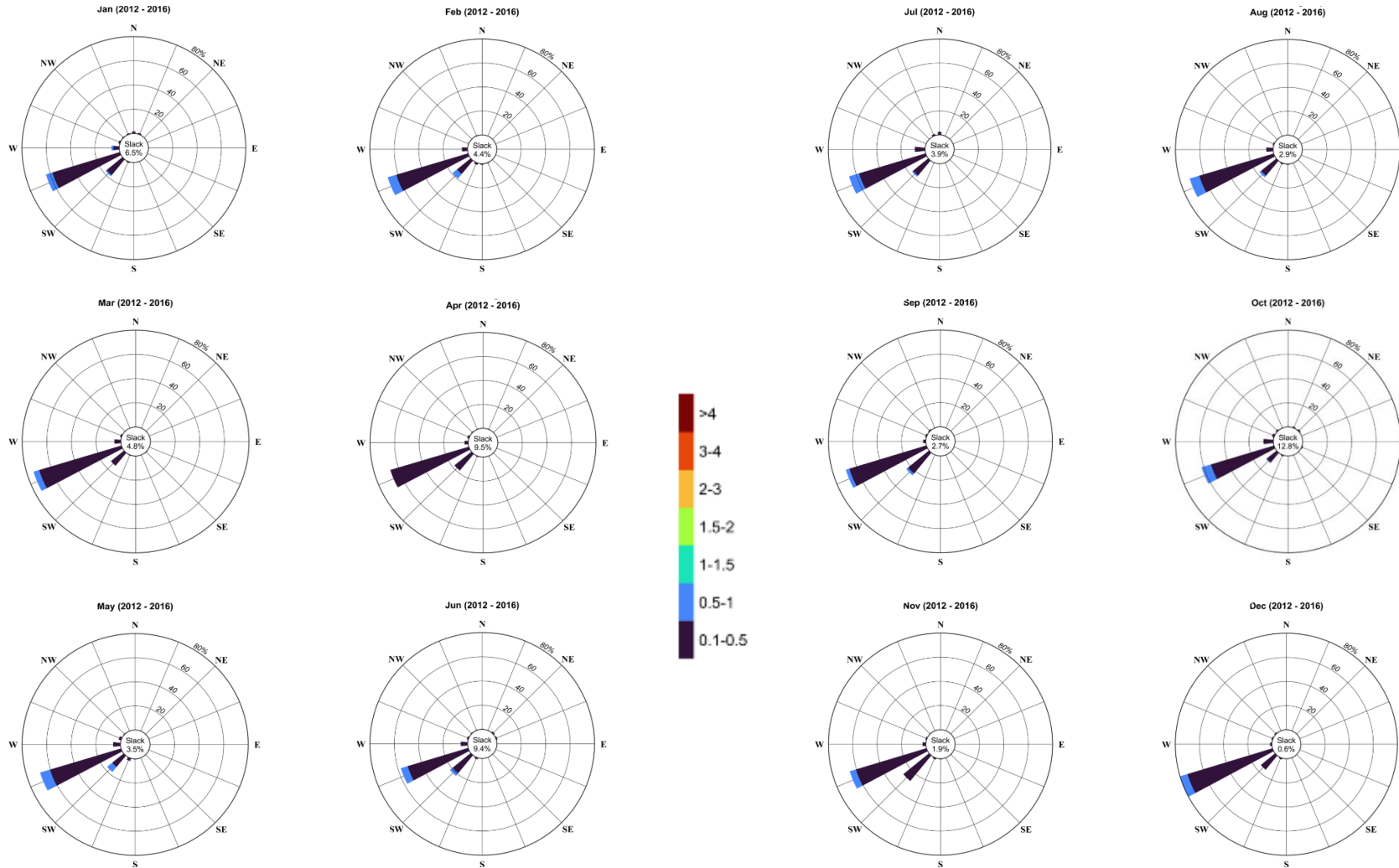


Figure 3-3 - Average monthly seabed current roses at Discharge 5 for 2012 – 2016 (colour bar represents current speed in m/s)

Figure 3-3 and Table 3-2 present the monthly current roses at the seabed for 2012 to 2016 and their associated statistics, respectively. The seabed currents present a low directional variability similar to the surface currents (Figure 3-3) and the dominant flow direction is to the WSW.

Table 3-2 - Yearly and monthly seabed current speed and direction statistics at Discharge 5

SPEED (M/S)	YRLY	JAN	FEB	MAR	APR	MAY	JUN	JUL	AUG	SEP	OCT	NOV	DEC
Median	0.3	0.3	0.4	0.3	0.3	0.4	0.3	0.3	0.3	0.3	0.3	0.3	0.3
Mean	0.3	0.3	0.3	0.3	0.3	0.4	0.3	0.3	0.3	0.3	0.3	0.3	0.3
Std. deviation	0.0	0.1	0.1	0.1	0.1	0.1	0.1	0.1	0.1	0.1	0.1	0.1	0.1
Minimum	0.0	0.0	0.0	0.0	0.0	0.0	0.0	0.0	0.0	0.0	0.0	0.0	0.1
Maximum	0.8	0.6	0.7	0.6	0.5	0.7	0.7	0.8	0.7	0.6	0.6	0.6	0.7
Most frequent direction	WSW	WSW	WSW	WSW	WSW	WSW	WSW	WSW	WSW	WSW	WSW	WSW	WSW
Strongest current direction	WSW	WSW	SW	WSW	WSW	SW	WSW	WSW	WSW	WSW	WSW	WSW	WSW

Figure 3-4 and Table 3-3 present the average monthly wind speed and direction statistics at 10 m elevation above sea level. Winds mainly occur in the east and west quadrants. The most frequent direction for stronger winds (>15 m/s) is from W over the five-year analysis period. The period from May to September also experiences mostly westerly winds.

Table 3-3 - Table 4: Yearly and monthly wind speed and direction statistics at Discharge 5

SPEED (M/S)	YRLY	JAN	FEB	MAR	APR	MAY	JUN	JUL	AUG	SEP	OCT	NOV	DEC
Median	8.4	7.5	7.5	8.2	7.7	7.7	9.6	9.6	9.2	9.7	8.9	8.6	7.8
Mean	8.7	7.5	7.6	8.3	8.0	8.2	9.9	10.1	9.6	9.9	8.9	8.6	7.8
Std. deviation	0.6	3.1	3.2	3.2	3.6	4.0	4.8	4.6	4.5	4.0	3.4	3.6	3.1
Minimum	0.1	0.2	0.3	0.4	0.3	0.3	0.4	0.3	0.5	0.4	0.6	0.6	0.1
Maximum	27.8	19.8	19.5	24.1	19.0	18.8	27.8	24.3	26.0	23.7	23.0	22.5	21.9
Most frequent direction	WSW	E	ENE	ENE	ENE	W	W	W	W	W	ENE	WSW	E
Strongest wind direction	W	W	W	W	W	W	W	ENE	W	W	W	W	WSW

In summary, the current data at Discharge 5 for the years 2012 to 2016 indicates flow at the sea surface mostly towards the SW for all months with some variability in speed, and mostly constant SW flow direction and speed at the seabed for all months. There are periods of the year (Feb, May and June) when occurrences of surface flow towards the north are also observed. The months of May to September also see an increase in the frequency and strength of winds from the west compared to other times in the year.

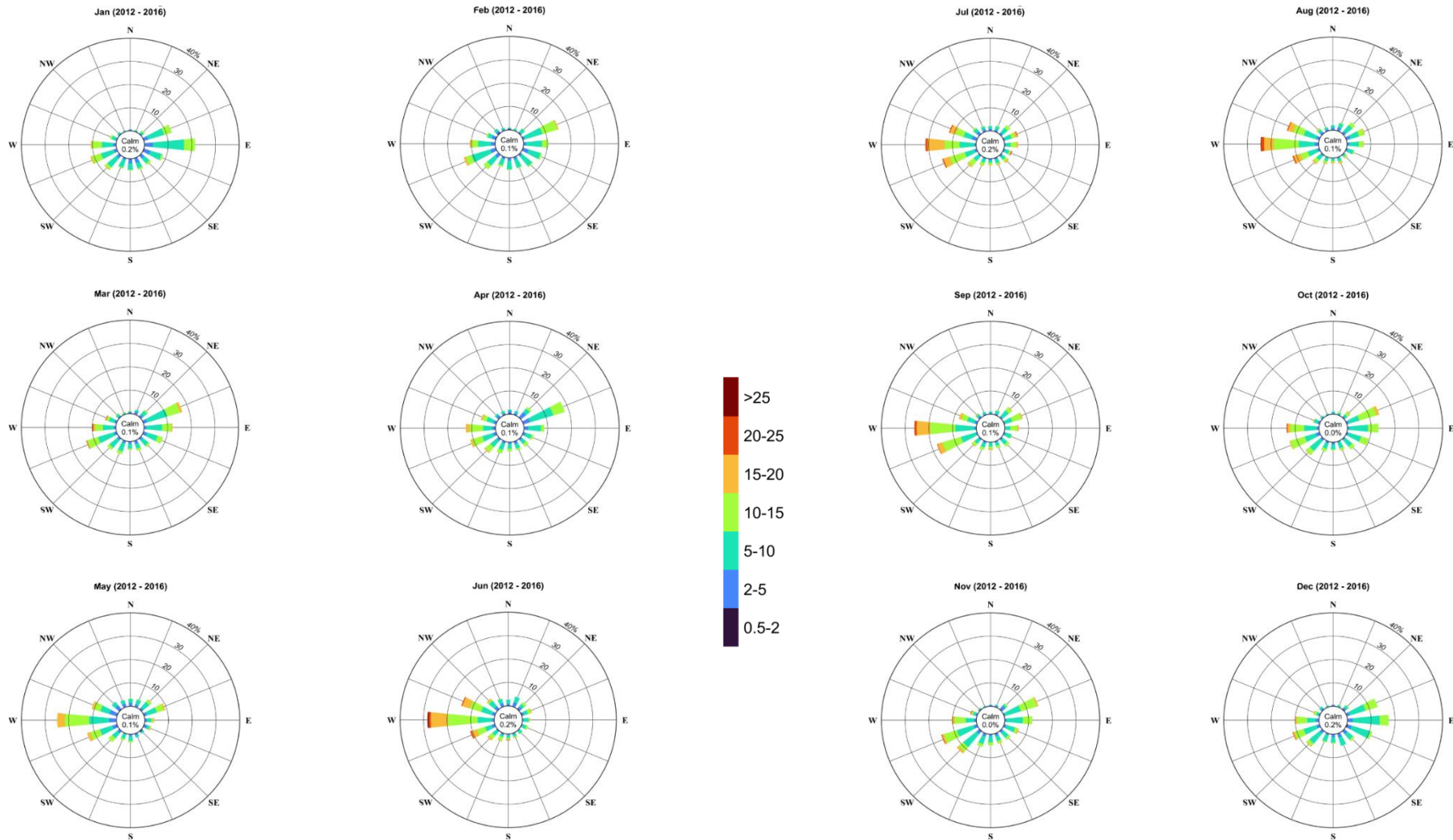


Figure 3-4 - Average monthly wind roses at Discharge 5 for 2012 – 2016 (colour bar represents wind speed in m/s)

3.1 SELECTION OF DRILLING DISCHARGE SIMULATION PERIODS FOR DISCHARGE 5

The methodology for identifying a suitably conservative start time for the drilling discharge simulations at Discharge 5 for Seasons 1 to 4 is identical to that described in Section 2.1. Similar to Discharge 4, the nearest MPA to Discharge 5 is the Southwest Indian Seamount Marine Protected Area, whose NE corner lies approximately 60.4 km to the SW as shown in Figure 2-5.

The two stages of well drilling at Discharge 5 are the same as for Discharge 4 and repeated below:

- Riserless phase – representing the first 270 hrs of operations, which includes 54 hrs of discharge at the seabed and 216 hrs (9 days) of no discharge. The total mass of cuttings and drilling mud released at the seabed during this phase is 1127 tonnes and 2326 tonnes, respectively.
- Riser phase – representing the next 344 hrs of drilling operations, which includes 200 hrs of discharge at 10 m below the water surface and 144 hrs (6 days) of no discharge. The total mass of cuttings and drilling mud released during this phase is 478 tonnes and 4100 tonnes, respectively.

The current speed and direction data at the seabed and ocean surface were analysed at Discharge 5 to estimate the periods of time when the maximum combined seabed and surface transport of seawater towards the MPA occurred during each season in the 5-year metocean dataset.

3.1.1 SEASON 1- DECEMBER TO FEBRUARY

Figure 3-5 presents summary statistics of current speed and direction at the seabed for each month of Season 1. Maximum current speed tends to mostly remain in the range of 0.5 m/s to 0.7 m/s, while average speed mostly lies in the 0.3 m/s to 0.4 m/s range. The most frequently occurring flow direction for the strongest 10% of the seabed currents is almost always to the WSW with a couple of months in 2014 and 2016 showing stronger flows to the W and SW.

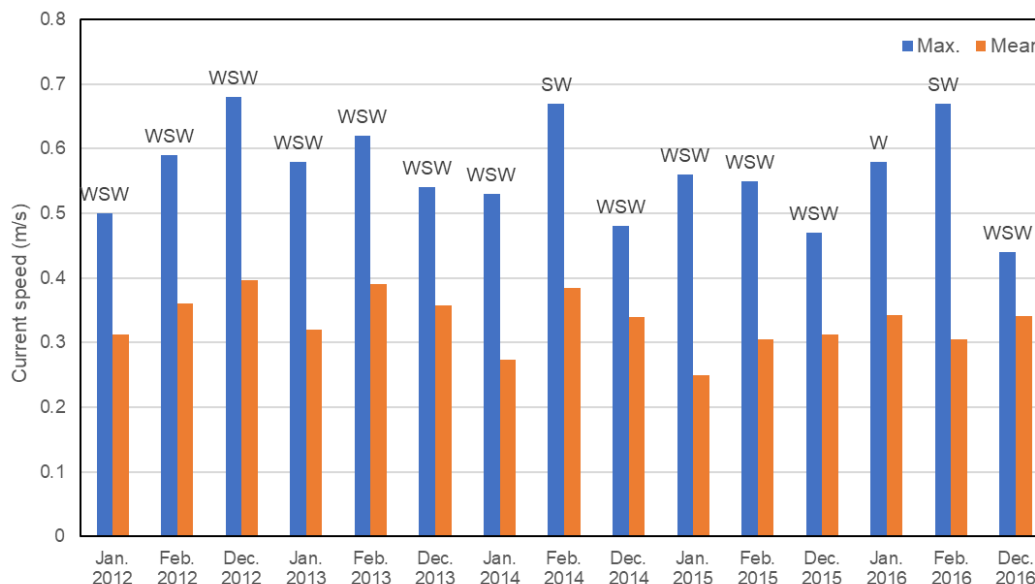


Figure 3-5 - Bottom current mean and maximum speed, and primary direction at Discharge 5 for Season 1 (2012 – 2016)

Figure 3-6 shows the current vectors at the seabed and surface at Discharge 5 for a 45-day period from 14 Dec 2015 to 27 Jan 2016. For clarity, the seabed and surface current vectors are scaled independently. The selected start time for the drilling discharge simulation in **Season 1 is 24 Dec 2015 at 0300 hrs**, as it yields the maximum combined seabed and surface transport of seawater towards the nearest MPA. The simulation periods for the riserless and riser phases of the well drilling are shown in Figure 3-6.

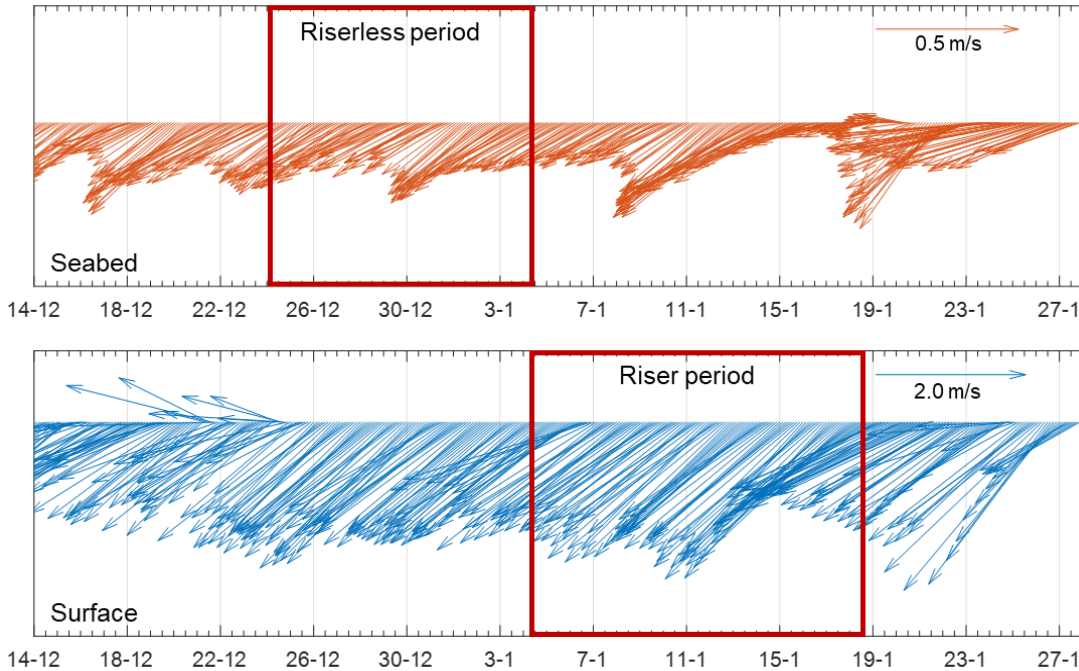


Figure 3-6 - Seabed and surface current vectors at Discharge 5 from 14 Dec 2015 to 27 Jan 2016 with boxes showing the period selected for drilling discharge simulation in Season 1

3.1.2 SEASON 2- MARCH TO MAY

Figure 3-7 presents summary statistics of current speed and direction at the seabed for each month of Season 2. Maximum current speed tends to mostly remain in the range of 0.5 m/s to 0.7 m/s, while average speed mostly lies in the 0.2 m/s to 0.4 m/s range. The most frequently occurring flow direction for the strongest 10% of the seabed currents is almost always to the WSW with a couple of months showing stronger flows to the SW.

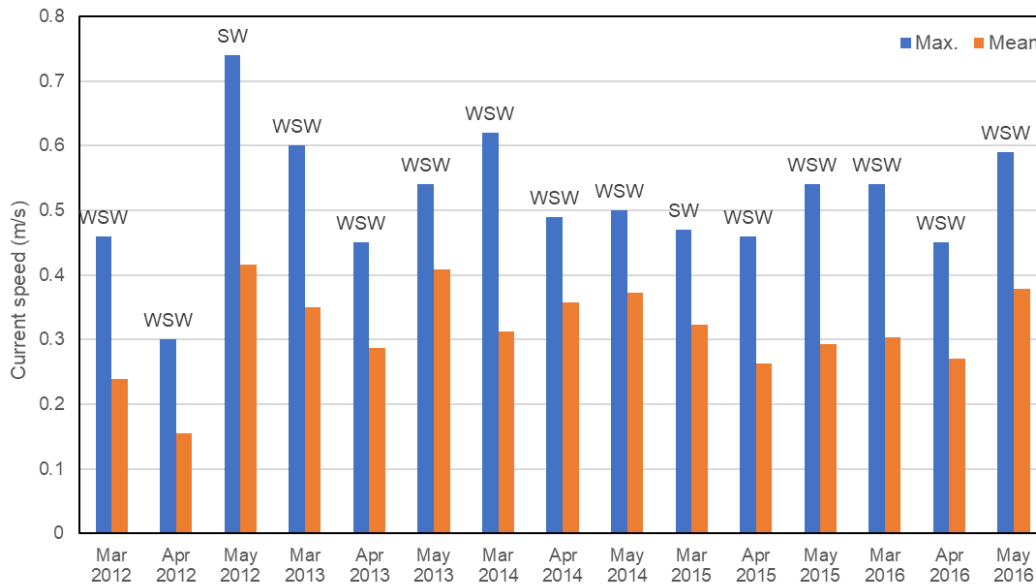


Figure 3-7 - Bottom current mean and maximum speed, and primary direction at Discharge 5 for Season 2 (2012 – 2016)

Figure 3-8 shows the current vectors at the seabed and surface at Discharge 5 for a 45-day period from 3 Mar 2013 to 16 Apr 2013. For clarity, the seabed and surface current vectors are scaled independently. The selected start time for the drilling discharge simulation in **Season 2 is 12 Mar 2013 at 0900 hrs**, as it yields the maximum combined seabed and surface transport of seawater towards the nearest MPA. The simulation periods for the riserless and riser phases of the well drilling are shown in Figure 3-8.

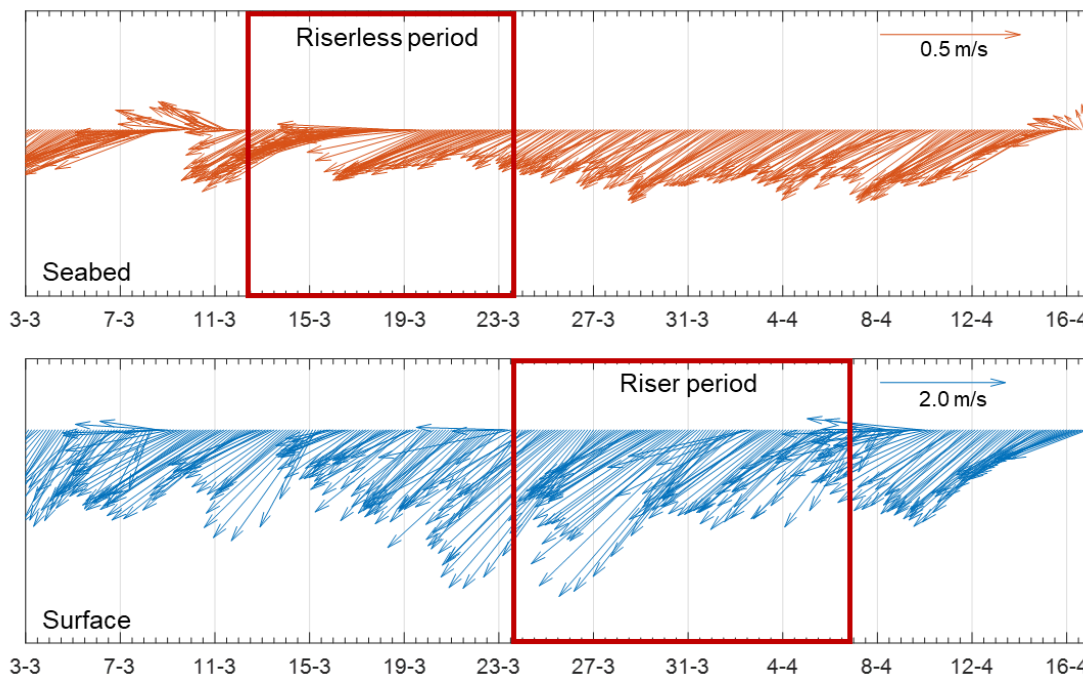


Figure 3-8 - Seabed and surface current vectors at Discharge 5 from 3 Mar 2013 to 16 Apr 2013 with boxes showing the period selected for drilling discharge simulation in Season 2

3.1.3 SEASON 3- JUNE TO AUGUST

Figure 3-9 presents summary statistics of current speed and direction at the seabed for each month of Season 3. Maximum current speed tends to mostly remain in the range of 0.5 m/s to 0.8 m/s, while average speed mostly lies in the 0.2 m/s to 0.4 m/s range. The most frequently occurring flow direction for the strongest 10% of the seabed currents is almost always to the WSW with just one month of June 2016 showing stronger flows to the SW.

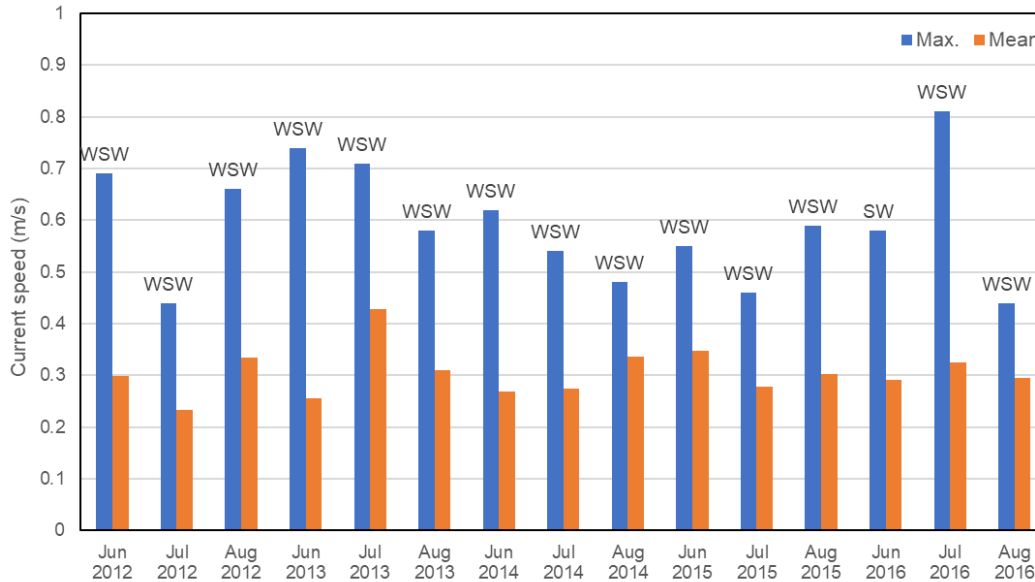


Figure 3-9 - Bottom current mean and maximum speed, and primary direction at Discharge 5 for Season 3 (2012 – 2016)

Figure 3-10 shows the current vectors at the seabed and surface at Discharge 5 for a 45-day period from 2 Aug 2015 to 15 Sep 2015. For clarity, the seabed and surface current vectors are scaled independently. The selected start time for the drilling discharge simulation in **Season 3 is 12 Aug 2015 at 0000 hrs**, as it yields the maximum combined seabed and surface transport of seawater towards the nearest MPA. The simulation periods for the riserless and riser phases of the well drilling are shown in Figure 3-10.

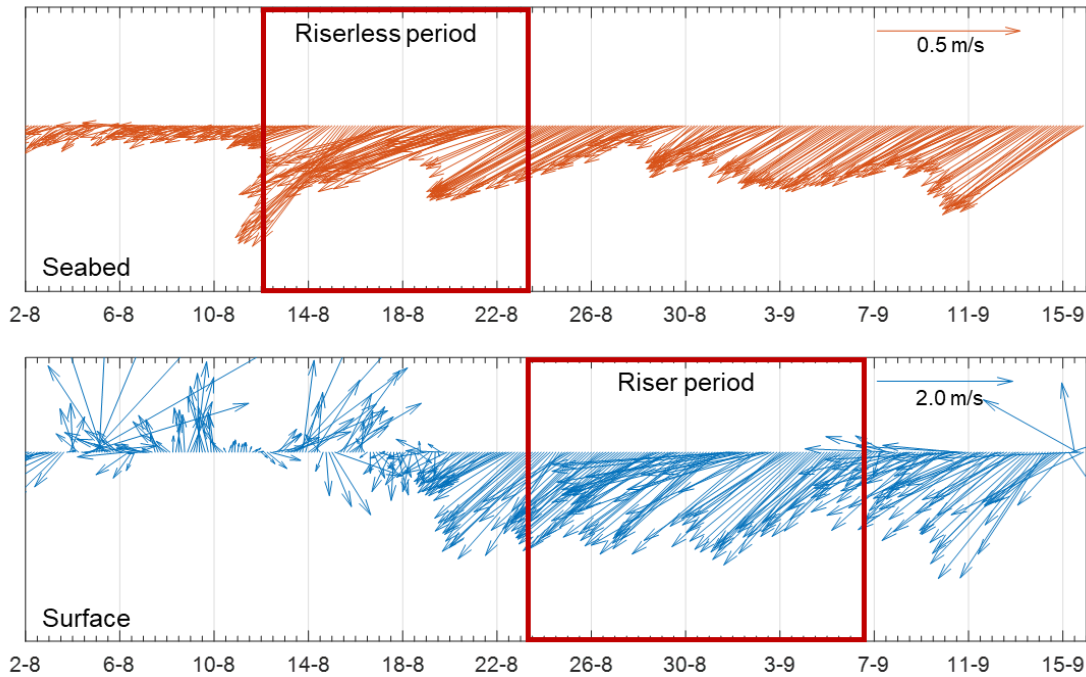


Figure 3-10 - Seabed and surface current vectors at Discharge 5 from 2 Aug 2015 to 15 Sep 2015 with boxes showing the period selected for drilling discharge simulation in Season 3

3.1.4 SEASON 4- SEPTEMBER TO NOVEMBER

Figure 3-11 presents summary statistics of current speed and direction at the seabed for each month of Season 4. Maximum current speed tends to mostly remain in the range of 0.5 m/s to 0.7 m/s, while average speed mostly lies in the 0.2 m/s to 0.4 m/s range. The most frequently occurring flow direction for the strongest 10% of the seabed currents is almost always to the WSW with a couple of months showing stronger flows to the SW.

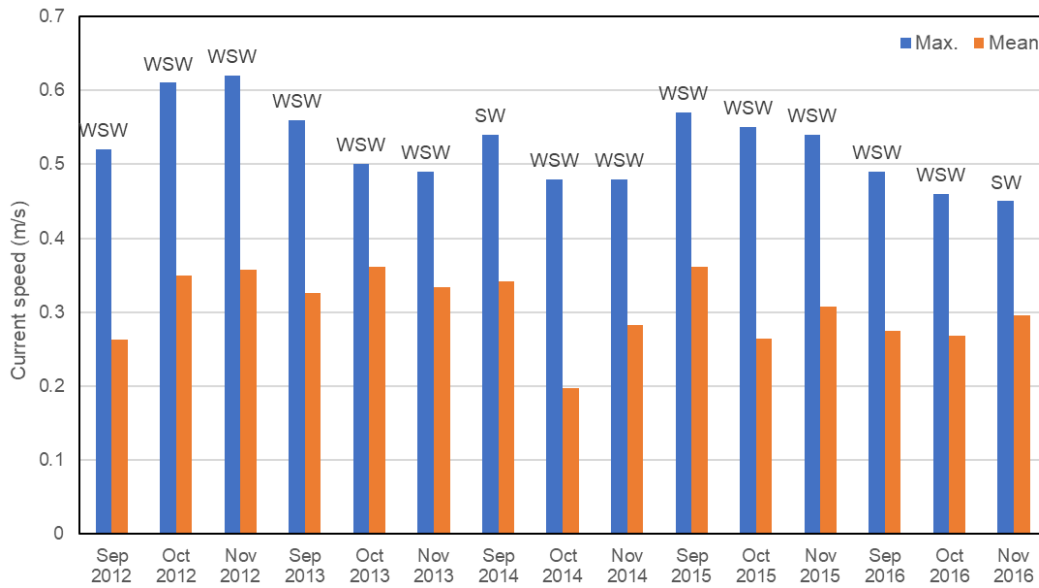


Figure 3-11 - Bottom current mean and maximum speed, and primary direction at Discharge 5 for Season 4 (2012 – 2016)

Figure 3-12 shows the current vectors at the seabed and surface at Discharge 5 for a 45-day period from 5 Oct 2015 to 18 Nov 2015. For clarity, the seabed and surface current vectors are scaled independently. The selected start time for the drilling discharge simulation in **Season 4 is 15 Oct 2015 at 0300 hrs**, as it yields the maximum combined seabed and surface transport of seawater towards the nearest MPA. The simulation periods for the riserless and riser phases of the well drilling are shown in Figure 3-12.

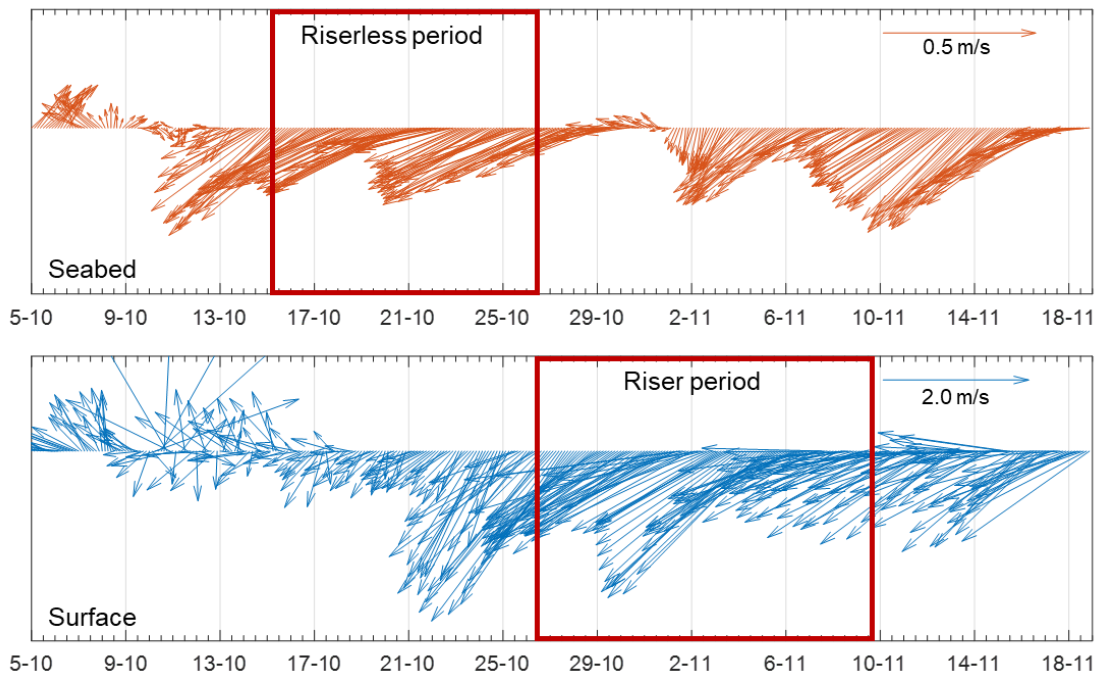


Figure 3-12 - Seabed and surface current vectors at Discharge 5 from 5 Oct 2015 to 18 Nov 2015 with boxes showing the period selected for drilling discharge simulation in Season 4

4 CONDENSATE PIPE LEAK LOCATION

Figure 4-1 shows the annual current and wind roses at the condensate pipe leak location - 35°6'58.41" S, 22°23'1.66" E. The surface current flows more often towards the SW like at Discharge 4 and 5, but there is more frequent occurrence of strong flows to the NE and NNE. Current speeds at the seabed are mainly to the WSW and SW and rarely exceed 0.5 m/s. Winds are mostly E-W and display similar characteristics as at Discharge 4 and 5.

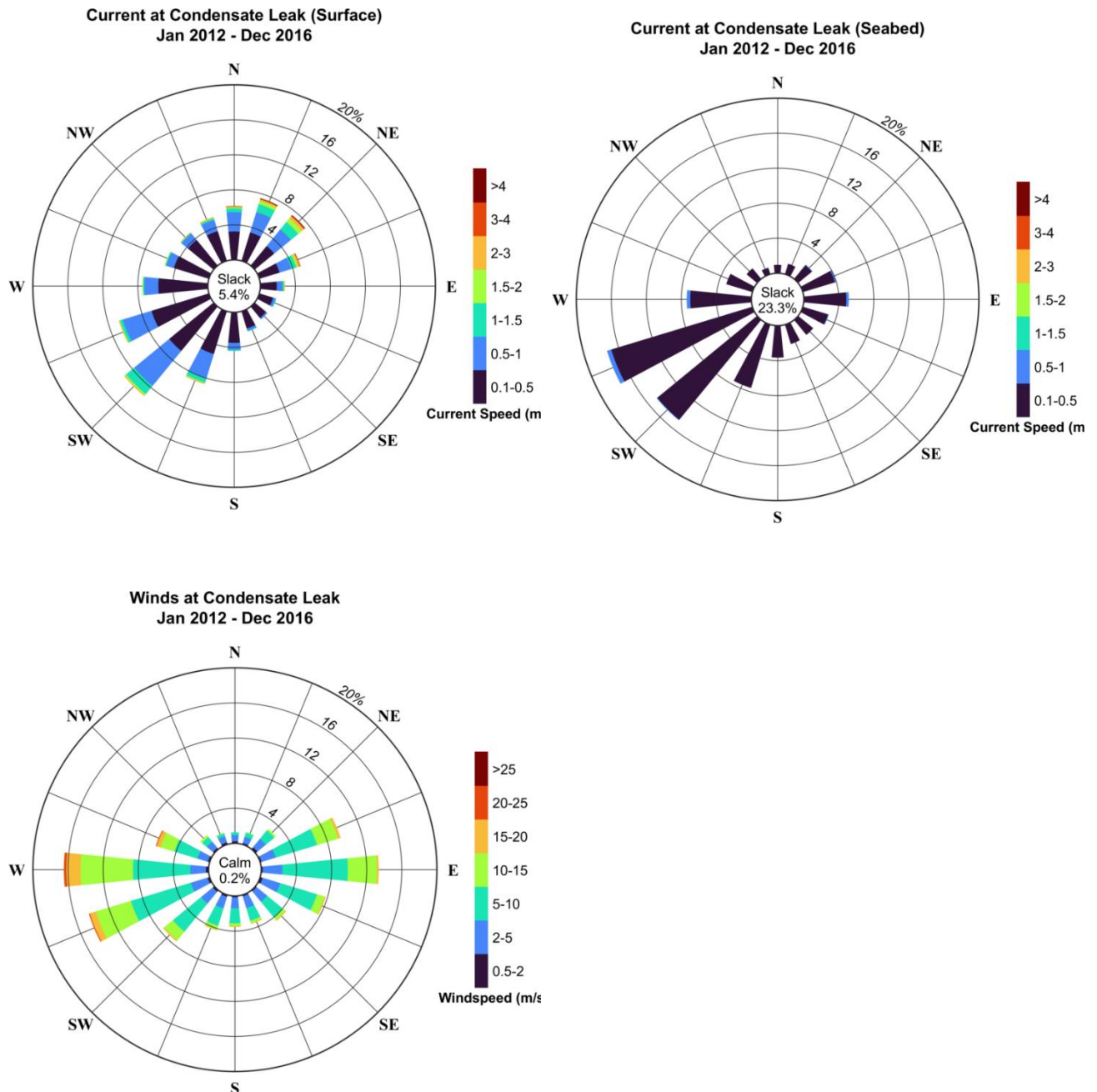


Figure 4-1 - Average annual current and wind speed roses at Pipe Leak location for 2012-2016

Table 4-1 summarises statistics of surface current at the Pipe Leak location. While the surface current usually flows to the SW for most of the year, the direction switches to the NE quadrant during the months of May to Aug. The strongest flows are almost always towards the NNE or NE. Peak current speed reached almost 5 m/s in the 5-year dataset although monthly median speeds generally vary between around 0.3 m/s and 0.5 m/s over the course of the year.

Table 4-1 - Yearly and monthly surface current speed and direction statistics at Pipe Leak location

SPEED (M/S)	YRLY	JAN	FEB	MAR	APR	MAY	JUN	JUL	AUG	SEP	OCT	NOV	DEC
Median	0.4	0.3	0.4	0.4	0.4	0.3	0.4	0.5	0.4	0.4	0.4	0.4	0.3
Mean	0.5	0.4	0.4	0.4	0.5	0.4	0.6	0.6	0.6	0.6	0.5	0.5	0.4
Std. deviation	0.4	0.3	0.3	0.3	0.3	0.3	0.6	0.5	0.5	0.5	0.3	0.4	0.3
Minimum	0.0	0.0	0.0	0.0	0.0	0.0	0.0	0.0	0.0	0.0	0.0	0.0	0.0
Maximum	5.0	2.0	1.9	2.3	2.7	2.3	5.0	3.3	3.8	3.5	3.5	3.0	2.6
Most frequent direction	SW	SW	SW	SW	SW	NNE	NE	NE	NE	SW	SW	SW	SW
Strongest current direction	NNE	NE	NNE	SW	NNE	ENE	NNE	NE	NE	NNE	NE	NNE	NE

Figure 4-2 shows average monthly surface current roses at the Pipe Leak location for 2012 to 2016. The surface current flows towards the SW quadrant in the months of January to April and October to December. The surface current is directed towards the NE and SW quadrants in the months of May to September, however the north-easterly currents are consistently stronger in those months.

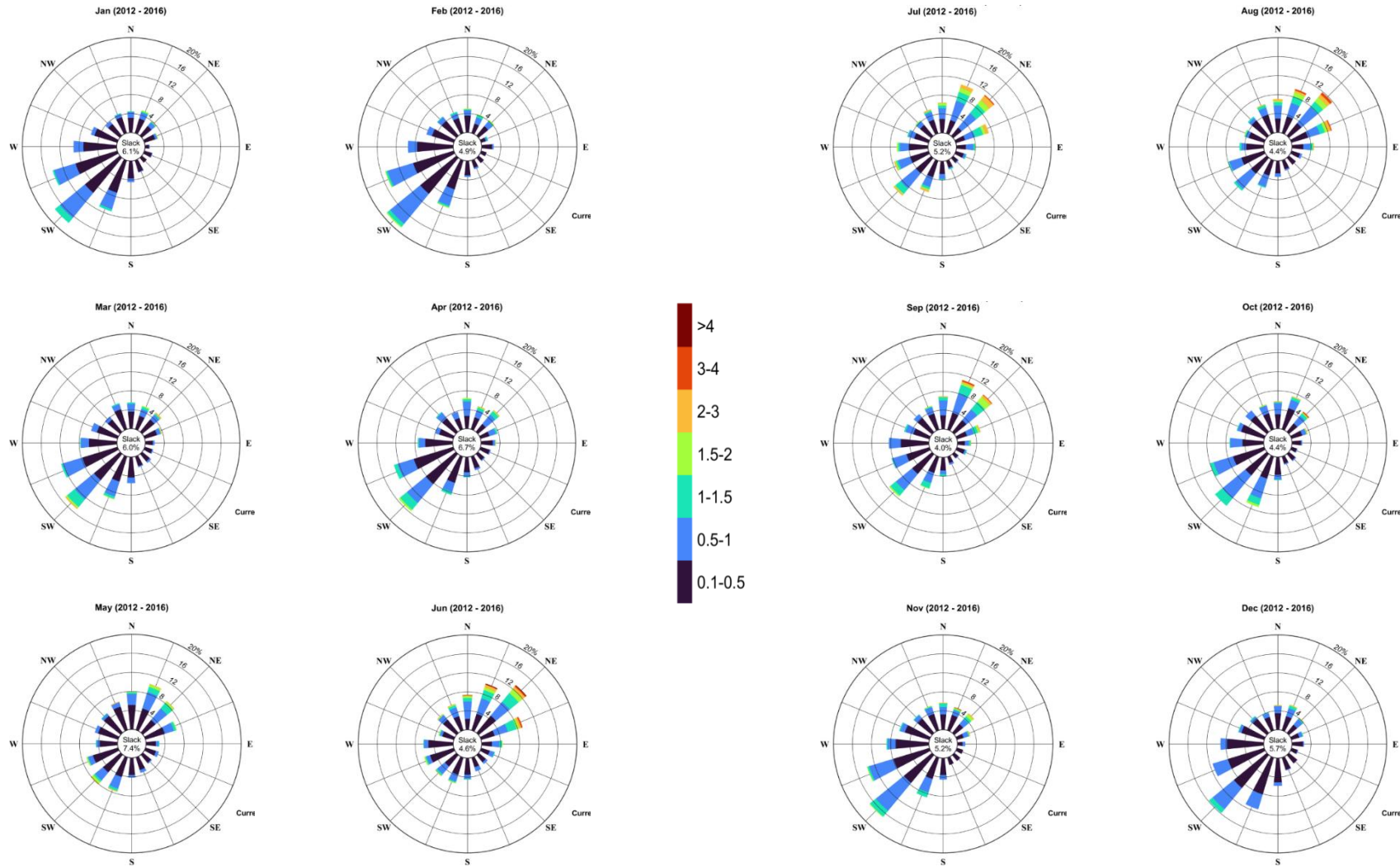


Figure 4-2 - Average monthly surface current roses at Pipe Leak for 2012 – 2016 (colour bar represents current speed in m/s)

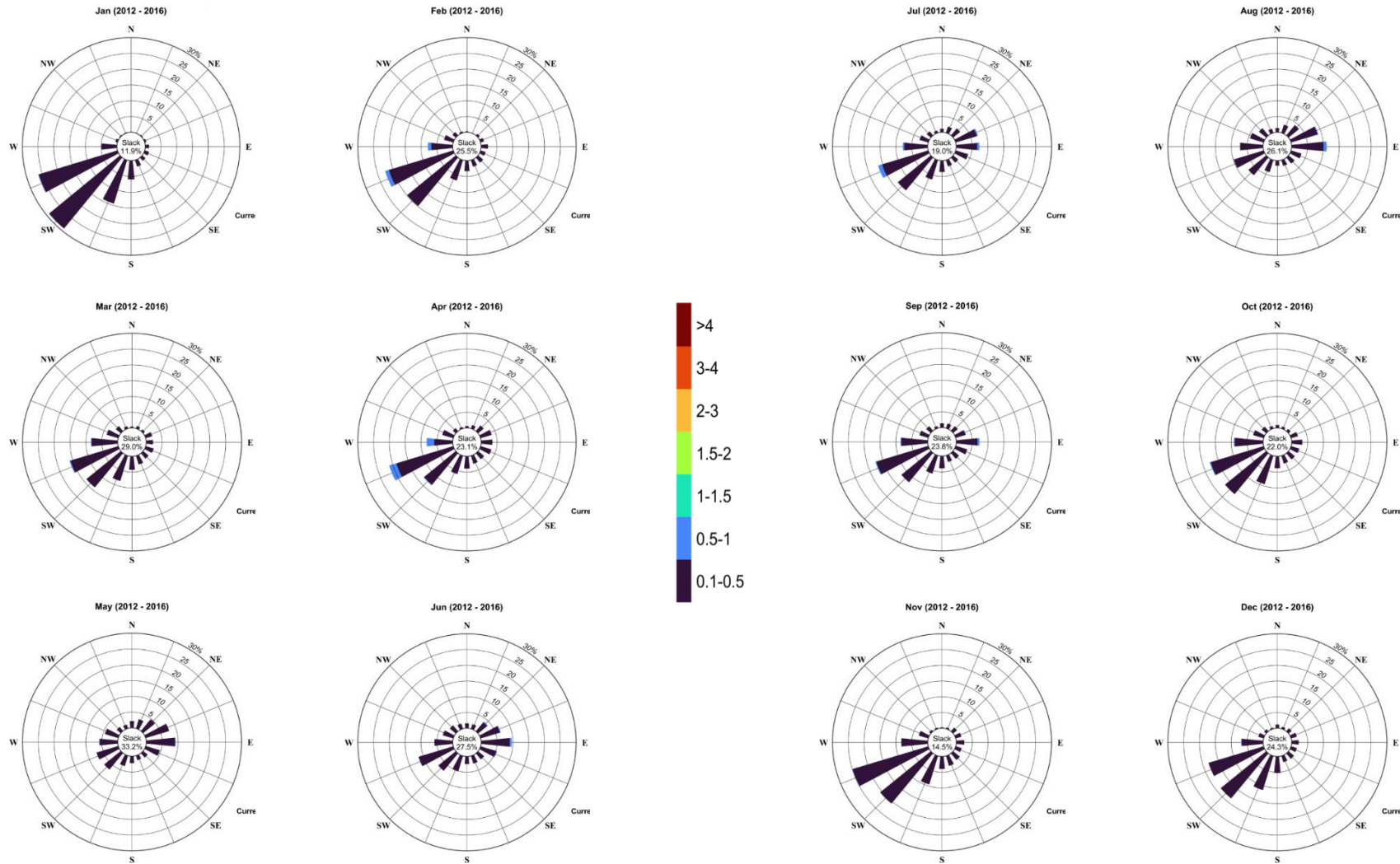


Figure 4-3 - Average monthly seabed current roses at Pipe Leak for 2012 – 2016 (colour bar represents current speed in m/s)

Statistics of the seabed current at the Pipe Leak location are summarised in Table 4-2. The seabed current is directed to the SW quadrant for most of the year except for the months of May and August, which see the most frequently occurring seabed current direction switching to an easterly flow. The strongest flows are almost always towards the east or WSW. Peak current speed reached 0.8 m/s in the 5-year dataset although monthly median speeds generally remain at 0.2 m/s over the course of the year.

Table 4-2 - Yearly and monthly seabed current speed and direction statistics at Pipe Leak location

SPEED (M/S)	YRLY	JAN	FEB	MAR	APR	MAY	JUN	JUL	AUG	SEP	OCT	NOV	DEC
Median	0.2	0.2	0.2	0.1	0.2	0.1	0.2	0.2	0.2	0.2	0.2	0.2	0.2
Mean	0.2	0.2	0.2	0.2	0.2	0.1	0.2	0.2	0.2	0.2	0.2	0.2	0.2
Std. deviation	0.1	0.1	0.1	0.1	0.1	0.1	0.1	0.1	0.1	0.1	0.1	0.1	0.1
Minimum	0.0	0.0	0.0	0.0	0.0	0.0	0.0	0.0	0.0	0.0	0.0	0.0	0.0
Maximum	0.8	0.5	0.7	0.6	0.8	0.6	0.7	0.7	0.7	0.6	0.6	0.5	0.5
Most frequent direction	WSW	SW	WSW	WSW	WSW	E	WSW	WSW	E	WSW	WSW	WSW	WSW
Strongest current direction	W	WSW	W	ENE	W	E	E	WSW	E	E	E	WSW	WSW

Figure 4-3 shows the average monthly seabed current roses at the Pipe Leak location for 2012 to 2016. The seabed current at the Pipe Leak location is directed towards the southwest quadrant in the months of January to April and September to December. The seabed current flows both eastward and to the southwest quadrant in the months of May to August.

Table 4-3 and Figure 4-4 present the statistics of hourly-average wind speed at 10 m elevation for the Pipe Leak location. Winds mainly blow from the eastern and western sectors from October to April. However, in the months of May to September westerly winds dominate in frequency of occurrence as well as strength. The most frequent direction for stronger winds (>15 m/s) is from W over the five-year dataset.

Table 4-3 - Yearly and monthly wind speed and direction statistics at Pipe Leak location

SPEED (M/S)	YRLY	JAN	FEB	MAR	APR	MAY	JUN	JUL	AUG	SEP	OCT	NOV	DEC
Median	7.3	6.6	6.5	7.2	6.6	6.4	8.0	8.6	8.0	8.6	8.1	7.6	6.8
Mean	7.6	6.8	6.7	7.2	6.9	6.9	8.4	8.9	8.5	8.7	8.0	7.7	6.9
Std. deviation	3.7	2.9	3.1	3.3	3.4	3.7	4.5	4.4	4.3	3.8	3.3	3.5	3.0
Minimum	0.1	0.2	0.4	0.5	0.2	0.1	0.3	0.2	0.1	0.6	0.6	0.1	0.3
Maximum	24.5	18.1	17.5	19.9	19.3	18.2	24.5	21.7	22.6	22.3	21.8	22.5	21.0
Most frequent direction	W	E	E	E	ENE	W	W	W	W	W	E	E	E
Strongest wind direction	W	W	W	W	W	WSW	W	W	W	W	W	WSW	WSW

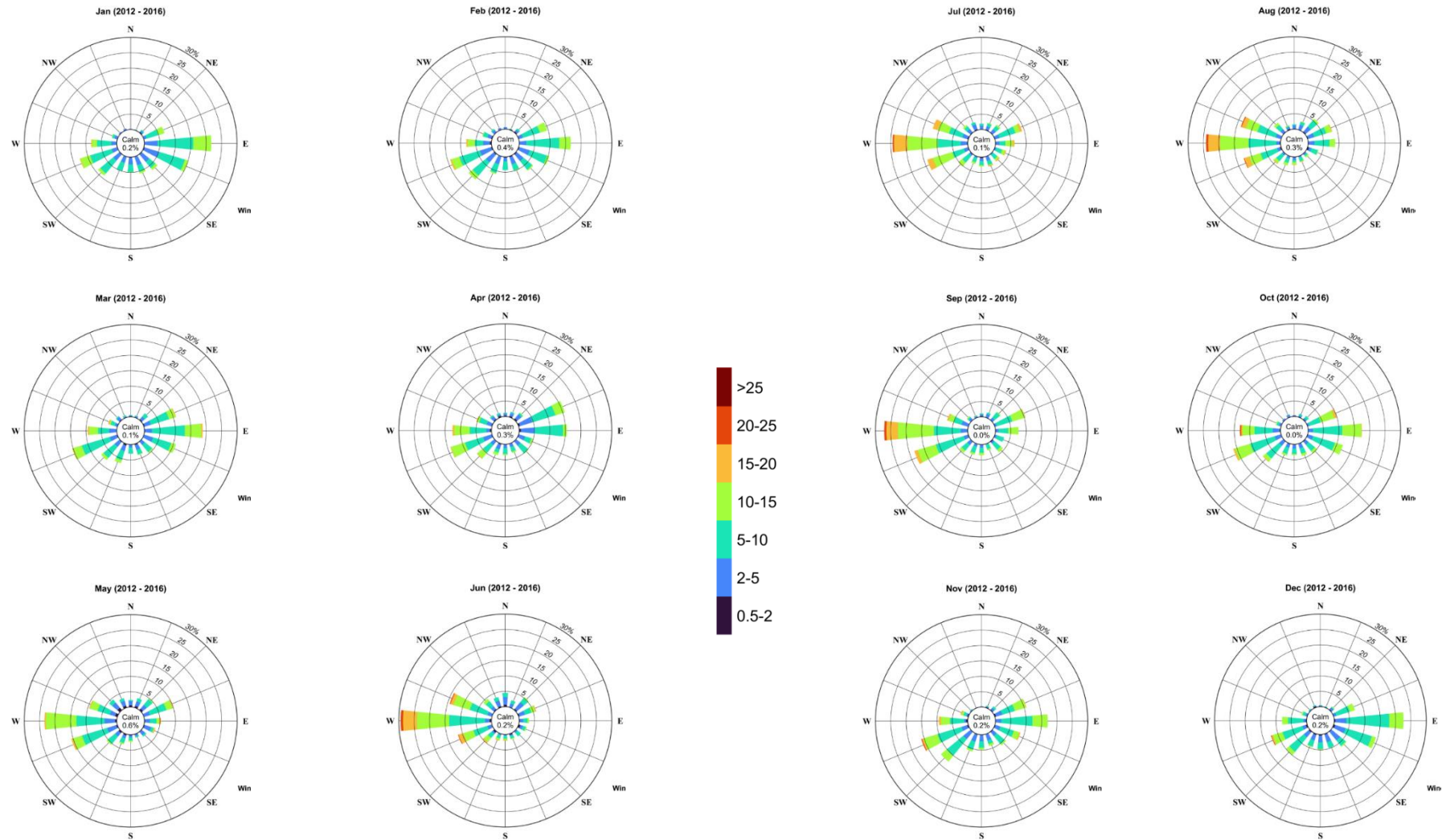


Figure 4-4 - Average monthly wind roses at Pipe Leak for 2012 – 2016 (colour bar represents wind speed in m/s)



5 STUDY LIMITATIONS

WSP Canada Inc. (WSP) has prepared this document in a manner consistent with the level of care and skill ordinarily exercised by members of the engineering and science professions currently practising under similar conditions in the jurisdiction in which the services are provided, subject to the time limits and physical constraints applicable to this document. No warranty, express or implied, is made.

This document, including all text, data, tables, plans, figures, drawings, and other documents contained herein, has been prepared by WSP for the sole benefit of Total Energies. This report represents WSP's professional judgement based on the knowledge and information available at the time of completion. WSP is not responsible for any unauthorized use or modification of this document. All third parties relying on this document do so at their own risk.

The factual data, interpretations, suggestions, recommendations, and opinions expressed in this document pertain to the specific project, site conditions, design objective, development and purpose described to WSP by Total Energies and are not applicable to any other project or site location. In order to properly understand the factual data, interpretations, suggestions, recommendations, and opinions expressed in this document, reference must be made to the entire document.

This document, including all text, data, tables, plans, figures, drawings, and other documents contained herein, as well as all electronic media prepared by WSP are considered its professional work product and shall remain the copyright property of WSP. Total Energies may make copies of the document in such quantities as are reasonably necessary for those parties conducting business specifically related to the subject of this document or in support of or in response to regulatory inquiries and proceedings. Electronic media is susceptible to unauthorized modification, deterioration, and incompatibility and therefore no party can rely solely on the electronic media versions of this document.

6 REFERENCES

- Bailey, D.F., J. Hermes, P. Penven, T. Bornman, W. Goschen (2022). An investigation of sea level and circulation response during a coastal trapped wave event on the Eastern Agulhas Bank, South Africa. *Continental Shelf Research*, **240**, 104698.
- Beal, L.M. and H. L. Bryden (1997). Observations of an Agulhas Undercurrents, *Deep-Sea Res.*, **44(9)**, 1715-1735.
- Beal, L.M. (2009). A time series of Agulhas undercurrent transport. *J. Phys. Oceanography*, **30**, 2436-2450.
- Beal, L.S. S. Elipot, A. Houk and G.M. Leber (2015). Capturing the Transport Variability of a Western Boundary Jet: Results from the Agulhas Current Time-Series Experiment (ACT),. *Journal of Physical Oceanography*, **45**, 1302-1324.
- Boyd, A.J. and F.A. Shillington (1994). Physical forcing and circulation patterns on the Agulhas Bank. *S.A. J. Sci.*, **90**, 114-122.
- Goschen, W. and E.H. Schumann (1990). Agulhas Current variability and structure off the Cape province, South Africa. *J. Geophys. Res.*, **95(C1)**, 667-678.
- Hutchinson, K. (2018). Seasonality of the Agulhas Current with respect to near- and far-field winds. *Phd Thesis*, University of Cape Town, 176pp.
- Krug, M. J. Tournadre and F. Dufois (2014). Interactions between the Agulhas Currents and the eastern margin of the Agulhas Bank, *Continental Shelf Research*, **81**, 67-79.
- Largier, J.L. and V.P. Swart, V.P.(1987). East -west variation in thermocline breakdown on the Agulhas Bank. In: *The Benguela and Comparable Ecosystems*, Payne, A. I. L., Gulland, J. A. and K. H. Brink (Eds). *S. Afr. J. mar. Sci.*, **5**, 263-272.
- Largier, J. P. Chapman, W.T. Peterson and V.P. Swart (1992). The western Agulhas Bank: circulation, stratification and ecology, *South African Journal of Marine Science*, **12(1)**, 319-339, DOI: 10.2989/02577619209504709
- Lutjeharms, J.R.E. and M.J. Roberts (1988). The Natal Pulse: An extreme transient on the Agulhas Current., *J. Geophys. Res.*, **93 (C1)**, 631-645.
- Lutjeharms, J.R.E., R. Catzel and H.R. Valentine (1989). Eddies and other boundary phenomena of the Agulhas Currents, *Cont. Shelf. Res.*, **9(7)**, 597-616.
- Lutjeharms, J.R.E., O. Boebel, P.F.C. van der Vaart, W.P.M. de Ruijter, T. Rossby and H.L. Bryden (2001). Evidence that the Natal Pulse involves the Agulhas Current to its full depth. *Geophysical Research Letters*, **28(18)**, 2449-2452.
- Lutjeharms, J.R.E., P. Penven and C. Roy (2003). Modelling the shear edge eddies of the southern Agulhas Current. *Cont. Shelf Res.*, **23**, 1099-1115.
- Pearce, A.F and M.L. Gründlingh (1982). Is there a seasonal variation of the Agulhas Current? *Journal of Marine Research*, **40(1)**, 177-184.



- Russo S.R., J. Veitch, M. Carr, G. Fearon and C. Whittle (2022) An intercomparison of Global Re-analysis products for southern Africa's major oceanographic features. *Front. Mar. Sci.* 9:837906. doi: 10.3389/fmars.2022.837906.
- Roualt, M.J. and F. Penven (2011). New perspectives on the Natal Pulse from Satellite observations, *J. Geophys. Res.*, **116**, C07013, doi:10.1029/2010JC006866.
- Schumann, E.H., G.J.B . Ross and W.S. Goschen (1988) Cold water events in Algoa Bay and along the Cape south coast, South Africa, in Marc/April 1987. *S.A. J. Sci.*, 84, 581-584.
- Swart, V.P. and J.L. Largier (1987). Thermal structure of the Agulhas Bank water. In: *The Benguela and Comparable Ecosystems*, Payne, A. I. L., Gulland, J. A. and K. H. Brink (Eds). *S. Afr. J. mar. Sci.*, **5**, 243-253
- Tedesco, P., J. Gula, C., Ménesguen, P. Penven and M. Krug (2019). Generation of submesoscale frontal eddies in the Agulhas Current. *Journal Geophysical Research: Oceans*, **124**, 7606–7625. <https://doi.org/10.1029/2019JC015229>.
- TotalEnergies. (2022). *Drilling Discharge Modeling Technical Report*.



7 CLOSURE

We trust the above meets your present requirements. If you have any questions or requirements, please contact the undersigned.

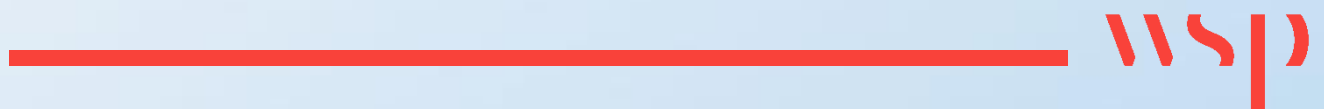
Ashwin Gadgil, PhD, EIT
Coastal Engineer & Hydrodynamic Modeller

Sundar Prasad, PhD
Senior Principal Coastal Engineer

Marieh Rajaie, PhD, EIT
Water Resources Specialist

Appendix A

SATOCEAN HYDRODYNAMIC DATABASE: CALIBRATION AND VALIDATION





MEMO

Exploration & Production

TEPSA/OPS – TEPsa/2020-0098/OPS.PL

Destinataire : C. MICHEL (EP/AF/A-FE/ZA-TEP/HSEQ) To E. GROENEWALD (EP/AF/A-FE/ZA-TEP/HSEQ)	Expéditeur : P. LATTES (EP/AF/A-FE/ZA-TEP/OPS) From T. MAJA (EP/AF/A-FE/ZA-TEP/OPS)
Copie : Copy	Date : April 21 st 2020
Object : 3D current model calibration and methodology – South Blocks - South Africa. Subject	Philippe LATTES Signature numérique de Philippe LATTES Date : 2020.06.09 13:20:38 +0200

1 Background

Block 11B/12B is characterized by harsh environmental conditions. Total Hs and surface winds show clear seasonality signals with best conditions occurring during austral summer. Another aspect that affects Block 11B/12B is the core of the Agulhas Current. This warm and saline current is formed by several oceanic currents in the Indian ocean and is the second strongest current in the world.

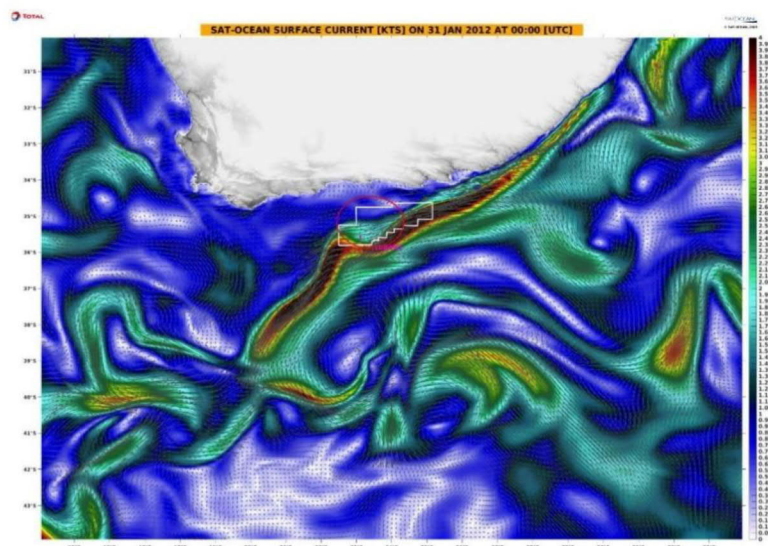


Figure 1: Current speed map of current flow over the southern African region showing the Agulhas Current system for January 2012. A shear edge eddy (red circle) cross the 11B/12B block is demarcated by a white polygon.

TOTAL Classification: Restricted Distribution

TOTAL - All rights reserved



MEMO

A great portion of the 11B/12B block lies on the pathway of the Agulhas Current, a fast and narrow western boundary current flowing along the eastern and southern coasts of South Africa. The core of the current is generally positioned across the block and is occasionally perturbed by shear edge eddies (see Figure 1) generated upstream south of Port Elizabeth (34° S) and or Natal pulse anomalies generated offshore Durban. During passage of these anomalies, the current speeds over the block are either weakened or reinforced with an associated change in flow direction and depending on the behavior of the anomaly (see Figure 2).

Current speeds of up to and exceeding 6 knots have been recorded within the core of the current associated with meanders. Current direction can change in response to change in winds and or progression of large eddies. The Agulhas Current does not present any seasonality as the anomalies impacting the current flow, in addition to weather, are sporadic and difficult to predict.

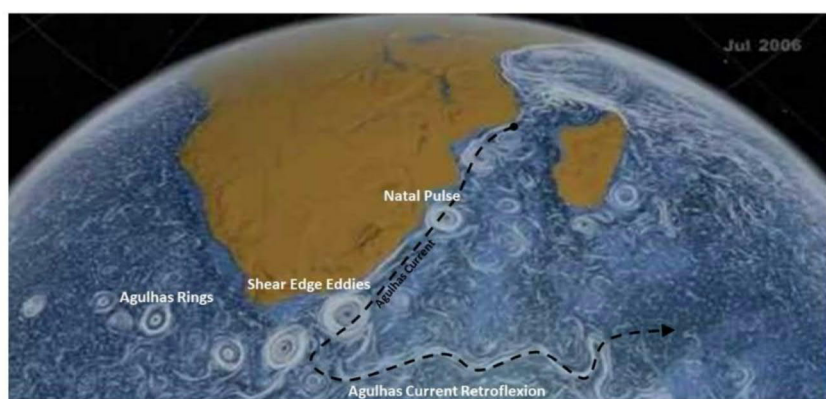


Figure 2 Large current eddies due to shear stress induced by the coast and continental shelf in South Africa

2 SAT-OCEAN Model description

SAT-OCEAN have developed innovative and exclusive technologies based on in-situ, satellite sea surface temperature, wind and altimetric data by which absolute ocean currents and winds are computed, anywhere in the world.

In effect, coupled inverse/direct modeling approaches combined with the data allow us to measure these quantities from space with very high spatial (1/32°) and temporal resolutions (3-hour output time step) over the model emprise (see Figure 1). Figure 1: Current speed map of current flow over the southern African region showing the Agulhas Current system for January 2012. A shear edge eddy (red circle) cross the 11B/12B block is demarcated by a white polygon.).

Several studies have shown that upper layer oceanic features can be monitored from satellite measurements over long periods of time. SAT-OCEAN merge up to 9 sensor data sets and produce analyzed SST fields accurate to 0.3°C on average compared to surface drifting buoys' temperature measurements. Monitoring the ocean's surface at such resolutions yields the ability to compute absolute 3-dimensional currents

TOTAL Classification: Restricted Distribution

TOTAL - All rights reserved



MEMO

worldwide. In addition, SAT-OCEAN model data are cloud free and can be produced up to every 3 hours at a 7-10 km resolution in space from 1998.

SAT-OCEAN inverse/direct model is controlled by very accurate SST analyzed fields, together with wind satellite analyzed data and altimetric data, leading to high resolution current fields. Over several areas of the world including offshore South Africa, this new approach has yielded accurate current estimates with respect to simultaneous on-site measurements (ADCP, HF radars, current meter and buoys' velocities).

SAT-OCEAN also provides high quality analyzed satellite wind data, either in real time or spanning over the past 25 years. The data can be used for design or to assist offshore operations.

3 Satellite observations and Ocean Currents Monitoring

3.1 Satellite data

SAT-OCEAN bases its ocean current computations on several data sets, stemming from scatterometers (for the model forcing winds) as well as from altimeter-based and Sea Surface Temperature satellite observations (to be assimilated in the HYCOM based ocean current model).

3.2 QSCAT and SSMI satellite wind data

Satellite wind scatterometry data are processed for the purpose of forcing the 3D Navier-Stokes direct circulation model.

The data are extracted from the GSFC database (public access), and wind magnitude and direction images are processed (flagged for rainy areas, bad data, projected and calibrated against anemometer data).

The processed data are then merged via objective mapping and spectral fusion. Analyzed wind fields are produced in real time every 3 hours at a 0.125° spatial resolution.

3.3 Geostationary imagery

The geostationary raw data are routinely obtained from the GMS satellite series which cover the area of interest. SAT-OCEAN produces SST images via a methodology analogous to the one described for the AVHRR imagery (section 3.4).

The GOES image series presents a 5 km spatial resolution over the area of concern and 24 to 48 images are available each day, depending on the availability of the data.

3.4 TRMM TMI and AQUA AMSR-E imagery

TOTAL Classification: Restricted Distribution

TOTAL - All rights reserved



MEMO

The TRMM (Tropical Rainfall Measuring Mission), TMI (TRMM Microwave Imager) and AMSR-E AQUA SST image series are extracted in real time from the GSFC (Goddard Space Flight Center) data base (public access). The SSTs are already computed and the projection, geolocation and error correction are already applied. The TMI and AMSR-E measurement technology is such that the ocean is always visible no matter the cloud coverage, except over regions where it is raining. The TMI and AMSR-E image spatial resolution is about 25 km and the area is covered twice a day.

3.5 Polar Orbiting NOAA Satellite AVHRR imagery

Satellite AVHRR (Advanced Very High Resolution Radiometer) Level 1b high resolution imagery is extracted in real time from the NOAA (US National Oceanographic and Atmospheric Agency) Satellite Active Archive server (public access). The level 1b data is very similar to the Level 0 on-board recorded measurement.

The AVHRR image series presents a 1 km (Local Area Coverage) to 4 km (Global Area Coverage) spatial resolution and 10-12 images are available each day, depending on the number of orbiting satellites.

The raw satellite data are processed in real time at SAT-OCEAN including: channels 1 to 5 linear and non-linear calibrations, geolocation, clock drift and satellite attitude (roll, pitch and yaw) error corrections, Lambert Azimuthal Equal Area projection, multi-channel cloud detection and sea surface temperature (SST) will be computed using split, dual or triple window algorithms from the 5 processed channels.

3.6 Satellite altimeter data

Several altimeters are and have been orbiting with a worldwide coverage. Among those, some are performing measurements in spectral bands dedicated to ocean circulation.

SAT-OCEAN will process the data set over the area of concern for the study, calibrate and cross-calibrate all the data to construct an altimeter-based series over the area.

3.7 HF radars and ADCP

ADCP data have been recorded during seismic campaigns and dedicated surveys over the 11B/12B block and have been used for SAT-OCEAN model calibration. In addition, several HF radars installed and operated by TOTAL located along the coast (between Mossel Bay and Port Elizabeth) allowed to monitor surface current since February 2018 over a large offshore area. These data are available every 30 minutes at 6km resolution. This monitoring allows accurate historical and real time monitoring of the surface currents over the block 11B/12B and has been used for model validation/calibration.



MEMO

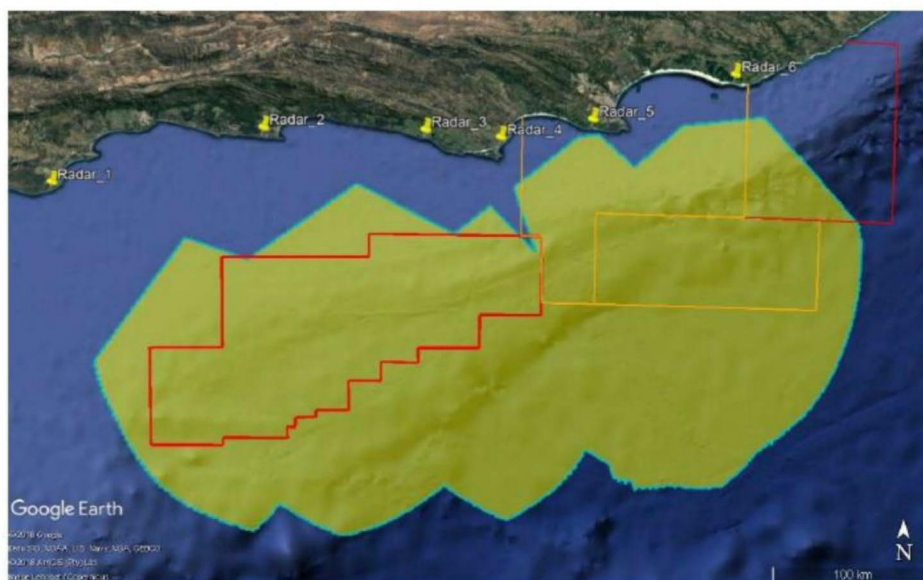


Figure 3 Coverage with 6 radar stations

4 Methodology

4.1 Ocean current computation

SAT-OCEAN ocean current modeling is based on HYCOM (Hybrid Coordinate Ocean Model - Bleck, 2001). HYCOM is a generalized hybrid vertical coordinate model widely recognized as a powerful and efficient tool for ocean modeling. To this state of the art model, SAT-OCEAN brings a significant methodology innovation in using it in an inverse way: the "data" drives the model where the dynamics is fitted onto it to yield 3D absolute ocean currents.

SST cloud-free fields are produced from merged sensor data sets with a very high spatial and temporal resolution and a 0.2°C rms error compared to simultaneous *in situ* measurements. From there, a regression coefficient calculation derived from simultaneous altimetric fields and historical Temperature / Salinity (T/S) profiles yields 3D temperature and salinity, daily: the obtained 3D T/S is called SAT-OCEAN dynamic climatology and represents as closely as possible the 3D state of the ocean over a given region.

The 3D T/S data is then strongly being assimilated in HYCOM/SAT-OCEAN model, strongly in the sense that it is given very little freedom to the model, and are very close to performing an inversion of forcing data, for the ocean circulation (except in the mixed layer which is highly driven by the forcing wind stress). Another way to present this is to say that ocean currents is fitted with high quality 3D satellite data, rather than obtaining current "data" from a model.

TOTAL Classification: Restricted Distribution
TOTAL - All rights reserved



MEMO

SAT-OCEAN also make a quantitative use of *in situ* data to calibrate the model when available (section 4.2).

A first 1/16° assimilated global model in-house run is used that covers the global ocean domain. Then, a fine resolution 1/32nd degree configuration of the assimilated model will cover a very large target area covering the offshore South Africa area of concern. The run will encompass 34 layers, with an about 10-layer sampling of the thermocline and a 3-hour output time step.

4.2 Calibration

Where TOTAL HF Radar and ADCP *in situ* current measurements are available, SAT-OCEAN performs a calibration and validation of their 3D ocean current model against the field data. Many mooring data as possible are used to perform the model calibration, including previous drilling campaigns and extensive seismic survey-based hull mounted ADCP on site current measurements. However, model calibration and validation at the deeper layers remain always more challenging due to the lack of measurements and are generally less reliable than at the surface where a larger quantity of data measurements are available. For each data set, current speed and direction measurements are extracted at all times and depths from all the provided files, and time-depth arrays are built. Specific procedures are then developed and applied (SVD decomposition, Kalman filtering etc.) to process the data at each measurement site such that it can be used for quantitative comparison and assimilation into the current model.

The pre-processed measurements are then used by SAT-OCEAN to extract the best calibration scheme for obtaining an improved time-depth dataset at each of the mooring sites. The outcome of this approach significantly improves the correlation between the modeled currents and the measurement series. Typically, SAT-OCEAN derive a calibration scheme over a learning data subset and evaluate the result over the remainder set, providing solid ground for the calibration scheme generalization to periods beyond learning periods. The final calibration scheme is applied to the entire ocean current historical/hindcast period to obtain calibrated hindcast datasets at every mooring location.

A calibration of the full South African south blocks dataset is finally performed. Spatial correction fields are derived in order to quantify at all ocean locations the influence of the locally calibrated currents at the mooring sites and of the modeled currents at each grid point of the hindcast domain.

The methodology results in a fully calibrated ocean current data set that takes the best advantage of the HF radar and ADCP on-site data available and of the assimilated model hindcast.



MEMO

4.3 Validation: currents and winds

4.3.1 Surface current

The SAT-OCEAN model currents were compared against observational data from HF radar for the purpose of validation. Only currents at the surface could be validated due to limited or no data at the sub-surface and for this exercise, 30 days of surface current observations from a single point were extracted from the HF radar dataset. The comparison of modelled currents with observations offers an opportunity to assess the ability of the SAT-OCEAN model to represent the current variability from the extracted data. Time series data starting from 10/03/2020 and ending on 10/04/2020 is presented in Figure 4 below.

From the visual inspection of the presented time-series in Figure 4 and scatter plots in Figure 5, surface current observations are generally coherent with SAT-OCEAN currents during the 30-day period. The SAT-OCEAN current presents a relative error RMS of 0.32kt. The increasing and decreasing patterns are consistent between the model and observations although there are slight differences in the magnitude of current speeds. The absolute mean bias between the SAT-OCEAN model and HF radar observations generally should not exceed 1 knot and there are occasional and slightly differences in the direction of the surface current flow.



Figure 4: Surface currents time-series from SAT-OCEAN (model) vs HF Radar (observations) for 30 days.



MEMO

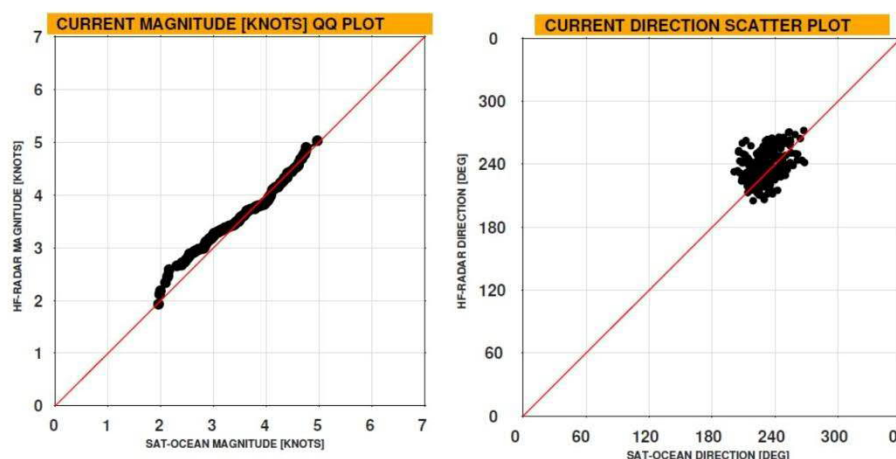


Figure 5 Current speed QQ plot and current direction scatter plot of SATOCEAN model vs observation for the considered period

For the given location, SAT-OCEAN modelled currents performed adequately indicating a reasonably fair representation of the surface current conditions over the 11B/12B block. The performance of the model may vary depending on features impacting the current flow e.g. a meandering core vs jet-regime state. Caution should be exercised when interpreting these results as they only represent validation at a single point within the block area (i.e. the Luiperd well location).

4.3.2 Winds

For the wind model validation, METAR (METeological Airport Report) wind observations are used as reference to compare with the model output. The comparison is made from a weather station wind dataset from Port Elizabeth which is located north-east outside the 11B/12B block along the South African coast. The Port Elizabeth location is within our observation area of interest with HF radars and therefore a relevant position for validation of the wind model. The time series comparison between the dates 10/03/2020 and 10/04/2020 is presented below in Figure 6.

Strong correlation between wind observations and model (see Figure 7) is recorded from the 30-day time series with the model explaining more than 88% of the variability in wind observations ($r = 0.94$ and $rms = 13$ kt). The SAT-OCEAN wind model provides coherent and consistent representation of the winds and is accurate in both magnitude and direction. Although the extreme wind conditions at 11B/12B can often exceed that of Port Elizabeth, the SAT-OCEAN model has proven its adequacy in capturing and representing wind conditions over a larger area including the full extent of the 11B/12B block.

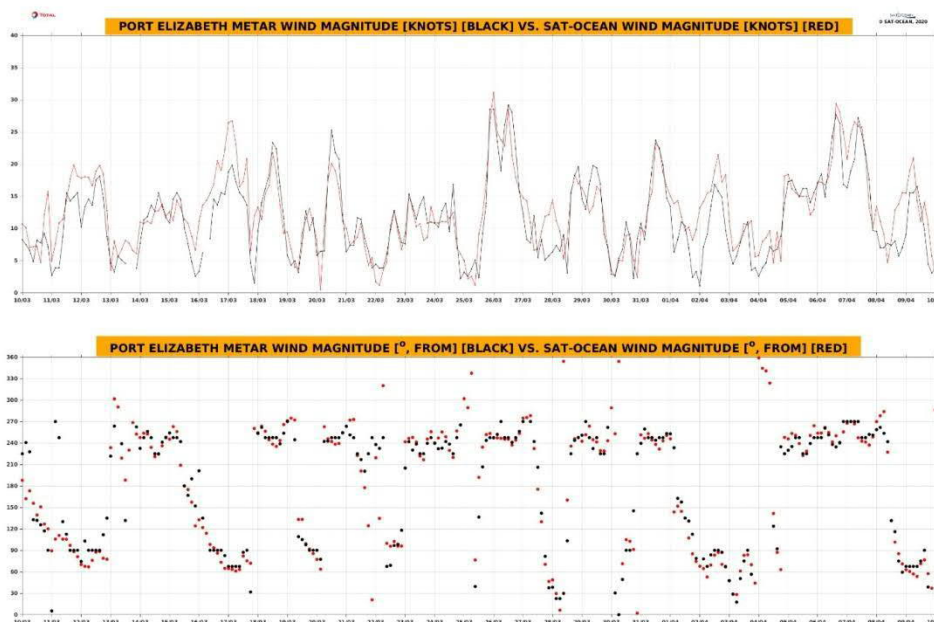



Figure 6 Surface winds time-series from SAT-OCEAN (model) vs METAR (observations) for 30 days.

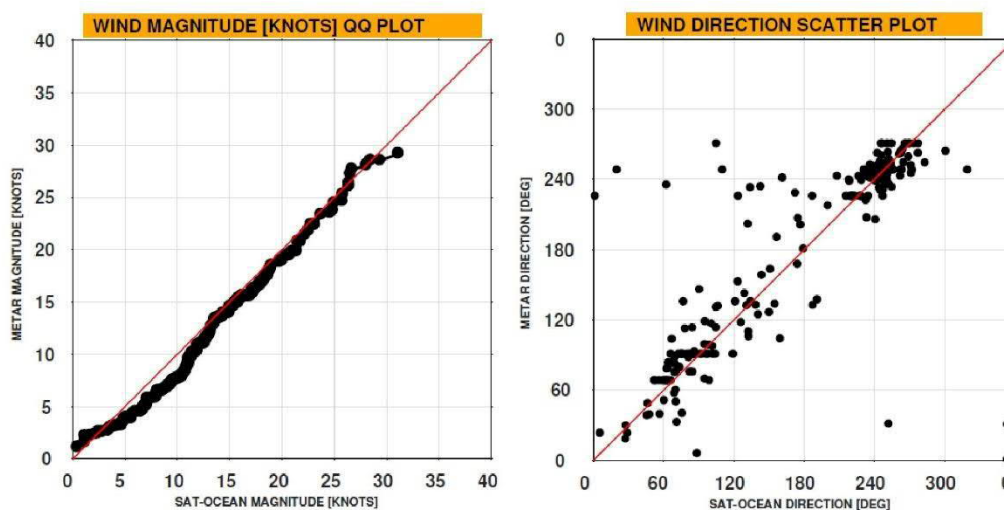
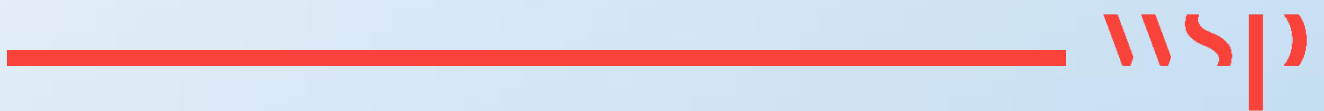


Figure 7 Wind speed QQ plot and wind direction scatter plot of SATOCEAN model vs observation for the considered period

TOTAL Classification: Restricted Distribution
 TOTAL - All rights reserved

Appendix B

DOCUMENT LIMITATIONS





DOCUMENT LIMITATIONS

This document has been provided by WSP Group Africa Pty Ltd (“WSP”) subject to the following limitations:

- i) This Document has been prepared for the particular purpose outlined in WSP’s proposal and no responsibility is accepted for the use of this Document, in whole or in part, in other contexts or for any other purpose.
- ii) The scope and the period of WSP’s Services are as described in WSP’s proposal, and are subject to restrictions and limitations. WSP did not perform a complete assessment of all possible conditions or circumstances that may exist at the site referenced in the Document. If a service is not expressly indicated, do not assume it has been provided. If a matter is not addressed, do not assume that any determination has been made by WSP in regard to it.
- iii) Conditions may exist which were undetectable given the limited nature of the enquiry WSP was retained to undertake with respect to the site. Variations in conditions may occur between investigatory locations, and there may be special conditions pertaining to the site which have not been revealed by the investigation and which have not therefore been taken into account in the Document. Accordingly, additional studies and actions may be required.
- iv) In addition, it is recognised that the passage of time affects the information and assessment provided in this Document. WSP’s opinions are based upon information that existed at the time of the production of the Document. It is understood that the Services provided allowed WSP to form no more than an opinion of the actual conditions of the site at the time the site was visited and cannot be used to assess the effect of any subsequent changes in the quality of the site, or its surroundings, or any laws or regulations.
- v) Any assessments made in this Document are based on the conditions indicated from published sources and the investigation described. No warranty is included, either express or implied, that the actual conditions will conform exactly to the assessments contained in this Document.
- vi) Where data supplied by the client or other external sources, including previous site investigation data, have been used, it has been assumed that the information is correct unless otherwise stated. No responsibility is accepted by WSP for incomplete or inaccurate data supplied by others.
- vii) The Client acknowledges that WSP may have retained sub-consultants affiliated with WSP to provide Services for the benefit of WSP. WSP will be fully responsible to the Client for the Services and work done by all its sub-consultants and subcontractors. The Client agrees that it will only assert claims against and seek to recover losses, damages or other liabilities from WSP and not WSP’s affiliated companies. To the maximum extent allowed by law, the Client acknowledges and agrees it will not have any legal recourse, and waives any expense, loss, claim, demand, or cause of action, against WSP’s affiliated companies, and their employees, officers and directors.
- viii) This Document is provided for sole use by the Client and is confidential to it and its professional advisers. No responsibility whatsoever for the contents of this Document will be accepted to any person other than the Client. Any use which a third party makes of this Document, or any reliance on or decisions to be made based on it, is the responsibility of such third parties. WSP accepts no responsibility for damages, if any, suffered by any third party because of decisions made or actions based on this Document.

WSP GROUP AFRICA (PTY) LTD



Building 1, Maxwell Office Park
Magwa Crescent West, Waterfall City
Midrand, 1685
South Africa

wsp.com

PUBLIC